SSC-7

Magnetic Errors in the SSC

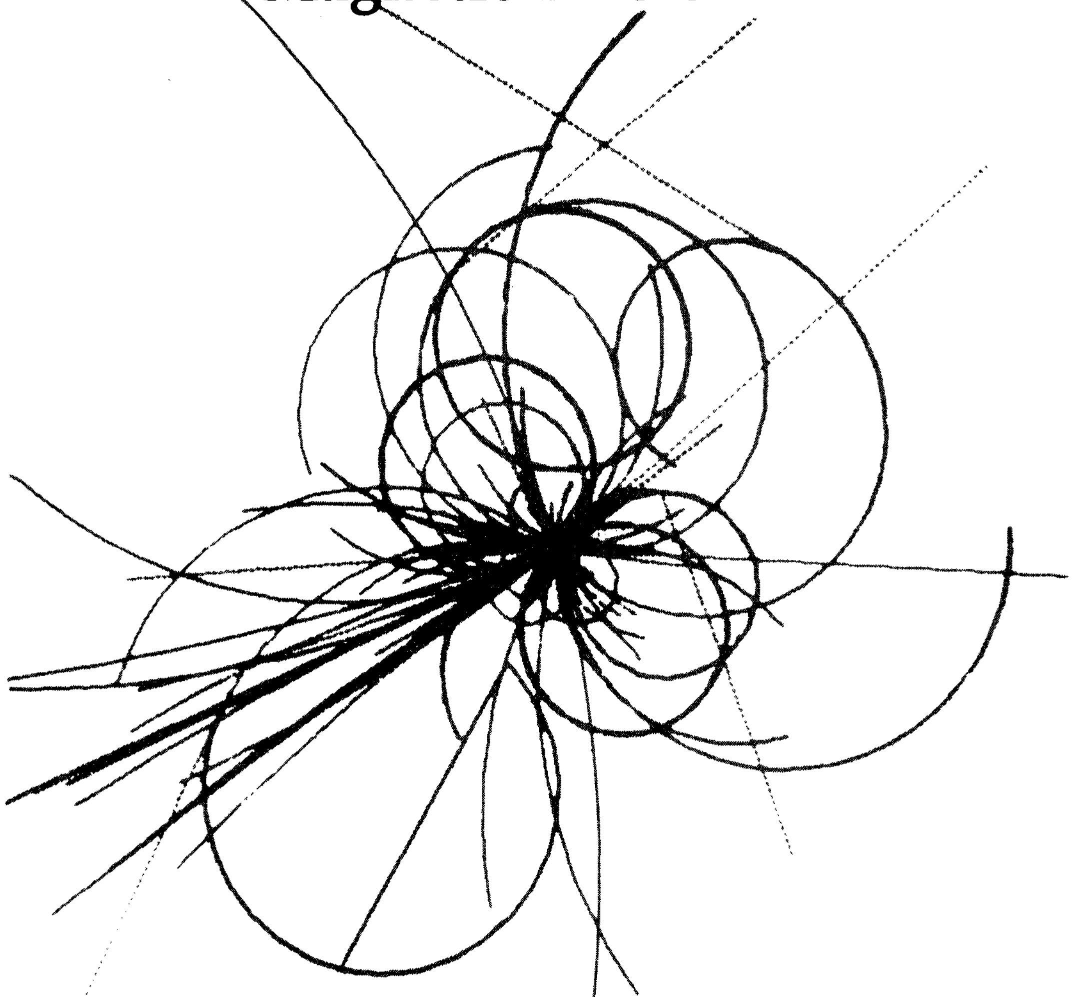

Preliminary Report of the Magnetic-Errors Working Group of the SSC Aperture Workshop

H.E. Fisk, W.S. Gilbert, M.A. Green,
W.V. Hassenzahl, R.B. Meuser, J.M. Peterson,
S. Pissanetsky, R. Scanlan, C.E. Taylor,
P.J. Wanderer, and W.A. Wenzel

April 1985

SSC-7

MAGNETIC ERRORS IN THE SSC

Preliminary Report of the Magnetic-Errors Working Group
of the SSC Aperture Workshop

J. M. Peterson
SSC Central Design Group,* c/o Lawrence Berkeley Laboratory, Berkeley, CA 94720

and

H. E. Fisk
Fermi National Accelerator Laboratory, P. O. Box 500, Batavia, IL 60510

and

W. S. Gilbert, M. A. Green, W. V. Hassenzahl,
R. B. Meuser, R. Scanlon, C. E. Taylor, and W. A. Wenzel
Lawrence Berkeley Laboratory, Berkeley, CA 94720

and

S. Pissanetsky
Texas Accelerator Center, The Woodlands, TX 77380

and

P. J. Wanderer
Brookhaven National Laboratory, Upton, NY 11973

April 1985

*Operated by Universities Research Association, Inc. under contract with the U. S. Department of Energy

TABLE OF CONTENTS
MAGNETIC ERRORS IN THE SSC

LIST OF TABLES

LIST OF FIGURES

LIST OF FIGURES (continued)

Summary

Magnetic Errors In the SSC
P.J. Wanderer

The four magnet types discussed in this report are briefly described in Section I of this report. However, for most purposes a discussion of random construction errors needs to deal with only two classes of magnets: collared cosine-theta (Designs A, B, D) and superferric (Design C). They are discussed in Section II and Section III, respectively. Magnetization effects in the cosine-theta magnets are treated in Section IV.

The report on superferric magnets is in two main parts. The first deals with the two-current version of the magnet (Fig. II.1), for which extensive calculations of both random and systematic magnetic field errors have been done. Two one-meter one-in-one models and a one-meter two-in-one model of this design have been successfully tested. Magnetic field data are available from the first two one-in-one models and have been compared with calculations. There is generally good agreement between the calculated and measured harmonics. The two currents were successfully adjusted for zero sextupole at all fields. However, approximately 8 10^{-4} units of sextupole remain unaccounted for and the presence of several 10^{-4} units of skew quadrupole and octupole is blamed on known imperfections in the conductor insulation. Random multipole errors were estimated by listing the sources and magnitudes of mechanical errors and calculating their effects on the fields. The results are presented in the last lines of Tables II.4 and II.6. The committee has reviewed the estimates of mechanical errors and is in general agreement with them. However, confirmation by measurement of a number of identical magnets is highly desirable. The effects of magnetization and remanent fields are calculated to be small. As yet no information exists on the fields of the magnet ends.

The second main part of the superferric discussion describes the three-current version of this magnet. The presence of the third current and a magnetic shunt allows control of the decapole at all excitations. The higher systematic multipoles are calculated to be 2 10^{-4} units at most (Table II.7). The random multipoles of the two-current and three-current designs are expected to be much the same, although the effects of placement errors in the third conductor remain to be calculated. Crosstalk between the two apertures is calculated to be negligible. As yet there is no information on scaling of error effects with aperture.

The superferric section briefly discusses an alternate approach, using pole face windings (Section II.9; also Appendix A). This approach, if successful, would allow the field to be increased to 4T.

The discussion of cosine-theta magnets begins with a review of the magnetic field data for the Tevatron and CBA dipoles (Section III.1). The Tevatron and CBA magnet diameters differ by nearly a factor of two, but the rms variations of the random errors at two-thirds radius are much the same. This suggests that the best approach to estimating errors for the SSC designs is an appropriate scaling law, although it is not obvious how the random errors will scale as the coil thickness approaches 2 cm, the size of the inner radius. (The data from the three 3.2-cm 2-in-1's, although limited, suggest that some sort of scaling law holds.) The results of three different approaches to estimating the errors are presented. The method of Fisk averages the Tevatron and CBA results after extrapolating the random dimensional errors to SSC diameters with a dependence of $r^{1/2}$ (Section III.3). Meuser calculates the sensitivity of field errors to 15 specific construction errors and then fits to the rms widths of the Tevatron and CBA multipole distributions to determine the sizes of the specified mechanical errors (Section III.4). Meuser extrapolates the dimensional errors to the SSC diameter assuming a $r^{0.3}$ law. Herrera's list of construction errors is quite similar to Meuser's list, but he groups them according to the type of symmetry or asymmetry they produce in the magnets before fitting them to the date (Section III.5). Herrera conservatively assumes that dimensional errors are independent of coil radius. Meuser's and Herrera's fits to the Tevatron and CBA data are quite good, typically 0.2 and 0.3 x 10^{-4} units (Section III.6). The predictions of all three models for SSC cosine-theta magnets are typically within 20% of one another (Table III.8). A prediction for the rms variation of the multipole errors to be expected for the SSC cosine-theta magnets is made by taking the average of the three predictions for each multipole (Table III.9). As noted above, the limited data from the 3.2 cm and 5 cm magnets (Section III.1) generally support these methods of analyzing magnet errors. Variations in the quadrupole terms due to mispositioning of the collared coils in the yoke are treated separately for the cold-iron designs (Section III.8). As was done at Fermilab, precise control of the positioning can be used to substantially reduce the quadrupole terms generated earlier in the production process.

A similar table of the projected random multipole variations for the superferric design also has been prepared, but it is based on very limited data. A summary of the projected random errors is given in Table S-1. The purpose of this table is to provide a starting point for the tracking programs. It is not to be taken as a final table, since that must ultimately depend on magnet measurements.

The systematic multipoles of Tevatron and CBA magnets are summarized in Table III.2, for terms higher than the sextupole. For both types of magnets, the difference between the calculated and measured values is 0.4 units or less for 18-pole and higher terms. The CBA data confirm that wedges can be used to control these terms. There is substantial flexibility in the actual choice of

Table S-1
RMS MULTIPOLE VARIATIONS
PROJECTED FOR SSC MAGNET DESIGNS
a_n, b_n = skew, normal coefficient of 2(n+1)-pole
Units are 10^{-4} at 1 cm
Data of 7/30/85

Multipole Coef	Design A and D(4 cm)					Design B				
	σ_{geom}	σ_{Pers} 5μ	σ_{Pers} 9μ	σ_{Tot} 5μ	σ_{Tot} 9μ	σ_{geom}	σ_{Pers} 5μ	σ_{Pers} 9μ	σ_{Tot} 5μ	σ_{Tot} 9μ
a_0	5.9	-	-	-	-	5.6	-	-	-	-
b_0	3.0	-	-	-	-	2.8	-	-	-	-
a_1	0.70	.09	.15	.71	.72	3.6	.07	.11	3.6	3.6
b_1	0.70	.09	.15	.71	.72	1.75	.07	.11	1.75	1.75
a_2	0.61	.09	.14	.62	.63	0.59	.05	.08	.59	.60
b_2	2.01	.47	.75	2.06	2.15	1.94	.36	.56	1.97	2.02
a_3	0.69	0	0	.69	.69	0.60	0	0	.60	.60
b_3	0.35	0	0	.35	.35	0.30	0	0	.30	.30
a_4	0.14	0	0	.14	.14	0.11	0	0	.11	.11
b_4	0.59	.03	.07	.59	.59	0.46	.01	.02	.46	.46
a_5	0.16	0	0	.16	.16	0.11	0	0	.11	.11
b_5	.059	0	0	.059	.059	0.042	0	0	.042	.042
a_6	.034	0	0	.034	.034	.022	0	0	.022	.022
b_6	.075	.01	.01	.076	.076	.048	0	0	.048	.048
a_7	.030	0	0	.030	.030	.017	0	0	.017	.017
b_7	.016	0	0	.016	.016	.0091	0	0	.0091	.0091
a_8	.0064	0	0	.0064	.0064	.0033	0	0	.0033	.0033
b_8	.021	0	0	.021	.021	.011	0	0	.011	.011
a_9	.0056	0	0	.0056	.0056	.0026	0	0	.0026	.0026
b_9	.0030	0	0	.0030	.0030	.0014	0	0	.0014	.0014
a_{10}	.0012	0	0	.0012	.0012	.00050	0	0	.00050	.00050
b_{10}	.0071	0	0	.0071	.0071	.0030	0	0	.0030	.0030

$\sigma_{pers}(b_{2,4,6}) = 0.10\, b_{2,4,6}$ = rms variation of persistent-current multipole coef. due to variations in critical current density and temperature at injection.

$\sigma_{pers}(a_1, b_1, a_2)$ are due to random sextupole-correction-coil errors.

$\sigma^2_{tot} = \sigma^2_{pers} + \sigma^2_{geom}$(at injection).

Table S-1, RMS Multipole Variations (continued)
Units are 10^{-4} at 1 cm
Data of 7/30/85

Multipole Coef	Design C					Design D (5 cm)				
	σ_{geom}*	σ_{Pers} 9μ	σ_{Pers} 20μ	σ_{Tot} 9μ	σ_{Tot} 20μ	σ_{geom}	σ_{Pers} 5μ	σ_{Pers} 9μ	σ_{Tot} 5μ	σ_{Tot} 9μ
a_0	-	-	-			5.5	-	-	-	-
b_0	-	-	-			2.8	-	-	-	-
a_1	3.1	.01	.03	3.1	3.1	0.56	.06	.09	.56	.57
b_1	1.2	.01	.03	1.2	1.2	0.56	.06	.09	.56	.57
a_2	1.1	.01	.03	1.1	1.1	0.41	.04	.07	.41	.42
b_2	1.	.06	.13	1.	1.	1.4	.29	.47	1.4	1.5
a_3	1.3	0	0	1.3	1.3	0.40	0	0	.40	.40
b_3	0.8	0	0	.8	.8	0.20	0	0	.20	.20
a_4	0.8	0	0	.8	.8	.07	0	0	.07	.07
b_4	0.4	0	0	.4	.4	.29	.01	.02	.29	.29
a_5	0.7	0	0	.7	.7	.069	0	0	.069	.069
b_5	0.4	0	0	.4	.4	.025	0	0	.025	.025
a_6	0.7	0	0	.7	.7	.012	0	0	.012	.012
b_6	0.5	0	0	.5	.5	.028	0	.01	.028	.028
a_7						.0094	0	0	.0094	.0094
b_7						.0050	0	0	.0050	.0050
a_8						.0017	0	0	.0017	.0017
b_8						.0057	0	.0057	.0057	
a_9						.0013	0	0	.0013	.0013
b_9						.00069	0	0	.00069	.00069
a_{10}						.00024	0	0	.00024	.00024
b_{10}						.0014	0	0	.0014	.0014

* Based partly on measured variations among the first six model magnets (types NF2C, WF2C, and WF3CMS) and partly on estimated random construction errors. From S. Pissanetzky and W. MacKay, private communications.

the systematic multipoles for both the one-in-one designs (B and D) and for the two-in-one design (A), at levels of a few tenths of a unit. The calculated effect of excitation on the systematics of the two-in-one magnet is about 0.6 units in the normal quadrupole and sextupole terms and less than 0.1 for higher terms (Table III.12). A summary table of the systematic multipole strengths expected for each magnet type is presented also (Table S-2).

Section IV discusses the effects of magnetization on the field shape of cosine-theta magnets at SSC injection. Subsections IV.1 and IV.2 summarize the calculations and measurements of the magnetization of bare conductors as well as the sextupole fields in magnets with NbTi filament sizes in the range 10μm to 20μm. At fields near 0.3 T, which corresponds to SSC injection, there is agreement within 30 percent or better between measurements and calculations (e.g., a 4-cm dipole with 20μm filaments in Figure IV.16.) Predictions of the magnetization sextupole for magnets with conductor having filament sizes in the range 2μm to 20 μm, for magnet types A, B, and D are given (Figures IV.3-.8).

In addition to the overall level of magnetization, it is important to consider fluctuations due to variations in the superconductor; these amounted to about 9 percent rms in the Tevatron dipoles (Section IV.5). It is also necessary to consider the sawtooth variation caused by the 0.25K (maximum) change in helium temperature along a cryogenic loop (Section IV.6). This is calculated to produce an rms variation equal to 1.5 percent of the persistent-current sextupole. As can be seen from the entries in Table S-1, these effects do not significantly increase the total rms variation beyond that expected from construction errors.

With the assumption that it will be necessary to correct the magnetization effects "locally" (i.e., with coils inside the main dipoles rather than in the separate spool pieces), Section IV.4 reviews three possible approaches. The

Table S-2
Systematic Multipoles Projected for SSC Magnet Designs
b_n = normal coefficient of 2(n+1)-pole
units: 10^{-4} at 1 cm
Data of 7/30/85

	b_1	b_2	b_4	b_6	b_8	b_{10}	b_{12}
Design A[a]							
geometry, Inj.	0	-.9	0	.2	.8	0	-
geometry, 20 Tev	-.4	-.2	0	.2	.8	0	-
persistent, 5μ, Inj.	0	-4.7	.30	.07	-	-	-
persistent, 9μ, Inj.	0	-7.5	.67	.13	-	-	-
Design B[b]							
geometry, Inj. & 20 TeV	0	.07	-.07	.09	-.14	.014	-
persistent, 5μ, Inj.	0	-3.6	.08	0	-	-	-
persistent, 9μ Inj.	0	-5.6	.24	0	-	-	-
Design C							
geometry, Inj.[c]	0	0	0	.5	.1	-	-
geometry, 20 TeV[c]	0	0	0	1.5	.2	-	-
persistent, 20μ, Inj.[d]	0	1.3[g]	-	-	-	-	-
remanent H, Inj.[d]	0	1.1[g]	-	-	-	-	-
Design D(4 cm)[e]							
geom, Inj.	0	-0.05	-.16	-.03	.15	.19	-.05
geom, 20 TeV	0	2.	-.16	-.03	.15	.19	-.05
persistent, 5μ, Inj.	0	-4.7	.30	.07	-	-	-
persistent, 9μ, Inj.	0	-7.5	.67	.13	-	-	-
Design D(5 cm)							
geom, Inj.[f]	0	-.037	-.086	-.012	.044	.041	-.0079
geom, 20 TeV[f]	0	1.47	-.086	-.012	.044	.041	-.0079
persistent, 5μ, Inj.	0	-2.9	.10	.03	-	-	-
persistent, 9μ, Inj.	0	-4.7	0.23	.07	-	-	-

a. Coil configuration C-5, 2-in-1 BNL SSC Tech. Note 19
b. Coil configuration OPTI 824 (FNAL)
c. Data on superferric design WF3CMS (TAC)
d. Data on superferric design NF2C (TAC)
e. Coil configuration PK-15, (BNL)
f. Scaled from D(4 cm)
g. Can be canceled by current adjustment

first two use sextupole coils, in one case powered by an external power supply and in the other case powered by flux linkage with the magnetization sextupole. In the third case, superconductor is distributed appropriately inside the dipole so that the inherent diamagnetic property of the superconductor itself cancels the sextupole induced in the main windings. The important features of these three possibilities are summarized in Table IV.6.

MAGNETIC ERRORS IN THE SSC

I. Introduction

The objective of the Magnetic-Errors Working Group (Group C of the SSC Aperture Workshop, November 1984) is a realistic appraisal of the magnetic multipole strengths likely to be present in the several types of superconducting magnets now under consideration for the Superconducting Super Collider.

The magnet designs considered are

(1) Magnet Design A of the SSC Reference Design Study (cosθ-type magnet in a two-in-one configuration, 4-cm inner-coil diameter, cold iron, originally without a collar but has evolved to a collared version),

(2) Magnet Design B of the Reference Design Study (cosθ-type magnet in a one-in-one configuration, 5-cm inner-coil diameter, "no" iron),

(3) Magnet Design C of the SSC Reference Design Study (super-ferric magnet in a two-in-one configuration),

(4) Magnet Design D (cosθ-type magnet in a one-in-one configuration, 4-cm and 5-cm inner-coil-diameter versions, cold iron, 15-mm collar).

The projected magnetic-multipole strengths presented here are based both on experience and on the calculated effects due to estimated placement errors and persistent currents in superconducting coils.

These projections will be updated as warranted when measurements on models of the new magnet designs become available.

The multipole nomenclature is defined by the following expansion of the magnet field in the central region of a dipole magnet:

$$B_y + i\,B_x = B_o \sum_{n=0} C_n (Z/R_R)^n$$

where B_o = Magnitude of the dipole field (in the y-direction (vertical))

$C_o = 1$

$C_n = b_n + i\,a_n, \quad n \geqslant 1$

b_n = normal multipole coefficient, symmetric about the x-(horizontal) axis

a_n = skew multipole coefficient

n = 1 for quadrupole

n = 2 for sextupole, etc.

$Z = x + i\,y$

R_R = reference radius, either 2/3 of the inner-coil radius or 1 cm in this report.

II. Superferric Magnets, SSC Design "C"

Sergio Pissanetzky

II.1 Introduction

Historically, the following superferric design versions were developed successively at Texas Accelerator Center:

C1C - Crenellated, one current

NF2C - Narrow face, two currents

WF2C - Wide face, two currents

WF3CMS - wide face, three currents, with magnetic shunt.

This report first discusses version NF2C. Two magnets were built, measured, and compared with predictions. Version WF3CMS is also discussed. It is the favored superferric design at present. All 2C versions use two different currents in the coil, their ratio being adjusted in such a way that the sextupole coefficient b_2 is made equal to zero. The 3C version uses an additional small conductor with an independent current that is adjusted to make the decapole coefficient b_4 equal to zero.

II.2 Narrow-Face, Two-Currents Design NF2C

Two magnets, TAC001 and TAC002, each with a single bore, were built according to this design. The average measured dimensions of the laminations and superconducting coil are shown in Figure II.1.

Measurements were performed at BNL on both magnets. The results are given in Table II.1, and plotted in Figure II.2. The plots show that the two magnets behave essentially the same way within measurement and construction errors, except for a_1 and a_3. This exception is attributed to improper wrapping of the conductors in Kapton (the Kapton

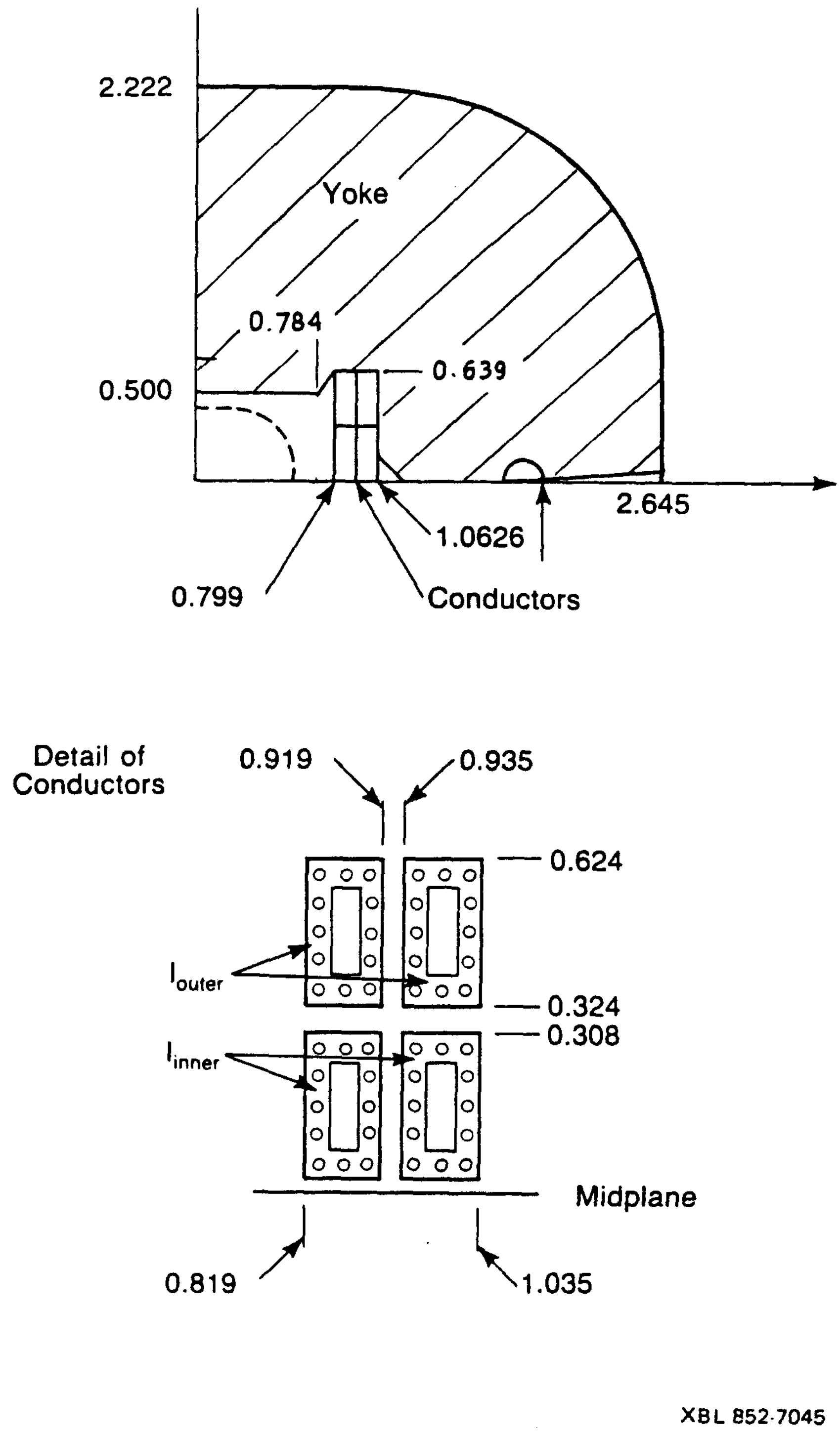

Figure II.1 Quadrant of narrow-face, two-current superferric Design NF2C and detail of conductor bundle. Dimension in inches.

Table II.1
Harmonics for Two T.A.C. Magnets.

Harmonics were measured with tangential coils. The two excitation currents were adjusted until the measured sextupole was close to 0. Harmonics ($x10,000/B_0$) are given at 0.4 inch. All values agree reasonably well with predicted numbers, thus showing that predictions can be met.

T.A.C. 001.

B_o	I_{in}	I_{out}	b_1	b_2	b_3	b_4	b_5	b_6	b_7	b_8	b_9
0.15T	584A	144A	3.4	-0.7	2.5	5.6	1.3	0.8	1.5	1.5	1.1
0.25	998	278	1.3	-0.2	2.1	5.6	0.9	2.0	0.1	1.5	0.2
1.03	4001	1220	0.5	-0.4	0.9	5.1	0.1	2.1	0.4	1.0	0.7
1.77	7002	1996	-0.2	-0.2	0.5	7.4	-0.1	2.5	0.9	-0.2	1.1
2.54	9523	4516	-0.3	0.0	-0.1	2.2	0.4	2.9	0.1	0.8	0.6
2.99	9313	9303	0.5	0.1	-1.3	-17.5	0.1	-0.8	1.2	0.7	0.2

B_o	B_oa_o	a_1	a_2	a_3	a_4	a_5	a_6	a_7	a_8
0.15T	-35G	-5.6	1.1	-2.1	-0.1	-0.3	-0.9	2.4	-1.7
0.25	0	-1.6	1.0	0.1	0.2	0.9	0.7	-0.8	0.5
1.03	0	3.7	0.7	1.6	0.0	0.7	0.3	0.2	0.1
1.77	-9	4.5	0.9	1.8	0.8	0.2	1.1	-0.2	0.9
2.54	-6	3.2	0.5	0.5	0.4	0.5	0.8	-0.3	0.6
2.99	-6	2.6	-0.2	-1.9	-1.0	-0.4	-0.4	0.4	0.3

T.A.C. 002.

B_o	I_{in}	I_{out}	b_1	b_2	b_3	b_4	b_5	b_6	b_7	b_8	b_9	b_{10}	b_{11}
0.15T	585A	145A	0.4	0.7	1.9	5.4	0.8	1.6	0.0	0.2	-0.3	-0.2	1.4
0.25	1000	280	0.2	0.0	1.4	4.5	1.0	2.0	-0.3	1.0	-0.8	0.2	-0.2
0.51	2000	590	-0.5	0.9	0.8	5.0	0.7	1.7	0.5	0.4	0.1	0.6	-1.2
1.03	3999	1217	-0.4	-0.1	1.2	4.5	0.5	2.1	0.1	0.9	0.7	-0.8	0.6
1.77	6999	2000	-0.6	-0.7	1.2	6.4	0.7	2.8	0.1	1.4	-0.3	1.0	-0.2
2.5	9518	4520	-0.4	-1.1	0.5	1.6	0.9	3.0	0.1	0.7	0.2	1.0	-1.5
2.98	9305	9295	-0.7	-0.2	-1.9	-17.4	0.1	-1.0	0.3	0.7	0.3	-0.2	-1.9

B_o	B_oa_o	a_1	a_2	a_3	a_4	a_5	a_6	a_7	a_8	a_9	a_{10}	a_{11}
0.15T	0G	-2.1	-2.0	-2.5	-0.2	-0.5	0.0	-0.3	0.1	1.3	0.4	0.7
0.25	-7	-2.7	-1.6	-1.7	0.2	-0.7	-0.2	-0.3	0.1	0.3	-1.0	-0.3
0.51	5	-3.4	-1.4	-1.8	-0.2	-0.5	-0.1	0.1	-0.6	0.3	0.5	-0.4
1.03	0	-3.5	-1.2	-2.0	0.0	-0.8	0.1	-0.4	-0.2	0.1	0.0	0.0
1.77	6	-3.5	-1.7	-2.3	0.1	-1.0	0.0	-0.8	0.0	-0.1	-0.1	0.1
2.53	-5	-3.4	-1.1	-1.2	-0.1	-1.0	0.2	0.1	-0.7	0.3	0.2	0.7
2.98	-4	-2.3	-0.5	3.0	-0.4	0.2	-0.3	0.0	-0.5	0.4	0.0	0.1

0388S

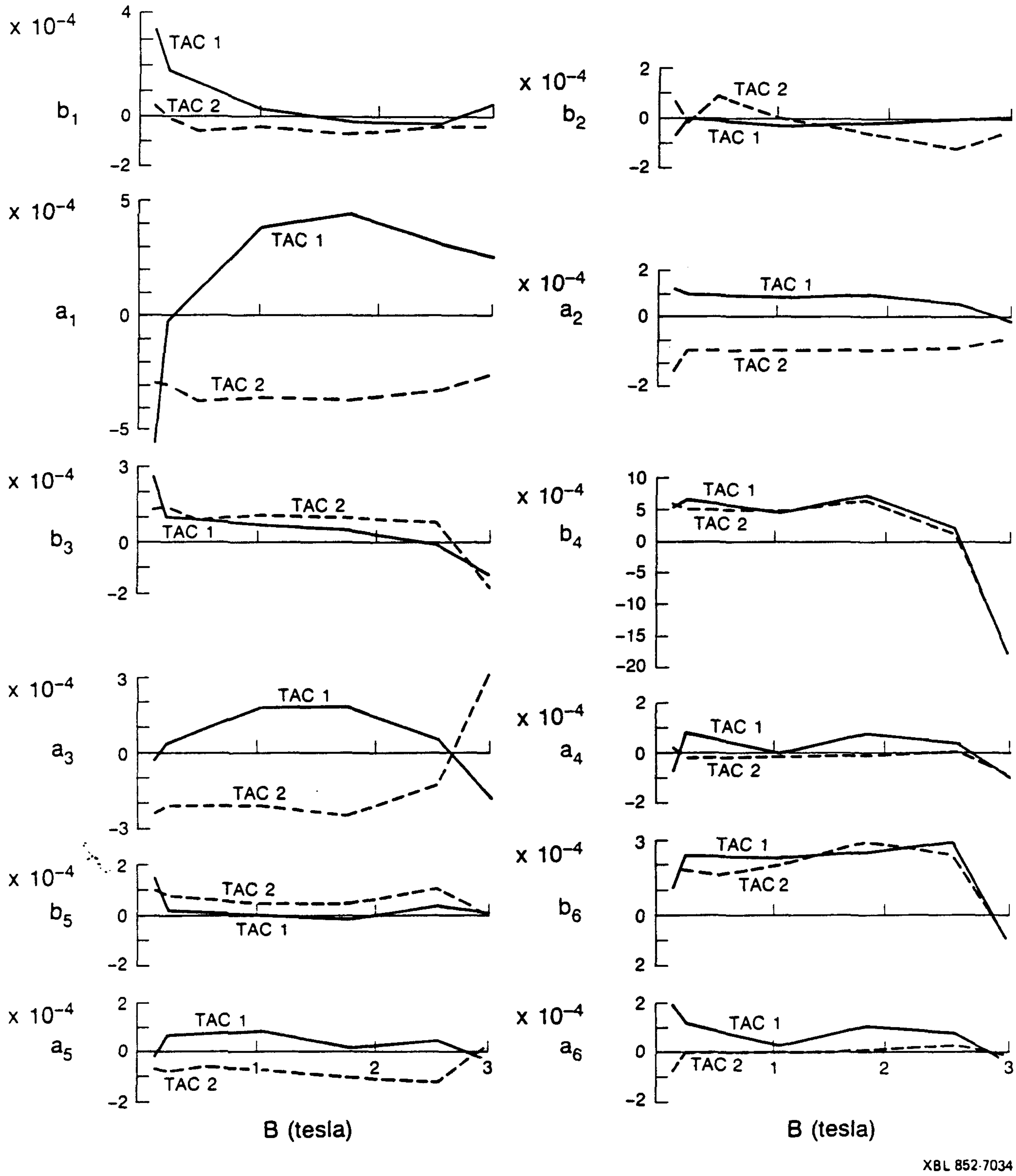

Figure II.2 Variation of measured multipole strengths with magnet excitation for magnet models TAC 1 and 2.

was over-lapping at the edges) which caused misplacement of the con ductors in the vertical direction; a_1 and a_3 are very sensitive to such a misplacement.

Predictions for TAC001 were obtained from a computer model (POISSON) that used the magnetic properties of 1008 steel corrected for 4.2°K and the measured average geometry for laminations and conductors. Table II.2 shows a comparison between calculated and measured symmetric multipoles. The two sets are not directly comparable because different currents were used: the currents used for measurement were experimentally adjusted until b_2 was less than 1 unit (10^{-4}), while the currents used for computation were those of a previous (bad) measurement on TAC001, and lack of computer time prevented them from being iterated until $b_2 = 0$. The sensitivity of b_2 to current ratio is 0.4 and 1.1 units/1.0 percent at injection and storage, respectively, so that most of the differences in b_2 can be accounted for in this way. The sensitivities of b_4 are 0.2 and 0.3, while b_6 is almost insensitive. The measured and calculated b_4 and b_6 are in good agreement because the sensitivities are so low, and the agreement could have been made even better if the current ratio had been adjusted to the correct values.

Comparisons between the measured and calculated skew multipoles a_1 and a_3 are also available. a_1 and a_3 should be zero by symmetry, but (accidentally) a 5-mil-thick shim was placed on one side of each stack of conductors, thus causing the conductors to shift vertically by an average 2.5 mil. Table II.3 shows a comparison between the measured and the calculated values. The agreement is excellent. The shim was then removed and new measurements were performed, which gave a_1 in the range -3.5 to 4.8 units and a_3 between -2.2 and 2.1. This indicated a

Table II.2
Symmetric Multipoles at 0.4 Inch
Measured in Magnet Model TAC001

I_{in}	I_{out}	B_o	b_2	b_4	b_6
584.79A	143.80A	0.14526T	-0.7×10^{-4}	5.6×10^{-4}	0.8×10^{-4}
998.97	281.79	0.25329	-0.2	5.6	2.0
2000.2	591.15	0.51360	0.2	4.8	1.7
3999.53	1218.20	1.03262	-0.4	5.1	2.1
7000.56	2002.06	1.77290	-0.2	7.4	2.5
9521.00	4523.09	2.53597	0.0	2.2	2.9
9317.71	9307.91	2.98804	0.1	-17.5	-0.8

Table II.3
Comparison between measured and calculated skew
multipoles a_1 and a_3 for TAC 001 with a 5 mil shim.

	Measured		Calculated	
B_o(T)	a_1	a_3	a_1	a_3
0.511	12.6×10^{-4}	3.9×10^{-4}	13.5×10^{-4}	3.6×10^{-4}
1.022	13.7	4.3	13.5	3.5
1.711	14.5	4.5	13.8	3.4
2.537	11.5	2.3	11.3	2.2
2.691	10.6	1.7	10.4	1.8
2.980	9.0	0.2	8.7	1.3

vertical misplacement of the conductors of about 2 mils on the average, a figure quite consistent with the overlapping of the 2 mil thick Kapton insulation discussed previously.

II.3 Random Errors in the Superferric Design

The calculation of random multipoles for superferric magnets is done in several steps. Refer to Tables II.4, II.5, and II.6. The steps are:

- Identification of sources of error. Several sources were identified and are listed in the first column of the three tables.
- Estimation of the accuracy for each source of error, Column 2.
- Number of occurrences for each error, Column 3.
- Sensitivity (or derivative) of each harmonic component with respect to each source of error. Not all are available at present, but those which are available are given in Tables II.4, II.5 and II.6. They were computed for version WF2C. Version WF2C is identical to NF2C, Figure II.1, except that the pole face is wider, so that the dimensions are those shown in Figure II.3 for the WF3CMS design.
- The error in each harmonic produced by each source is obtained as the product of the sensitivity, the accuracy, and the number of occurrences.
- The final total error of each harmonic is the square root of the sum of the squares of each contribution. These figures are incomplete because not all contributions are available, but it is believed that the most important contributions have been taken into account and that the final errors are representative in the cases of injection and storage. Not enough information is available at intermediate fields.

Table II.4

Magnetic Errors at Injection (B_o = 0.15 T)
TAC Superferric Magnets
January 1985
u = 1 "unit" = 10^{-4}

Source of Error	Accuracy	Number of Occurrences	B_o Sensit.	B_o Error	b_2 Sensit.	b_2 Error	b_4 Sensit.	b_4 Error	b_6 Sensit.	b_6 Error	a_1 Sensit.	a_1 Error	a_3 Sensit.	a_3 Error
Horizontal Misplacement of Conductor	1 mil	$\sqrt{16}$	0 gauss/mil	0 gauss	-0.02 u/mil	0.08 u	-0.005 u	0.02 u	-0.002 u	0.01 u	0	0	0	0
Vertical Misplacement of Conductor	3.8 mil total (all 16 conductors)		0	0	-0.08 u/mil	0.30 u					0.28 u/mil	1.1 u	0.08 u/mil	0.3 u
Gap Spacing	0.2 mil	$\sqrt{2}$ ($\sqrt{4}$ for B_o)	-1.5 gauss/mil	0.4 gauss	2.7 u/mil	0.76 u	0.03 u/mil	0.008 u	0.3 u/mil	0.09 u	0	0	0	0
Current Ratio	0.01%	$\sqrt{2}$	0	0	0.37 u/1%	0.005 u	0.20 u/1%	0.003 u	0.035 u/1%	0 u	0	0	0	0
μ Variations	2%	1	0.01 gauss/1%	0.02 gauss										
Up-Down μ Mismatch	2%	1	0 gauss/1%	0 gauss	0.01 u/1%	0.02 u	-0.01 u/1Δ	0.02 u	-0.005 u/1Δ	0.01 u				
Stacking Factor (0.998)	0.1%	1	0 gauss/1%	0 gauss	-0.002 u/1%	0 u								
Up-Down Stack Factor Mismatch	0.1%	1	0 gauss/1%	0 gauss	-0.004 u/1%	0 u	0.004 u/1%	0 u	0.005 u/1%	0 u				
$\sqrt{\Sigma(\text{Error})^2}$			0.4 gauss		0.8 x 10^{-4}		0.03 x 10^{-4}		0.09 x 10^{-4}		1.1 x 10^{-4}		0.3 x 10^{-4}	

0388S

Table II.5
Magnetic Errors at Intermediate Field (2.4 T)
TAC Superferric Magnets
January 1985
$u = 1$ "unit" $= 10^{-4}$

Source of Error	Accuracy	Number of Occurrences	B_o Sensit.	B_o Error	b_2 Sensit.	b_2 Error	b_4 Sensit.	b_4 Error	b_6 Sensit.	b_6 Error	a_1 Sensit.	a_1 Error	a_3 Sensit.	a_3 Error
Horizontal Misplacement of Conductor	1 mil	$\sqrt{16}$	0 gauss/mil	0 gauss							0	0	0	0
Vertical Misplacement of Conductor	3.8 mil total (all 16 conductors)		0	0										
Gap Spacing	0.2 mil	$\sqrt{2}$ ($\sqrt{4}$ for B_o)									0	0	0	0
Current Ratio	0.01%	$\sqrt{2}$	0	0							0	0	0	0
μ Variations	2%	1	gauss/1%	gauss										
Up-Down μ Mismatch	2%	1	4.8 gauss/1%	10 gauss	-0.5 u/1%	1.0 u	0.3 u/1%	0.6 u	0.2 u/1%	0.4 u				
Stacking Factor (0.998)	0.1%	1	gauss/1%	gauss										
Up-Down Stack Factor Mismatch	0.1%	1	42 gauss/1%	4.2 gauss	-3.5 u/1%	0.4 u	-0.7 u/1%	-0.07 u	-0.3 u/1%	0.03 u				

$\sqrt{\Sigma(\text{Error})^2}$ (incomplete)

0388S

Table II.6
Magnetic Errors at Storage (3 T)
TAC Superferric Magnets
January 1985
u = 1 "unit" = 10^{-4}

Source of Error	Accuracy	Number of Occurrences	B_o Sensit.	B_o Error	b_2 Sensit.	b_2 Error	b_4 Sensit.	b_4 Error	b_6 Sensit.	b_6 Error	a_1 Sensit.	a_1 Error	a_3 Sensit.	a_3 Error
Horizontal Misplacement of Conductor	1 mil	$\sqrt{16}$	-0.25 gauss/mil	1.0 gauss	-0.007 u/mil	0.03 u	-0.001 u/mil	0.004 u	-0.001 u/mil	0.004 u	0	0	0	0
Vertical Misplacement of Conductor	3.8 mil total (all 16 conductors)		0	0	-0.3 u/mil	1.14 u					0.18 u/mil	0.68 u	0.03 u/mil	0.11 u
Gap Spacing	0.2 mil	$\sqrt{2}$ ($\sqrt{4}$ for B_o)	-13 gauss/mil	3.7 gauss	0.18 u/mil	0.05 u	0.07 u/mil	0.02 u	0.01 u/mil	0.003 u	0	0	0	0
Current Ratio	0.01%	$\sqrt{2}$	0	0	1.1 u/1%	0.015 u	0.29 u/1%	0.004 u	0.047 u/1%	0.001 u	0	0	0	0
μ Variations	0.13%	1	39 gauss/1%	5.1 gauss	-0.3 u/1%	0.04 u	0.17 u/1%	0.022 u						
Up-Down μ Mismatch	0.18%	1	12 gauss/1%	2.2 gauss	-0.4 u/1%	0.07 u	-0.7 u/1%	0.13 u	2.1 u/1%	0.4 u				
Stacking Factor (0.998	0.1%	1	155 gauss/1%	16 gauss	-2.4 u/1%	0.24 u	-0.69 u/1%	0.07 u	-0.13 u/1%	0.013 u				
Up-Down Stack Factor Mismatch	0.1%	1	71 gauss/1%	7.1 gauss	-6.3 u/1%	0.63 u	-3.6 u/1%	0.36 u	-2.2 u/1%	0.22 u				
$\sqrt{\Sigma(\mathrm{Error})^2}$				19 gauss		1.1×10^{-4}		0.4×10^{-4}		0.5×10^{-4}		0.7×10^{-4}		0.1×10^{-4}

0388S

Accuracies: Laminations are obtained by stamping, and all internal dimensions can be controlled within ±0.2 mil. Each conductor is wrapped with 4 layers of 2-mil-thick Kapton. From measurements the Kapton thickness was shown to be constant within 0.1 mil. Measurements of conductor samples with Kapton insulation gave the following average dimensions: 0.3190 inch vertical, 0.1206 inch horizontal, with σ = 0.7 mil in both cases. Thus it is believed that the conductors can be horizontally placed with an accuracy better than ± 1 mil.

Concerning vertical misplacement of the conductors, the problem is more complicated because collective effects must be taken into account: if one conductor is taller than the average, or one layer of insulation is thicker or thinner, then all conductors of the stack will be displaced. The stack of four conductors is built to a total height of 1.416 inch, and then compressed by the laminations to 1.412 inch. Since the Young's modulus of Kapton or fiberglass is 20 times less than that of the conductors, most of the compression will be absorbed by the insulation. The final position of each conductor in the stack can be computed as a function of the individual errors in each conductor and the individual errors in the thickness of each layer of insulation, which are the truly independent variables. The final error can then be obtained as the RMS average over the independent errors. The final result (Ref. 40) was found to be 3.8 mil of misplacement in total for all 16 conductors, as reported in Tables II.4, II.5 and II.6.

The gap spacing is accurate to ±0.2 mil and the number of occurrences of this error is $\sqrt{2}$. In the case of B_0, however, the number of occurrences is $\sqrt{4}$ because B_0 also is sensitive to spacing left between the upper and lower laminations of the yoke at the median plane.

The current ratio is accurate to within 0.01 percent and there are $\sqrt{2}$ occurrences of this error.

The variation in magnetic permeability is shown by the histogram (Fig. II.3) of the measured values of magnetization in the iron laminations stamped from 1008 steel that were used in making magnets for the Fermilab debuncher and accumulator rings. The histogram shows variations in μ-values of about 1 to 2 percent. A 1-percent variation is found when the grain direction is oriented either parallel to the long dimension of the lamination or perpendicular to it, but the mean values of μ for these two cases differ by 1 percent, as shown in Figure II.4. This error may affect both the upper and lower laminations at any given position, and it can also cause a mismatch between the permeability of an upper lamination and the corresponding lower one.

A measured stacking factor of 0.998 was achieved for TAC001 and TAC002. The stacking factor will be set by requiring a uniform weight per unit length of the assembled yoke. The inaccuracy in the stacking factor will certainly be less than 0.1 percent. This inaccuracy also can manifest itself as a mismatch between the upper and the lower stack of laminations.

Several other sources of error were considered and discarded because they are insignificant. As examples we may mention: left-right stacking factor mismatch due to bending of the magnet to follow the curvature of the tunnel; deformation of pole tip caused by mechanical or magnetic forces; displacement of conductors due to magnetic forces or thermal cycling; etc.

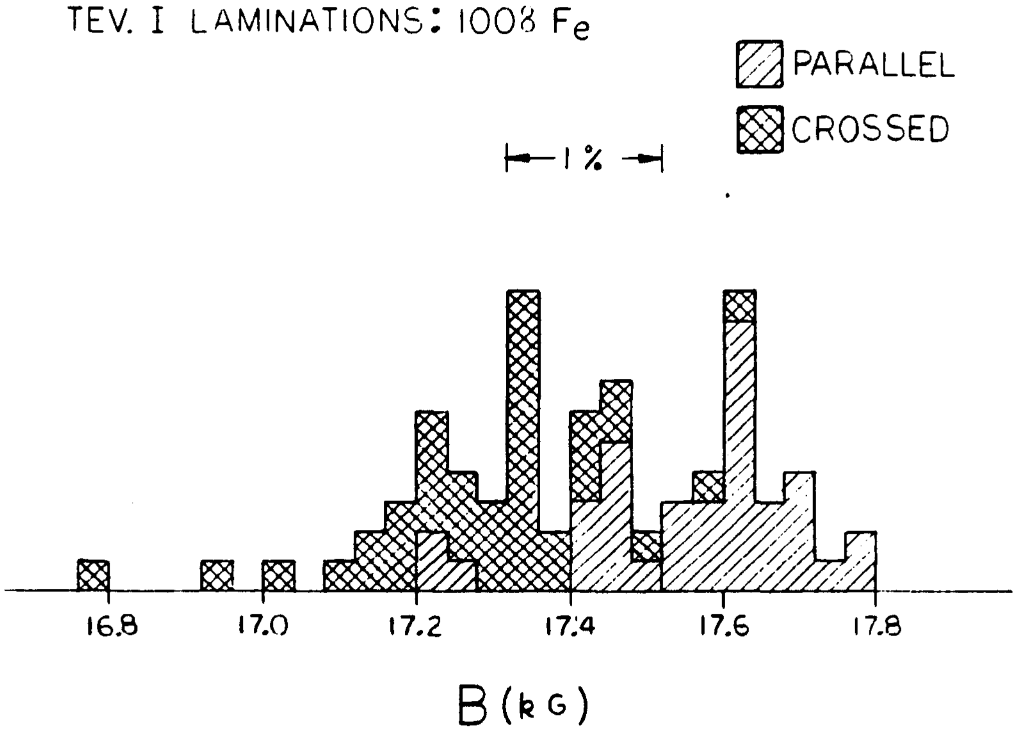

Figure II.3 Distribution of magnetization in Tevatron laminations at H = 80 oersted.

II.4 Error Sensitivities

The sensitivity to various errors are given in Tables II.4, II.5 and II.6. These tables also indicate which source of error is the most important in each case, thus providing guidelines for construction of the magnets. At injection, the errors in B_0 and b_2 are due almost entirely to gap spacing. There are no important errors in b_4 or b_6, but a_1 and a_3 are quite sensitive to conductor misplacement in the vertical direction, as was mentioned earlier.

At storage the error in B_0 is caused by the stacking factor, the error in b_2 by vertical misplacement of the conductors, the error in b_4 by the mismatch between the upper and lower stacking factors, and the error in b_6 by up-down μ-mismatch. a_1 and a_3 are again very sensitive to vertical conductor misplacement.

II.5 Fluctuations in Effective Magnetic Length

Local random fluctuations in B_0 were reported in the previous section. They are of the order of ±0.4 gauss at injection (0.15T) and ±19 gauss at storage (3T).

II.6 Persistent Currents and Remanent Fields

The effect of persistent currents in the superconductors at injection fields was analyzed for NF2C (Ref. 41). They produce a contribution to b_2 of less than 0.26 gauss if the filaments are 25 μm in diameter, or 0.19 gauss for 20 μm diameter. Since this is a systematic contribution, it can be compensated by adjusting the current ratio. The small values are due to the small amount of superconductor, to its large distance from the bore, and to shielding by the iron, which was taken into account in the calculations.

The remanent field for a material with coercive force 2.2 Oe (almost pure iron) is 15 to 17 gauss for NF2C (Ref. 42). A value of 17 gauss was measured for TAC001 with a sextupole content of 0.17 gauss. This is in excellent agreement with prediction. At injection, the remanent b_2 would be 1.1×10^{-4}, which is systematic and can be removed by adjusting the current ratio.

II.7 End Effects

Figure II.4 is a view of the end assembly for WF2C. Calculations of the effects of the ends are currently in progress.

II.8 The WF3CMS Superferric Design

The wide-face, three-current, magnetic-shunt model WF3CMS is the latest superferric design developed at TAC; see Figure II.5. A magnetic shunt 60-mil-thick of steel 1008 has been added next to the main coil, and there is an additional conductor right at the corner formed by the shunt and the pole face. This conductor is used to zero the decapole b_4, and the shunt helps to make the field in the bore more uniform. As an additional effect of the shunt, the field at the main coil becomes smaller, so that more current can be used and higher field values obtained than in previous designs.

The three currents are shown in Figure II.6 as functions of B_o. It is observed that the current in the decapole coil, I_c, is much less than in the main coil. Table II.7 shows the predicted systematic harmonics in the range 0.15 to 3.3T. Except for the last line of the table, all values of b_2 and b_4 will be made almost 0 by iterating the two

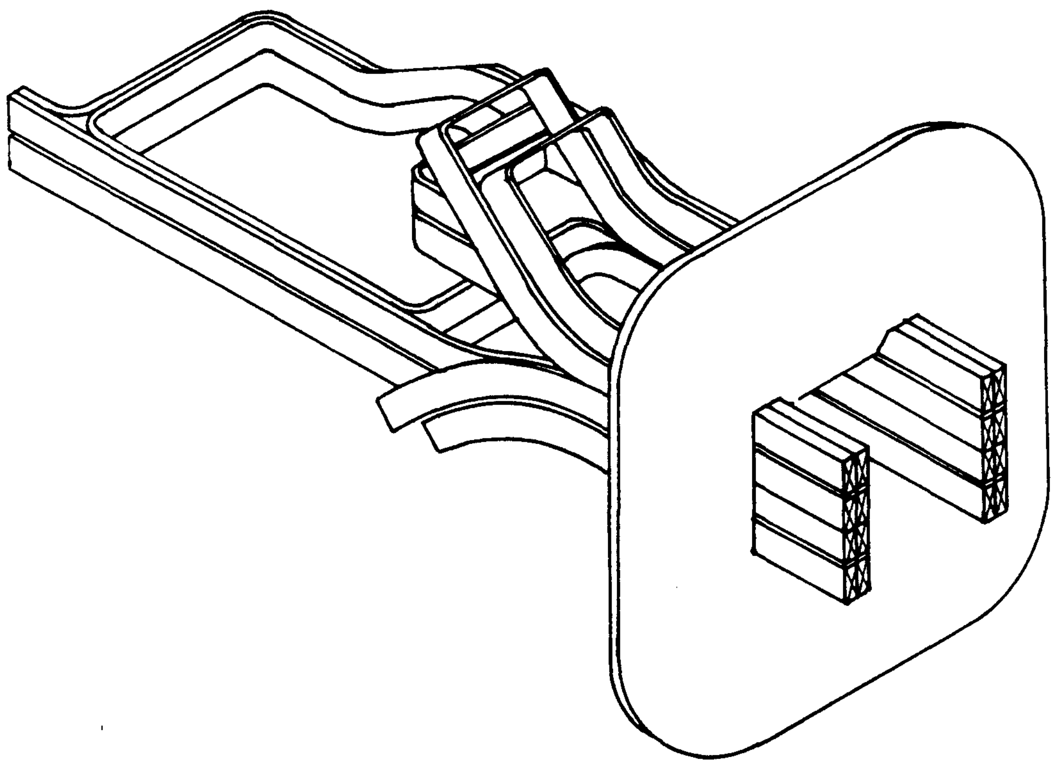

Figure 11.4 End assembly of superferric Design WF2C.

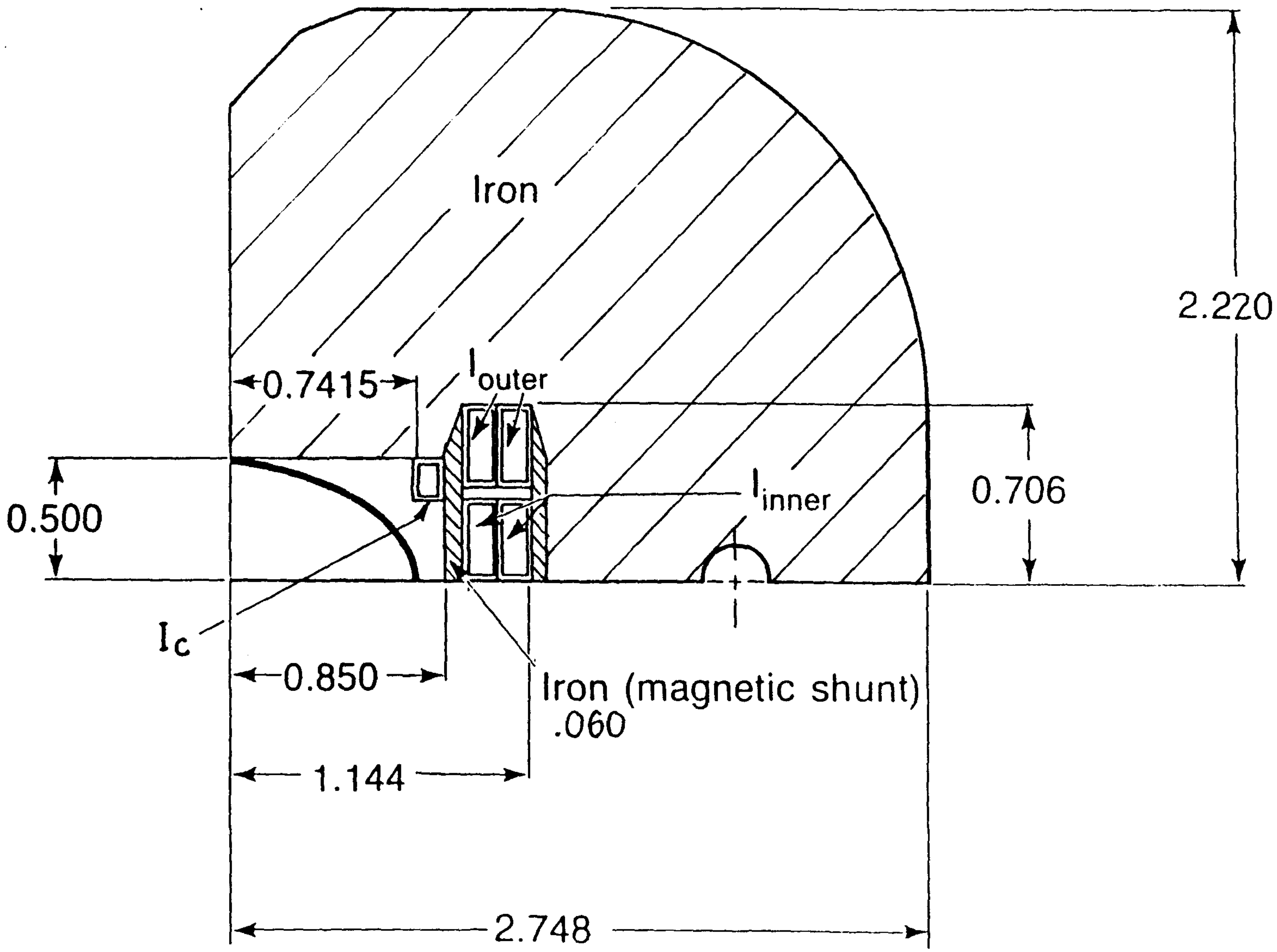

XBL 852-7041

Figure II.5 Quadrant of wide-face, three-current, magnetic-shunt superferric Design WF3CMs.

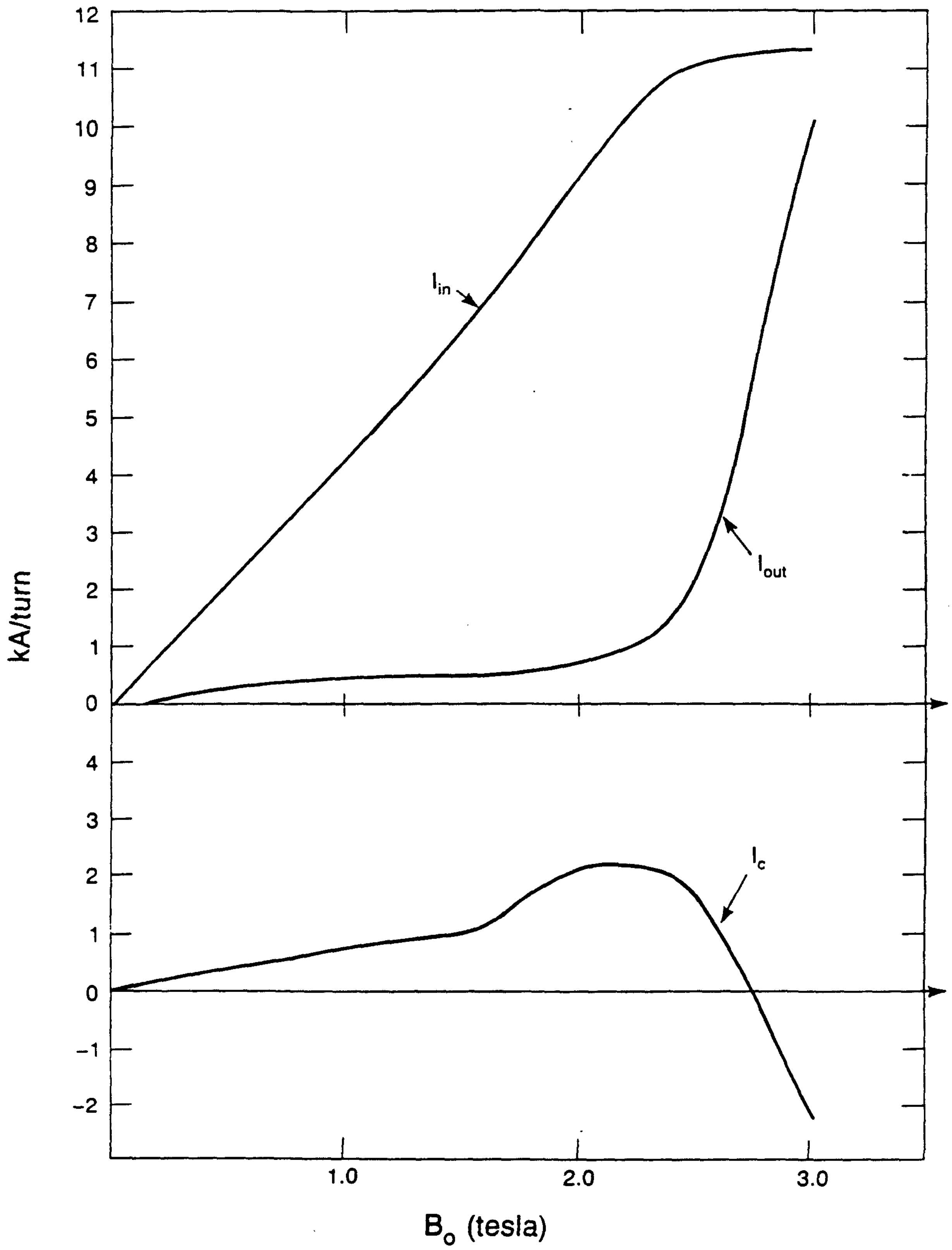

XBL 852-7036

Figure II.6 Variation of the three excitation currents in superferric Design WF3CMS.

current ratios when computer time permits. Additional tuning of the geometry is possible and is expected to produce values of b_6 and b_8 in the range + 1 to -1 x 10^{-4}.

Table II.7
Superferric Design "C" - WF3CMS
Systematic Multipoles as of 2/06/85
At 1 cm Radius

B_o(Tesla)	$b_2 x 10^{-4}$	$b_4 x 10^{-4}$	$b_6 x 10^{-4}$	$b_8 x 10^{-4}$	I_{in}(Amp)	I_{out}(Amp)	I_c(Amp)
0.1518	0.53	-0.07	0.76	0.13	685	0	175
1.0632	-0.43	-0.25	0.59	0.15	4575	425	800
1.6274	-0.72	2.10	1.70	0.31	7200	500	1200
2.4094	-1.12	1.70	1.54	0.25	10900	1450	2000
2.7940	0.42	-0.51	1.87	0.39	11250	6550	-500
2.9840	1.24	-1.90	2.01	0.16	11275	10225	-2400
3.3000	3.42	-15.54	-0.09	0.0	11400	13500	0

It is observed that I_c becomes negative above 2.7T. This is acceptable up to 3T, but above 3T, if I_c were negative, I_{out} would have to be too high, above the critical superconducting value. Thus, it is planned to keep I_{out} at the critical value while decreasing I_c above 3T in order to increase the total field in the gap. This will certainly introduce a sizable decapole b_4 and make the aperture smaller at 3.3T, a situation that might still be acceptable. This explains the presence of the last line in Table II.7.

Another possibility for achieving higher fields would be to put some more superconductor in the main coil.

Calculations of random harmonics for WF3CMS are in progress. The sensitivities to conductors misplacement and current-ratio errors are expected to be smaller than for WF2C because of the shielding effect of the magnetic shunt. Also, the inner conductor has a small current, and it is not likely to cause any serious errors.

The effect of the persistent currents in the main coil of WF3CMS will be even smaller than for WF2C because the field at the main coil is low, even at storage, and because the shunt provides additional shielding. The effect of the persistent currents in the inner conductor remains to be studied, but this is a small conductor and is not expected to cause significant difficulties.

II.9 Two-Mode Scaling Model for Superferric Dipoles

W.A. Wenzel

An approach that takes full advantage of the ubiquitous steel present in all active designs for the SSC dipoles must accommodate the saturation characteristics. With appropriate geometry the magnetic field dependence on excitation current can be described by a particularly simple model (32) whose characteristics can be inferred directly from the B-H dependence for good magnet steel. This is characterized by large permeability ($\mu > 10^3$) at low fields and unit differential permeability about a transition at $B = M \approx 2T$. Then for $B > M$ the field in the aperture is approximately the superposition of a $\mu = \infty$ (ferric) solution, excited at the current which gives $B = M$, and the $\mu = 1$ (super) solution for current in excess of this.

For any given material M sets the scale for B, H and the currents above and below M. The dipole field requires different but readily predictable current distributions corresponding to each of the two modes.

There are topological limitations on the applicability of the model. All parts of the steel boundary, especially the poletip, must saturate at the same excitation, and because B is a vector, effective superposition means that the field shape must be the same in both modes. Because it is impossible to satisfy these conditions exactly, the transition between modes is not infinitely sharp. We have learned from simulation studies, however, that at least one geometry is very forgiving. The results are discussed in Appendix A and summarized below.

We have studied (by POISSON) simulation up to 4.1T several current configurations which produce corrected dipole fields in a 1x2-in^2 rectangular aperture. The ferric mode requires a rectangular coil and the super mode required an equivalent of the well-known cosθ distribution for the non-ferric (or slightly-ferric) designs. Figure II.7a shows one of three configurations discussed in Appendix A. The results are summarized below in Table II.8. Those multipoles identified as "uncorrected" are obtained using only the main windings. Figure II.7b shows that above a transition current (~23kA) the multipoles are linear with current and proportional to each other. The dashed lines, in reasonable agreement with the simulation, are the calculated $\mu = 1$ (super) main-winding contributions to the sextupole and decapole.

These multipoles can be corrected with poleface current elements proportional to each other (see Appendix A) and to the

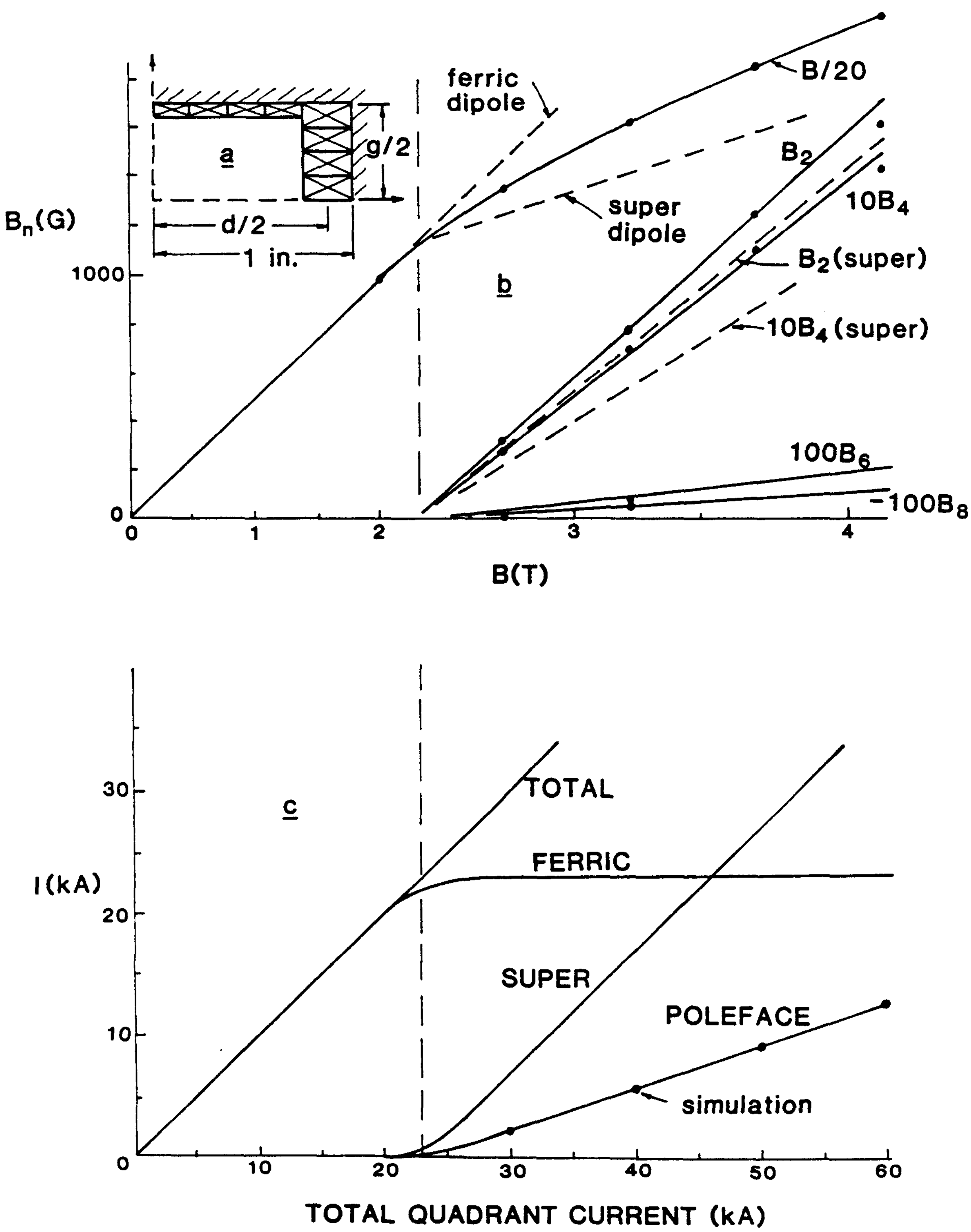

Figure II.7 Two-mode Scaling Model. (a) Quadrant of superferric magnet, (b) linearity of sextupole, decapole, and 14-pole strengths with dipole field, (c) distribution of ferric, super, and poleface currents.

Table II.8

Multipole content for current configuration a (Appendix A, and Figure A1). $b_n = B_n/B_o$. The upper (lower) numbers in each pair refer to the uncorrected (corrected) multipoles. The magnitude of the poleface current is scaled
to eliminate the sextupole at each dipole field. The ratios of poleface current elements are optimized at 2.7T and taken to be constant at all fields. At 60kA the simulated field is too low because the return saturates ($B \geq 2.37T$).

Quadrant Current (kA)	Eff. $\frac{B_o G}{8\pi I}$	Poleface Current (kA)	B_o(G)	$b_2(10^{-4})$	$b_4(10^{-4})$	$b_6(10^{-4})$	$b_8(10^{-4})$
20	0.994	0	19680	6.32	0.41	0.04	0.11
20	0.994	0.077	19674	0	-0.06	0.04	0.11
30	0.912	0	27084	120.08	10.20	-0.03	-0.06
30	0.907	2.253	26910	0	0	-0.03	-0.04
40	0.824	0	32618	239.15	21.47	0.26	-0.18
40	0.815	5.671	32270	0	0.29	0.06	-0.18
50	0.754	0	37299	329.10	29.43	0.37	-0.22
50	0.749	9.393	37063	0	-0.25	0.39	-0.28
60	>0.694	0	>41199	392.19	34.88	0.60	-0.31
60	>0.692	12.561	>41056	0	0.75	0.56	-0.40

main-winding current above transition. Figure II.7c shows the simulation results (from Table II.8) and a conceptual division of total quadrant current into the two modes. For this geometry one-third of the super-mode current is in the poleface windings. Although the main-winding currents for the two modes need not be physically separated, and were not separated in the simulation, doing this has an important advantage. With the independent ferric coil placed far from the center, the field quality at injection can be made relatively insensitive to coil position errors. For a high-field design any systematic sextupole from persistent currents at low fields can be tuned out with a small amount of super current.

Because most of the flux return is not saturated, the incremental dipole field above transition greatly exceeds the prediction for $\mu = 1$ (Figure II.7b). The steel promotes an efficient use of superconductor even for fields well above 4T. A calculation made in Appendix A finds that for the ferric design the superconductor requirements at 5T (7.5T) are at most 2/3 (3/4) those of a comparable non-ferric $\cos\theta$ design. Above transition this enhancement of the dipole field by the return yoke differs quantitatively from the effect on the higher multipoles. The simulation shows that the latter are not strongly affected by images in the fuzzy, receded high-permeability boundary, which would otherwise tend to distort the linearity observed in the super mode.

In Appendix A we have calculated the sensitivity of the dipole field (B_0) and sextupole field (evaluated at r=1cm) to M, which varies with steel characteristics. If we measure only current, then to keep $\Delta b_2 < 10^{-4}$ just above transition (worst case), we need to know M with relative accuracy $\Delta M/M \leq 2.4 \cdot 10^{-3}$. The corresponding uncertainty in B_0 depends on the aspect ratio of the aperture. For $g/d = 0.6$, where g is the vertical gap in the steel and d is the effective horizontal width of the high-field region, $\Delta B/B \leq 0.9 \cdot 10^{-3}$. The uniformity of magnets sharing the same current must be assured by measurement and selection and/or by scrambling the contributions from various steel production runs.

In summary, the two-mode ferric approach has several potential advantages over non-ferric designs: (1) Substantial savings in superconductor are possible at all interesting magnetic fields. (2) The corresponding reduction in stored energy simplifies quench protection. (3) The ferric coil may be located far from the center of minimize the effect of conductor placement errors at low fields. (4) The effects of persistent currents at injection are less because there is less superconductor and because the steel tends to damp the higher multipoles. (5) For rectangular geometry the steel yoke provides a very rigid, strong and inexpensive support for the coils. (6) The unsaturated yoke boundary decouples the fields of two apertures in the same cryostat, so that a rigid two-in-one over-under assembly is feasible.

II.10 Other Matters

Other magnetic-error investigations that are underway but incomplete include the effects of the other bore in a two-in-one configuration and the scaling of magnetic errors with aperture. These results will be reported in a later edition.

III. Cosθ Magnets

III.1 Systematic and Random Errors, Tevatron and CBA Experience

H.E. Fisk

To understand magnet errors in the cosθ magnets we consider separately the systematic and random errors. This section of the report deals with random errors due to conductor placement as well as systematic multipoles that occur for a given design. The cross sections for designs A (4-cm), B (5-cm), and D (4-cm) are shown in Figures III.1, III.2, and III.3.

In the calculation of random errors, the idea is to perturb the ideal location of conductor blocks and calculate the resulting fields. This implies that one must be able to supply both angular ($\Delta\theta$) and radial (Δr) errors to generate the resulting multipole perturbations. Since measurement of the location of conductors inside a magnet is not easily done, the rms widths of multipole moments have been used to determine the $\Delta\theta$'s and Δr's. Thus, the data on existing magnets are used in an attempt to understand errors.

Table III.1 and Figure III.4 give the rms multipole widths for Tevatron (Ref. 1), CBA, and other long magnets at two-thirds of the inner-coil radius. For the CBA magnets two numbers are given for each multipole. They correspond to a total magnet sample that includes some early developmental models and to a slightly smaller subset that includes only the magnets in the "field quality" series, (Ref. 2) in which the magnets were made as much alike as possible.

The Fermilab numbers are derived from the 772 dipoles installed in the Tevatron ring. The a_1 and b_1 are inferred from the shims that were required to off-center the collared coil in the iron, thus inducing quadrupole moments to cancel those built into the coil.

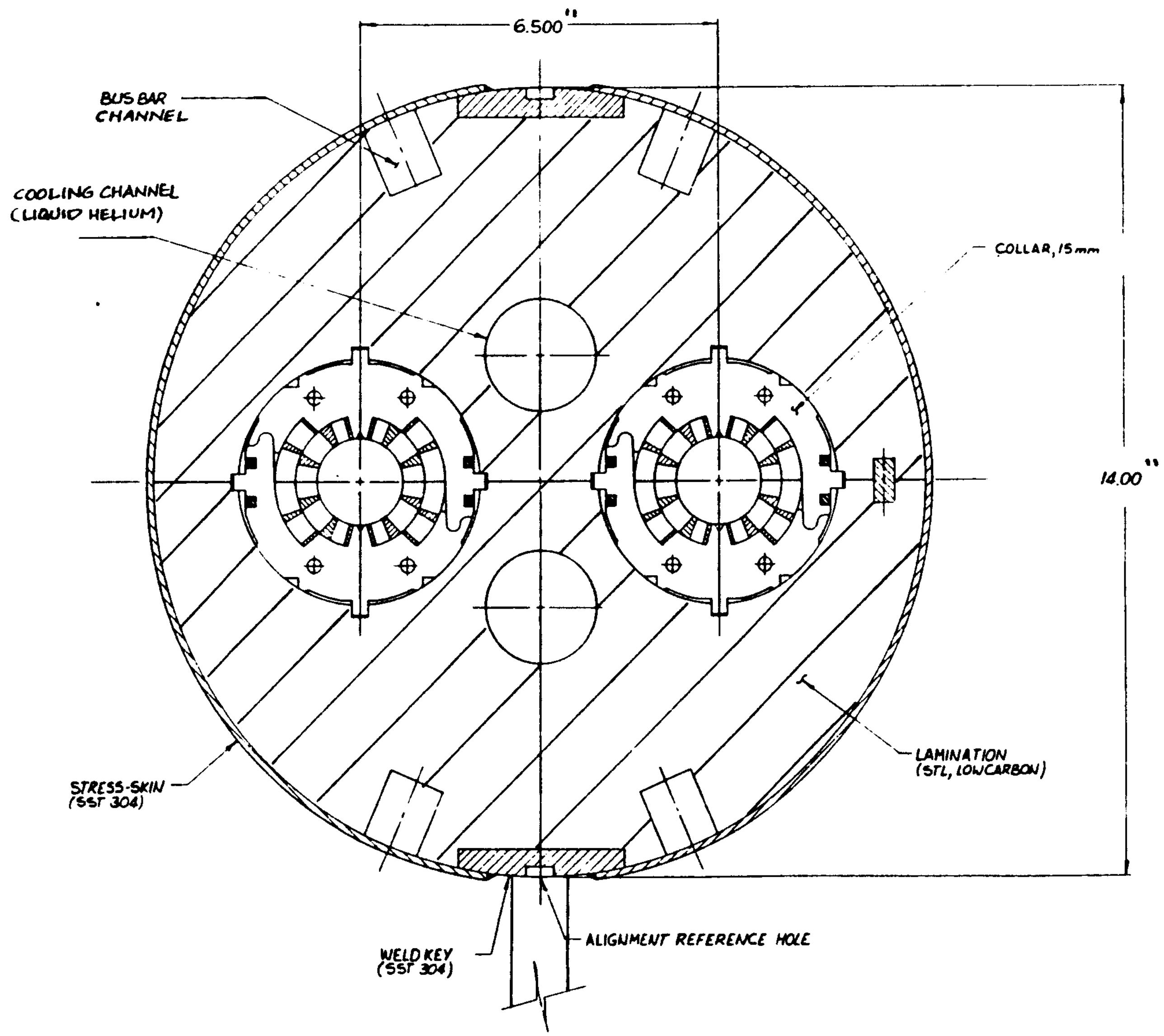

Figure III.1 Cross section of reference Design A, collared version. ID of inner coil is 4 cm.

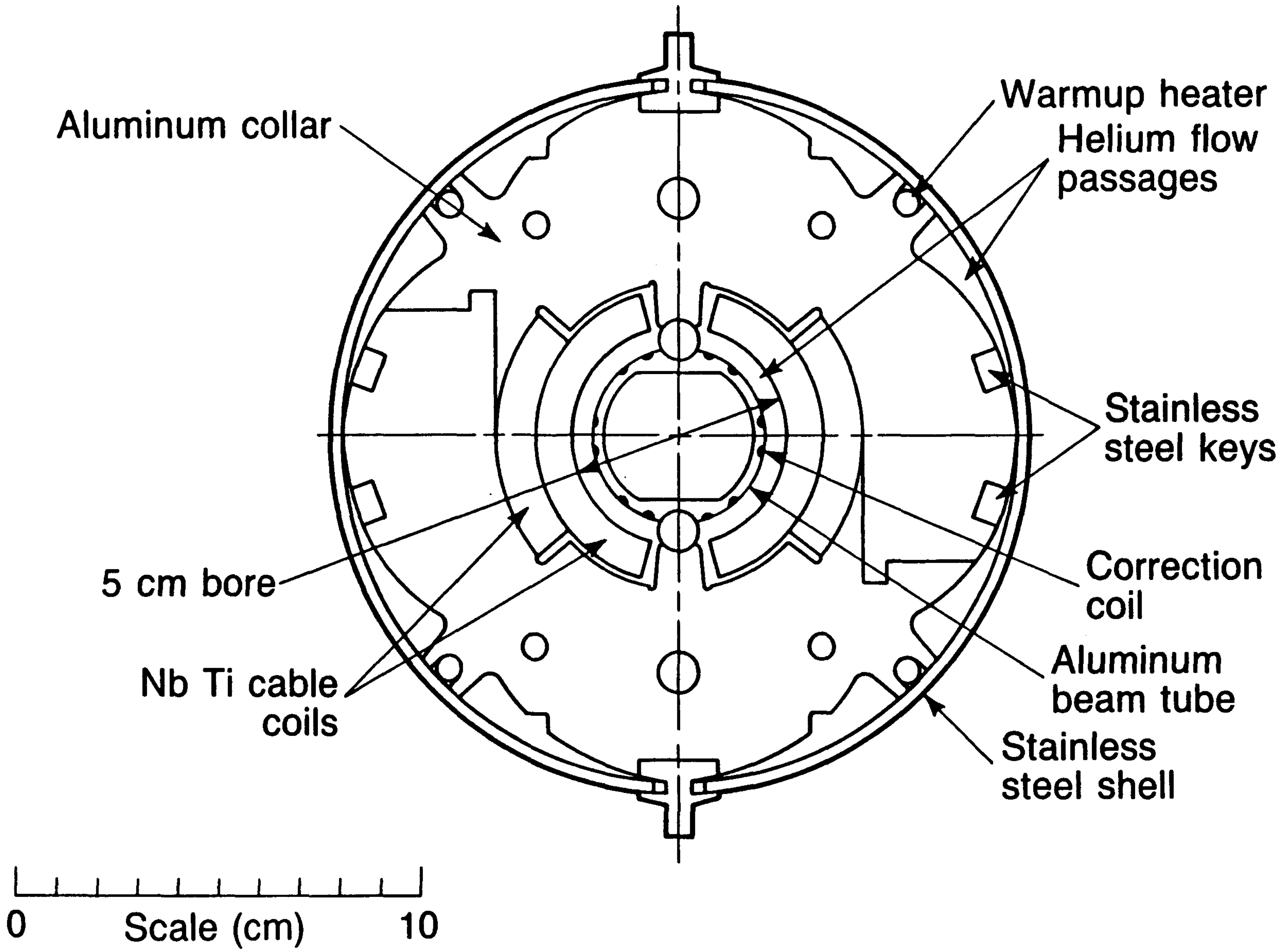

Figure III.2 Cross section of reference Design B.

XBL 852-6952

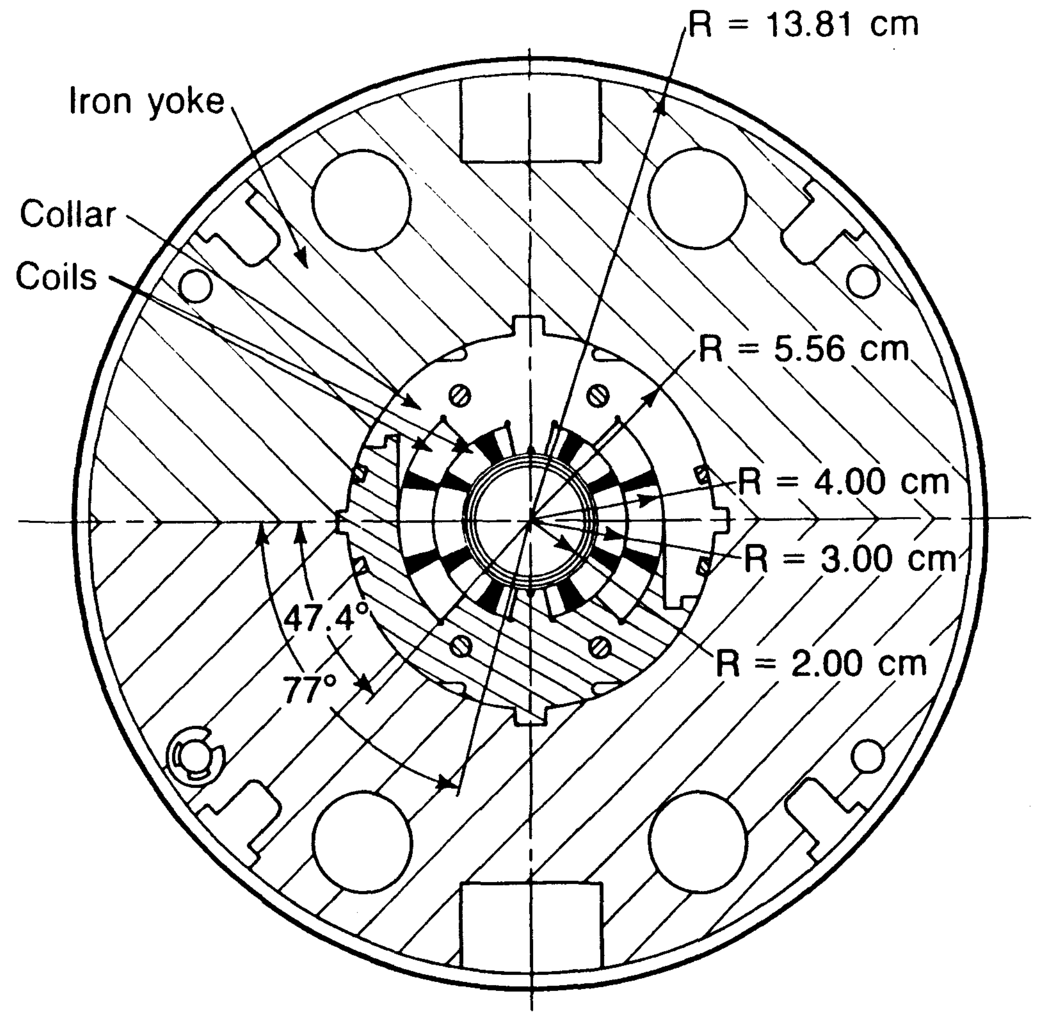

XBL 852-6951

Figure III.3 Cross section of reference Design D(4 cm)

Table III.1
RMS Multipole Widths for High Field Superconducting Dipoles

(in units of 10^{-4} at 2/3 of Inner-Conductor Radius)

	TeV	CBA[a]	HERA I[b]	HERA II[c]	Saclay
Aperture	7.6 cm	13.2 cm	7.6 cm	7.6 cm	10.2 cm
No. of Magnets	>700	15/10	2	4	3
b_1	1.9*	1.0/0.92	2.3	2.2	2.0
a_1	2.9*	2.8/2.64	4.3	2.4	2.9
b_2	3.1(2.5)	2.4/1.89	-1.0	2.2	1.8
a_2	1.2	0.4/0.46	0.3	0.8	0.7
b_3	0.8	0.2/0.23	0.8	1.1	1.2
a_3	1.5	1.3/0.72	0.6	2.5	0.9
b_4	1.3	1.1/1.16	1.4	1.0	1.3
a_4	0.5	0.2/0.18	0.3	0.6	0.9
b_5	0.3	---/0.1	0.4	0.3	---
a_5	0.6	---/0.1	0.8	1.5	---
b_6	0.5	---/0.2	---	---	---
a_6	---	---/0.1	---	---	---
b_8	0.3	---/0.1	---	---	---
b_{10}	0.3	---/0.1	---	---	---

* Inferred from shim data
Key shim dimensions were fixed
a) All CBA magnets/field quality series
b) Published data
c) Private communication

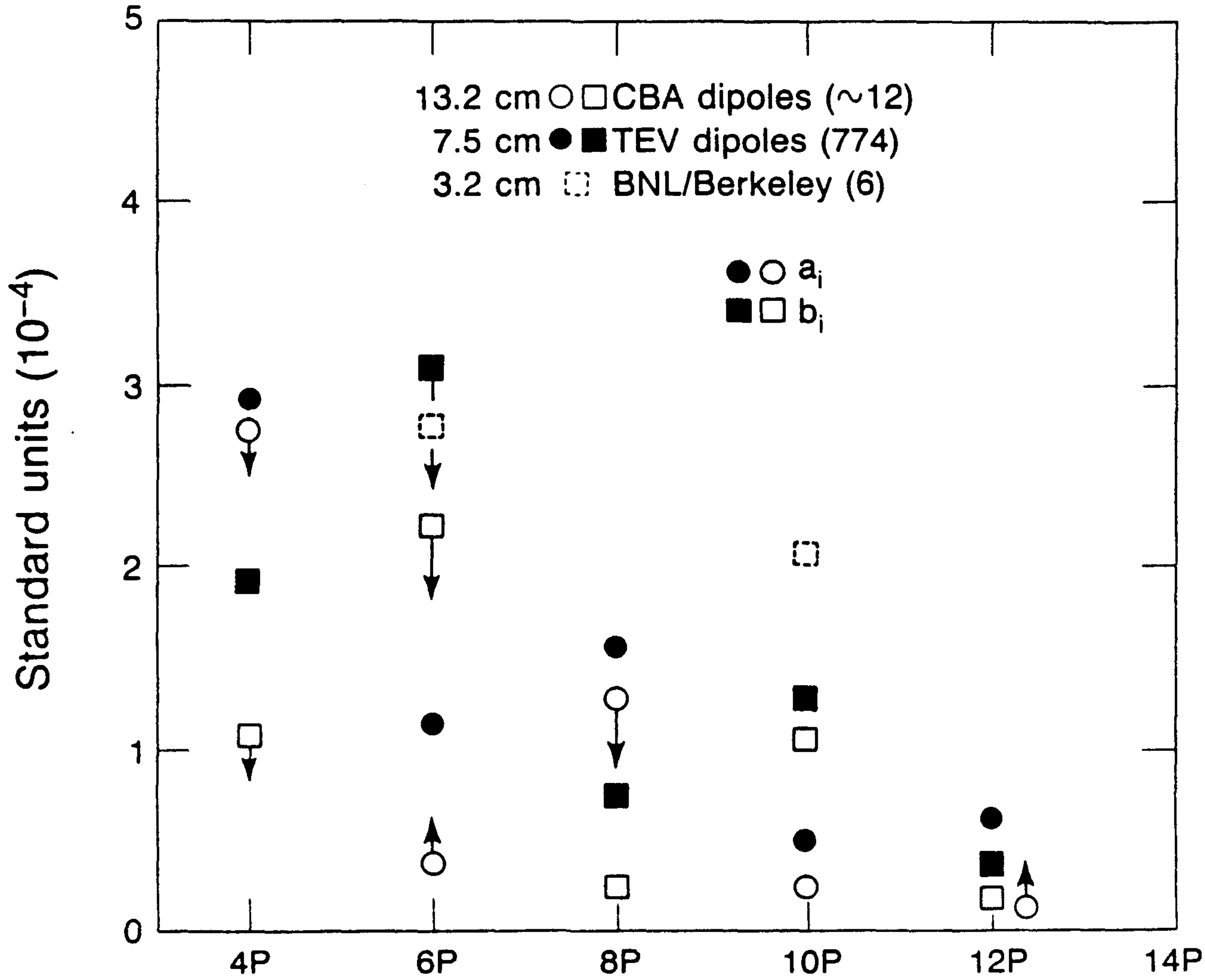

Figure III.4 RMS variation of multipole strengths at 2/3 coil radius in the CBA, Tevatron, and the 3.2-cm BNL/LBL models. The arrows indicate the variations listed in Table III.1.

All moments except normal sextupole, decapole, 14-pole, 18-pole, etc. are forbidden if the magnet obeys dipole symmetry. The measured mean and rms width of the allowed higher-order multipoles for Tevatron and CBA magnets are given in Table III.2.

Table III.2
Allowed Higher Multipoles in the Tevatron
and CBA Dipole Magnets
(at 2/3 the inner-coil radius)

coefficient		Tevatron (Ref 1) design	mean ± rms width	CBA (Ref 3) mean ± rms width
b_4	(Decapole)	1.0	-0.57 ± 1.32(x 10^{-4})	3.28 ± 1.16 (x 10^{-4})
b_6	(14-Pole)	4.4	5.48 ± 0.54	0.36 ± 0.22
b_8	(18-Pole)	-12.1	-12.52 ± 0.33	-0.27 ± 0.13
b_{10}	(22-Pole)	3.6	3.70 ± 0.26	0.12 ± 0.10

For the CBA magnets the 18- and 22-pole results in the table come from only four magnets. The non-zero values of the 14-, 18-, and 22-pole moments for the Tevatron dipole follow from the two-shell design without wedges. On the other hand, the CBA design with wedges gives small 14-, 18-, and 22-pole strengths. Two CBA prototypes iterated from the field-quality magnets had decapole coefficients within 1 unit of the design value.

In addition to the Tevatron and CBA magnets discussed above, several magnets with essentially the same cable and manufacturing techniques but with 3.2 cm ID have been successfully tested. The four 4.5m two-in-one magnets were made at BNL as part of the early SSC R&D effort (Ref. 35). The field shape data from these magnets, although limited to eight bores, is of interest because it bears on the question of whether the Tevatron and CBA manufacturing techniques can be extrapolated a factor of two from the Tevatron (four from CBA) to a diameter where the two-layer coil thickness and the inner radius are the same. For the allowed harmonics (b_2, b_4, b_6) the results are encouraging. The rms sextupole width was 2.8 units at 1 cm, comparable to the Tevatron and CBA results (Fig. III.4). Results for the sextupole are particularly interesting because this harmonic is one of the two largest contributors to rms variations in the CBA and Tevatron magnets. The decapole and 14-pole rms widths, 2.1 and 0.5 units respectively, are less than a factor of two worse than those from the larger diameter magnets. Most of the unallowed multipoles measured in the two bores of the fourth magnet were less than 0.5 units. (For the first three magnets, feeddown from the unusually large allowed harmonics limited the accuracy of the measurements.) The unallowed multipoles in the first two 4.5-meter Design D(4 cm) dipoles also are small (Ref. 30). These results support the idea, discussed below, that some scaling in errors can be expected down to the 4-cm and 5-cm diameters discussed for the SSC.

III.2 Predictions for SSC Dipoles

H.E. Fisk

Three different schemes have been used to calculate the random widths of multipole strengths expected for SSC cosθ magnets. All three schemes assume the dominant errors are those associated with conductor placement. The three schemes will be referred to as Fisk, Herrera, and Meuser. All the methods have different limitations, but the results are in reasonable agreement. The Fisk calculation, which assumes only azimuthal errors and has two parameters, probably underestimates the complexity of conductor motion, while the schemes of Herrera and Meuser permit a large number of conductor motions and give each a weight that is consistent with the Tevatron and CBA multipole data.

III.3 Fisk Method

H.E. Fisk

The Fisk method for finding rms multipole widths involves calculating the change in the $i^{\underline{th}}$ multipole field ΔB_{ij} due to a small change in azimuthal position, $\Delta\Theta_j$, of the $j^{\underline{th}}$ conductor block (Ref. 4). For conductor blocks that are in physical contact the correlations in angular position are taken into account. Two basic parameters δ and η are used. See Figure III.5a. The δ parameter refers to azimuthal coil-size mis-matching and η describes the angular difference between a half-coil's geometric center (as built) and its current-density center. Of the two parameters δ is the larger, about 1.1 to 1.4 mrad (normalized to about 20 cable thicknesses) for Tevatron magnets, with η being about half as big (Ref. 5). Multipoles for Tevatron quadrupoles are well described by this technique of calculating moments, as indicated in Table III.3a. The dipole-magnet moments are less well characterized, as shown in Table III.3b. In particular the normal and skew quadrupole and octupole moments are well described while the measured skew and normal sextupole moments are larger and smaller, respectively, than the calculated values.

Since the basic idea of accounting for rms multipole widths with azimuthal angular errors works reasonably well, we assume that both η and δ scale with inner conductor radius and that one can then calculate

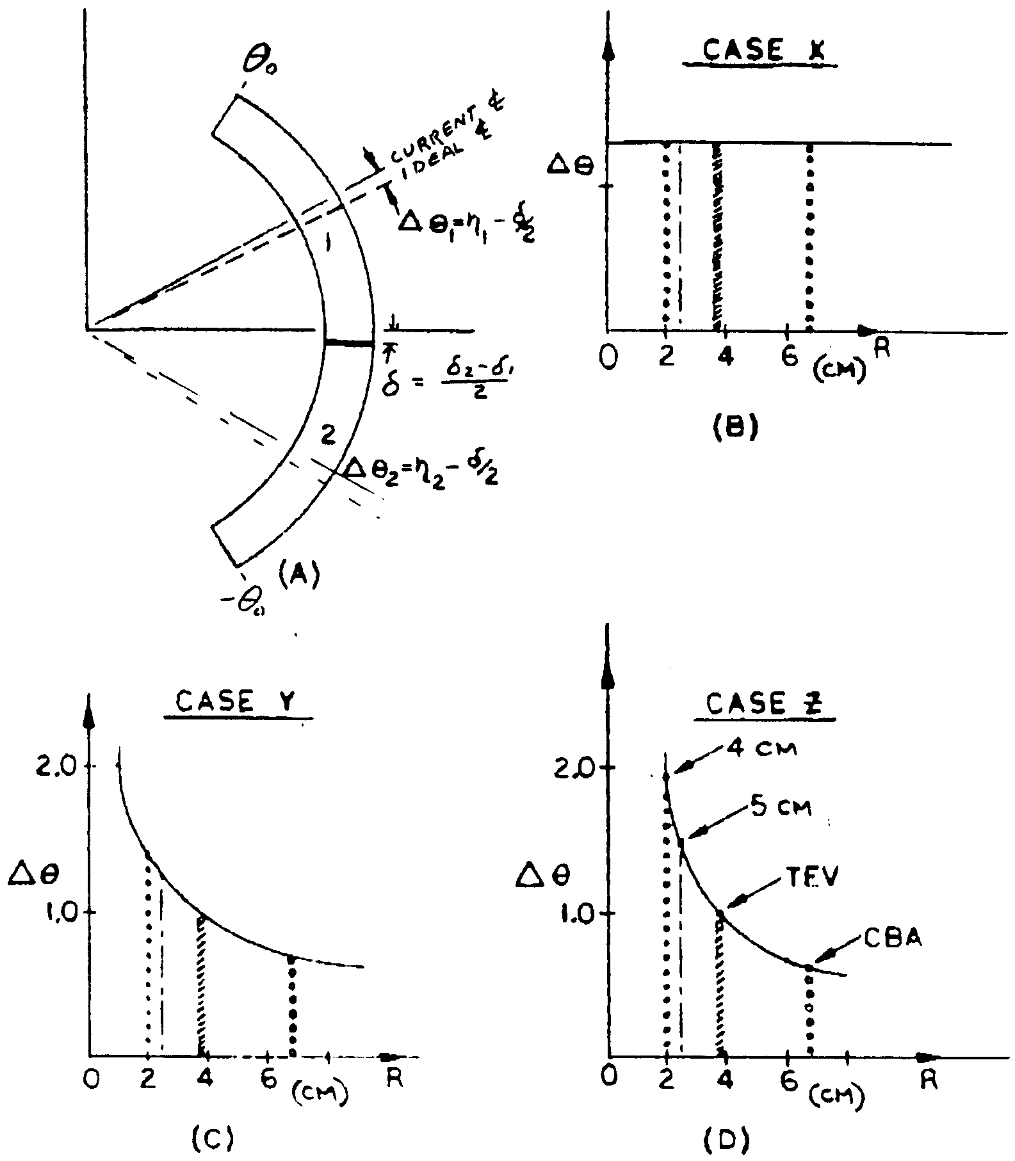

Figure III.5 Fisk model of magnet placement errors. (A) Diagram of model. δ is error in azimuthal width of coil 1 as built; η_1 is difference between geometrical center and current center of coil 1 as built. (B) Effect of scaling hypotheses X, (C) effect of hypothesis Y, (D) effect of hypothesis Z.

Table III.3
Fit of Fisk Model to Tevatron Data

III.3a RMS Moments for Tevatron Quadrupoles.
Units are 10^{-4} at 2/3 inner coil radius.

Multipole Coef.	Measured	Calculated
a_2	3.4	3.6*
b_2	3.7	3.6*
a_3	2.1	2.1 (fitted)
b_3	0.9	0.9 (fitted)
a_4	0.80	0.57*
b_4	0.74	0.57*

*Calculated using the fitted values of η = 0.44 mr and δ = 0.87 mr (coil matching).

III.3b RMS Moments for Tevatron Dipoles

	Measured	Calculated**
a_1	2.9	2.9
b_1	1.9	2.3
a_2	1.2	1.7
b_2	~2.5	1.5
a_3	1.46	1.35
b_3	0.77	0.56

**Calculated using η = 0.60 mr and δ = 2.20 mr (coil matching).

multipole widths at a new coil radius with a simple scaling law. This then permits one to scale from CBA and Tevatron magnets to those with smaller aperture if a scaling law is postulated. Three possible hypotheses have been investigated. We will call them, X, Y and Z. Case X (Fig. III.5b) assumes the azimuthal distance errors Δs are proportional to N, the number of cables. This results in angular errors that are independent of coil radius and further implies that the multipoles at 2/3 the inner-conductor radius are the same for CBA, Fermilab, and any magnet with smaller conductor radii. This hypothesis is somewhat inconsistent with the CBA and Fermilab data and is also inconsistent with the Tevatron quadrupole and dipole magnet data, where the azimuthal sizes are different.

For Case Y (Fig. III.5c) we let the azimuthal distance error Δs be proportional to $\sqrt{N}$, where N is the number of cables. Since $N = R\theta/T$, where R, θ, and T are, respectively, the conductor radius, angular extent, and cable thickness, the angular azimuthal error goes like $1/\sqrt{R}$. If the CBA data are scaled with this hypothesis, they give reasonable agreement with the measured Tevatron multipoles. Also the Tevatron quadrupole and dipole data, which have different numbers of turns in their windings, give azimuthal angular errors that are reasonably consistent with the $\sqrt{N}$ scaling. This comparison has been published in the Proceedings of the Snowmass Conference (Ref. 36).

For case Z we assume the Δs errors are fixed and independent of the number of cables. Since $\Delta\theta = \Delta s/R$, this case assumes angular errors that go like $1/R$. An extrapolation of the CBA data to the Fermilab radius would imply Tevatron moments that are 1.8 times those of CBA. This seems to be inconsistent with these data, although one might expect fixed minimum distance errors to play the major role in random multipole errors when Δs is reduced to a level of around 1 mil. The Tevatron angular errors of 1.1 to 2.3 mr when multiplied by 1", the inner conductor radius for design B, give Δs errors of 1 to 2 mils.

The predictions for 4- and 5-cm aperture magnets, based on case Y, the $1/\sqrt{R}$ scaling, are given in Table III.4. The estimates are generated by scaling the measured Tevatron and CBA moment widths at two-thirds the inner-conductor radius by $1/\sqrt{R}$ and then averaging the two extrapolated numbers. The predictions are reported at reference radii of two-thirds the inner conductor radius and 1 cm. The +/- values indicate the difference between the two extrapolated numbers and their average. One would obtain predicted multipoles that are significantly larger if the scaling law of 1/R were assumed for angular errors.

Table III.4
RMS Variation of Multipole Strengths* for
4-cm and 5-cm SSC Dipoles Scaled from
CBA and Tevatron Data by the Fisk Method

	4-cm Magnets [Designs A and D]		5 cm Magnets [Design B]	
	at 2/3 Rad	at 1 cm	at 2/3 Rad	at 1 cm
b_1	2.14 ± .46	1.61 ± .35	1.92 ± .42	1.15 ± .25
a_1	4.40 ± .40	3.31 ± .30	3.94 ± .35	2.36 ± .21
b_2	3.44 ± .35	1.94 ± .20	3.08 ± .31	1.10 ± .11
a_2	1.25 ± .41	0.71 ± .23	1.12 ± .37	0.40 ± .13
b_3	0.76 ± .34	0.32 ± .14	0.68 ± .31	0.15 ± .07
a_3	1.69 ± .38	0.72 ± .16	1.51 ± .33	0.32 ± .07
b_4	1.95 ± .16	0.62 ± .05	1.74 ± .14	0.22 ± .02
a_4	0.51 ± .18	0.16 ± .06	0.46 ± .16	0.06 ± .02
b_5	0.30 ± .12	0.07 ± .03	0.26 ± .10	0.02 ± .01
a_5	0.50 ± .32	0.12 ± .08	0.45 ± .29	0.035 ± .02

2/3 radius = 1.33 cm

2/3 radius = 1.67 cm

* The +/- in this table refer to the variations in extrapolated numbers that result from scaling the CBA and Tevatron data. An additional uncertainty of +50 percent of the rms widths should be assigned due to the uncertainty in the choice of model used to make the extrapolation.

III.4 Meuser Method

R.B. Meuser

The purpose of this study was three-fold: To attempt to understand the observed magnetic-field errors for some existing magnet systems in terms of the mechanical errors that produced the field errors; to use those results to predict the mechanical errors and corresponding field errors for the cosine-theta SSC dipole designs; and after a design is selected, to provide a basis for establishing manufacturing tolerances.

Thirty random mechanical-error modes that affect the positions of the coil boundaries, and which correspond directly to manufacturing specifications or dimensions of parts that can be easily measured, were identified. In addition, the effect of turn-to-turn variation in conductor width was considered. Of these thirty one, sixteen modes were selected for this study. Those modes are described in Table III.5 and illustrated in Figure III.6. The multipole sensitivities of SSC Magnet designs A and D(4 cm) to the different mechanical error modes are shown in Figure III.7, and those of design B in Figure III.8.

For both the CBA and Tevatron dipole magnets, reasonable values were assigned to the various error modes, and the corresponding field errors were evaluated. Then the mechanical errors were adjusted by trial and error to obtain a better correspondence between the calculated and measured field aberrations. The normal-dipole component was not included in this comparison, as it seemed reasonable that a major part of that was not the result of cross-section dimension variations but was instead simply the result of variation in the lengths of the magnets. The fitted mechanical errors are presented in Table III.6 and the corresponding field aberrations in Table III.7.

Table III.5
Description of Selected Error Modes

Mode No.		No. of Occurrences
1	Position of any one edge of either pole piece varies, inner coil.	4
2	As Mode 1 except outer coil.	4
3	Position of center line of either pole piece varies, both inner and outer coils.	2
4	Widths of both pole pieces vary collectively, inner coil.	1
5	As Mode 4 except outer coil.	1
6	Coil azimuthal width varies, top to bottom, both sides collectively, inner coil.	1
7	As Mode 6 except outer coil.	
8	Coil azimuthal width varies, side to side, either top or bottom half, inner coil.	2
9	As Mode 8 except outer coil.	2
10	Thickness of inner coil varies, both sides of top or bottom coil half in same sense.	2
11	Thickness of inner coil varies side to side, either top or bottom coil half.	2
12	As Mode 10 except outer coil.	2
13	As Mode 11 except outer coil.	2
14	Thickness of inter-layer insulation varies, any one quadrant.	4
15	Thickness of coil-to-iron insulation varies, any one quadrant.	4
16	Azimuthal width of conductor varies from turn to turn.	-

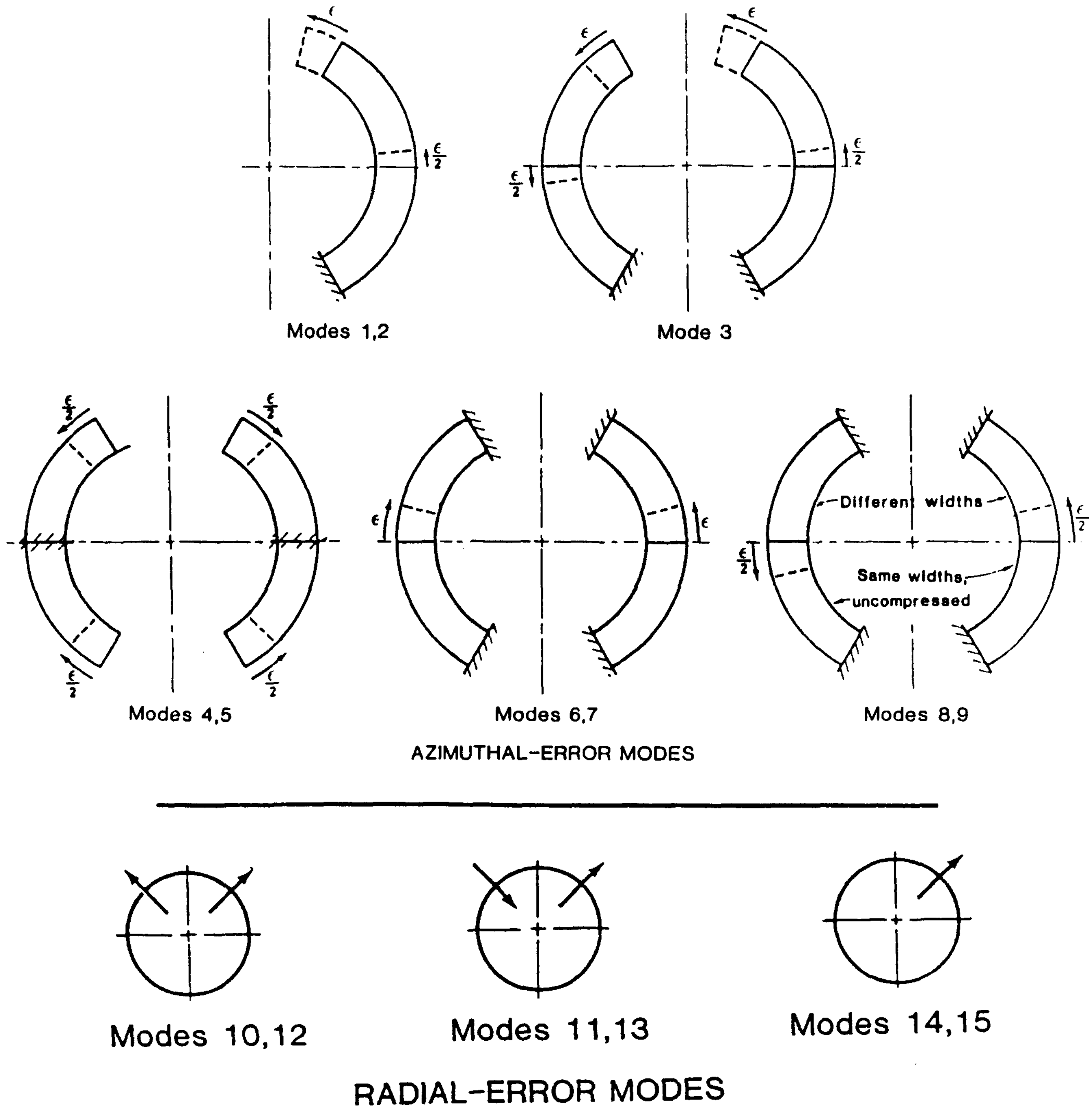

Figure III.6 Mechanical-error modes used by Meuser.

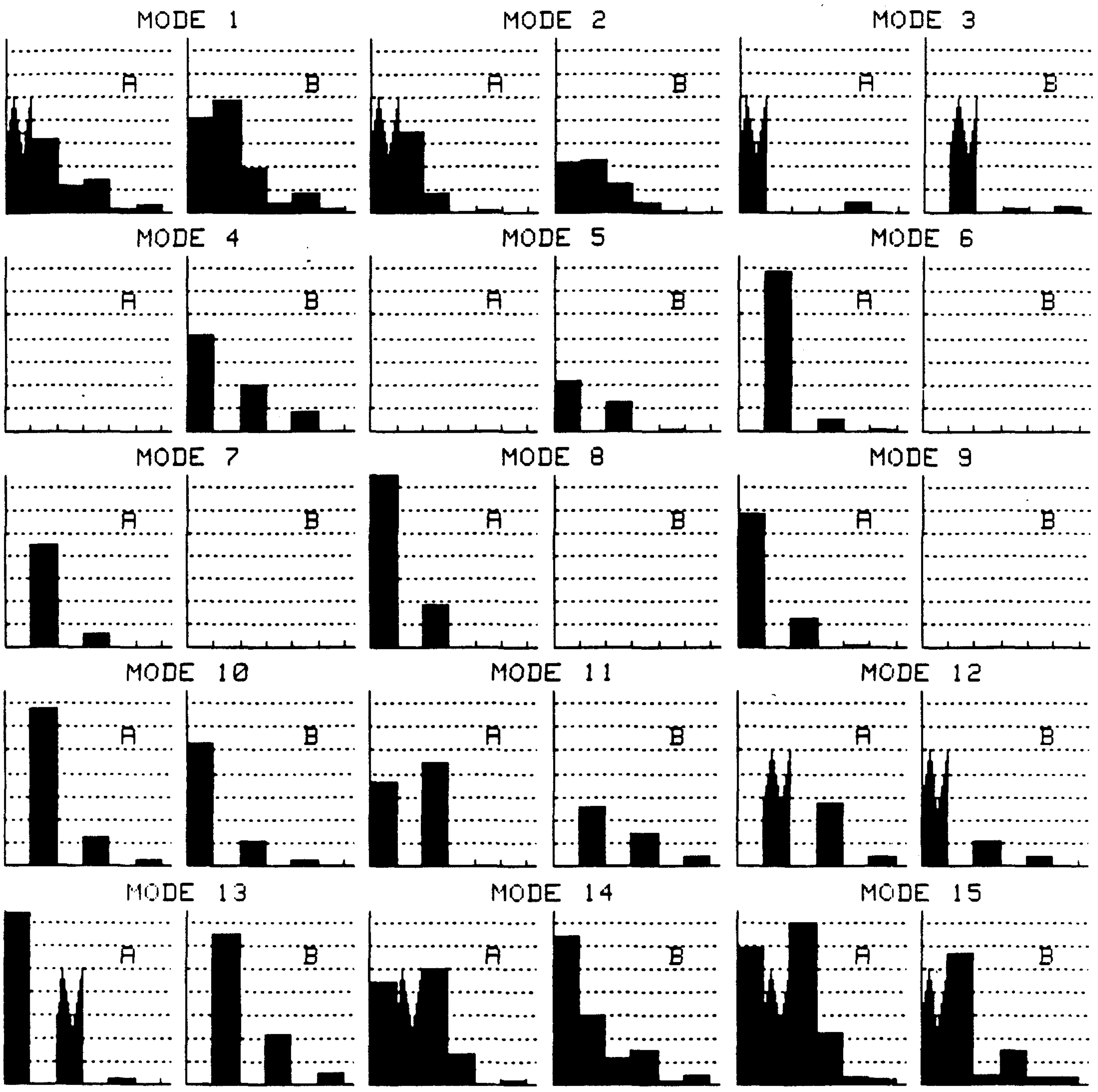

Figure III.7 Sensitivity of Designs A and D(4 cm) to the various error modes. Each division in the vertical scale represents a multipole strength at 1.33 cm of 1×10^{-4} of the dipole field per 0.1 mm of mechanical error. From left to right the columns represent dipole, quadrupole, sextupole, etc. "A" labels the skew components and "B" the normal components. Jagged barrs represent off-scale sensitivities (greater than 7.5×10^{-4} per 0.1 mm.

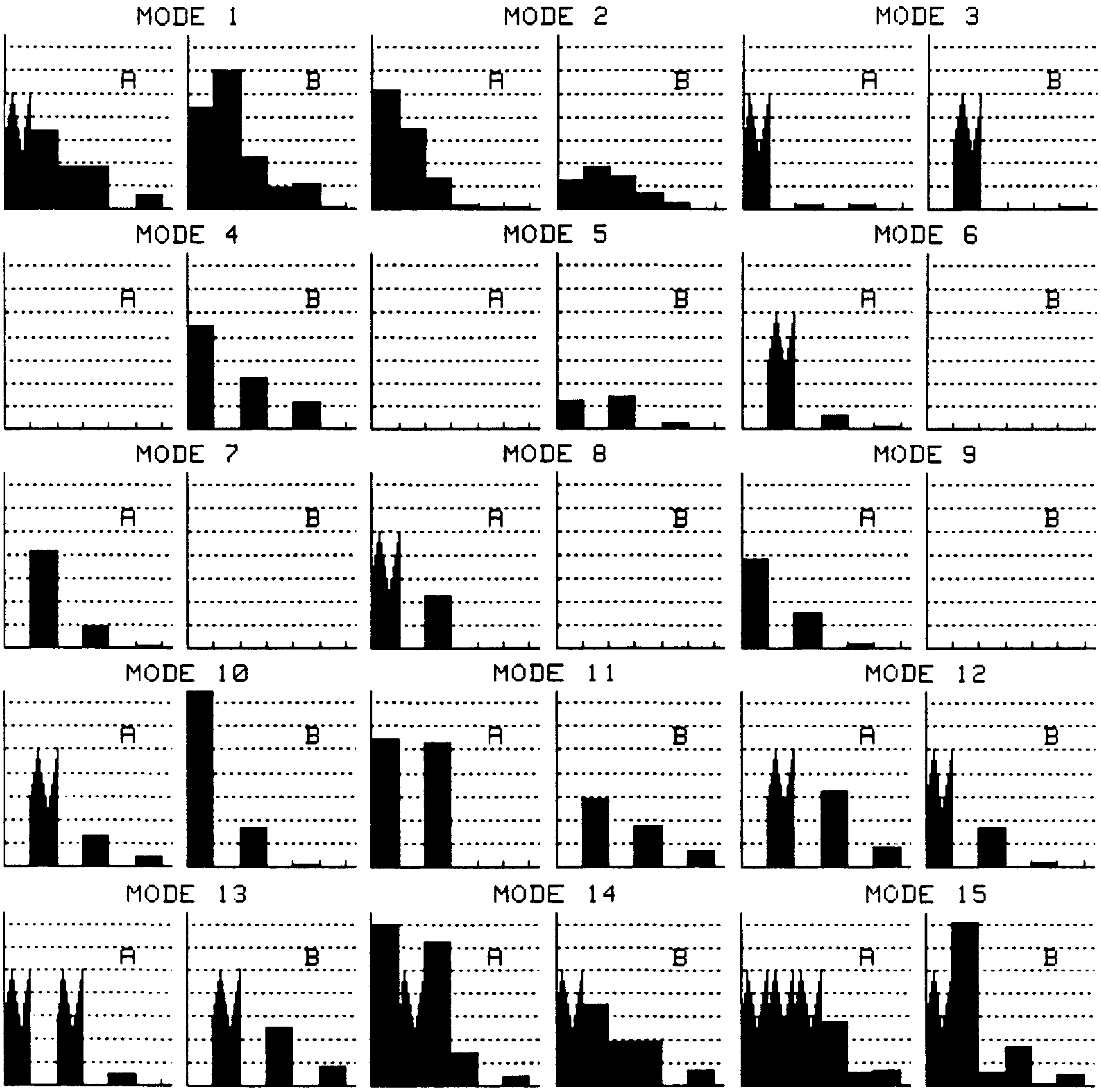

Figure III.8 Sensitivity of Design B to the various error modes. Each division in the vertical scale represents a multipole strength at 1.67 cm of 1×10^{-4} of the dipole field per 0.1 mm of mechanical error. From left to right the columns represent dipole, quadrupole, sextupole, etc. "A" labels the skew components and "B" the normal components. Jagged bars represent off-scale sensitivities (greater than 7.5×10^{-4} per 0.1 mm).

Table III.6
RMS Variation of Mechanical Errors in CBA and Tevatron Magnets
According to the Meuser Model (milli-inches)

Error Mode	Fitted Errors		Scaling Factors Based on Error $\propto \overline{r}^{0.3}$ Where $\overline{r} = r_1+0.2(r_2-r_1)$		
	CBA	Tevatron	From	To	Factor
1	0.95	1.77	CBA	Des A/D(4cm)	0.729
2	0.95	1.77	CBA	Des B	0.778
3	0.45	0.69	CBA	Des D(5cm)	0.772
4	6.55	4.54	TeV	Des A/D(4cm)	0.849
5	6.55	4.54	TeV	Des B	0.905
6	2.70	0.16	TeV	Des D(5cm)	0.899
7	2.70	0.16			
8	1.40	0.04			
9	1.40	0.04			
10	0.10	0.61			
11	0.20	0.06			
12	0.10	0.61			
13	0.20	0.06			
14	0.28	0.07			
15	0.17	0.09			
16	0.01	0.30			

Table III.7
The fit of the Meuser model to CBA and Tevatron Data
and the projected random multipole strengths for SSC Magnet Designs.
Units are 10^{-4} of the dipole component

No. of Poles	a (Real, Skew) Measured	Calculated	Difference	b (Imaginary, Non-skew) Measured	Calculated	Difference
CBA Dipole Magnets (Coefficients are normalized at 2/3 of the coil inside radius.)						
2		2.16			3.68	
4	2.64	2.91	.27	.92	.87	-.04
6	.46	.61	.15	1.89	2.04	.15
8	.72	.58	-.14	.23	.21	-.02
10	.18	.10	-.08	1.16	.79	-.37
12		.12			.034	
14	.11	.049	-.06	.22	.30	.08

RMS difference between measured and calculated coefficients is 0.17.
Maximum difference is 0.37.

No. of Poles	a (Real, Skew) Measured	Calculated	Difference	b (Imaginary, Non-skew) Measured	Calculated	Difference
Tevatron Dipole Magnets (Coefficients are normalized at 2/3 of the coil inside radius.)						
2		4.3			4.6	
4	2.9	2.9	0	1.9	2.2	.3
6	1.2	1.2	0	2.5	2.4	-.1
8	1.5	.9	-.6	.8	.6	-.2
10	.5	.3	-.2	1.3	1.2	-.1
12	.6	.3	-.3	.3	.2	-.1

RMS difference between measured and calculated coefficients is 0.26.
Maximum difference is 0.61.

SSC Dipole Magnets
(Coefficients are normalized at a radius of 10 mm.)

No. of Poles 2(n+1)	Design A/D(4cm) a_n	Design A/D(4cm) b_n	Design B a_n	Design B b_n	Design D(5cm) a_n	Design D(5cm) b_n
2	5.2	5.7	5.1	6.1	4.8	5.2
4	3.2	1.7	2.9	1.7	2.4	1.25
6	0.48	1.6	0.44	1.2	0.30	1.00
8	0.54	0.21	0.34	0.16	0.27	0.11
10	0.11	0.48	0.059	0.25	0.048	0.19
12	0.083	0.052	0.022	0.020	0.028	0.017
14	0.026	0.040	0.008	0.016	0.005	0.011
16	0.012	0.009	0.003	0.002	0.003	0.002
18	0.004	0.003	0.001	0.001	0.001	0.001
20	0.001	0.002	0	0	0	0

The correspondence between the final calculated and measured aberrations was within 0.17 unit rms for the CBA magnets and 0.26 unit rms for the Tevatron magnets. Without doubt the correspondence could be improved by additional empirical juggling of the mechanical errors, and by consideration of additional error modes. It is to be noted, however, that even a perfect correspondence between calculated and measured performances would not be proof that the mechanical errors had been assigned the correct values; several substantially different sets of errors could, conceivably, give equally good correspondence, and any correspondence could be entirely fortuitous.

These mechanical errors were used to predict field aberrations for the SSC magnets. However, since the SSC magnets are smaller in cross section than either the CBA or the Tevatron magnets, some reduction in the magnitude of the errors seemed appropriate; but a reduction in proportion to the magnet inner radius, for example, seemed too optimistic. It was estimated that the mechanical errors scaled as the 0.3 power of the effective coil radius, giving a 20 percent reduction in errors for a 50 percent reduction in radius. The effective coil radius was taken as the radius to a point 20 percent through the thickness of the coil from the inside, a value that has proved to give reasonably good results. The manufacturing errors were scaled from the CBA and Tevatron magnets to each of the SSC designs, and the corresponding field aberrations evaluated and averaged. The results are presented in Tables III.6 and III.7.

Referring to the projected multipole strengths for the SSC magnets in Table III.7 we note that Design B is only slightly better than Design D(4 cm) despite its larger coil inside diameter. Also, Design D(5 cm), having the same coil inside diameter as Design B, has a considerably higher field quality. This is evidently a consequence of Design B being an air-core design, whereas the others are iron-core designs. The iron simply increases the lower order multipole components, including the dipole component, more than it does the higher-order components.

III.5 Herrera Model

J.C. Herrera and P.J. Wanderer

A model of random errors in cosine theta magnets has been developed by Herrera et al and is described in detail in Ref. 8. In this report a brief summary of the method and the relevant results are presented. The model follows earlier work by Herrera (6, 7) in calculating the effect of random errors in the azimuthal and radial size and position of the blocks. (In this respect it is similar to Meuser's model.) The model calculates the random errors in accord with the basic symmetries of the dipole magnet. Thus for random errors in coil block position that preserve dipole symmetry, the rms variation in b2, b4, and b6 are calculated. For this four-fold symmetry-maintaining case, the inner and outer coils are given different angular variations. (This was found necessary in order to fit the rms variation in b4.) Next, the top-bottom symmetry of the coil was broken, producing a1, a3, and a5. Finally, the left-right symmetry of the coil was violated, yielding the other multipoles. The model reproduces the zig-zag pattern in the rms variation in the CBA and Tevatron harmonics, where the odd-n skew multipoles (such as the quadrupole) are larger than the corresponding normal terms, with the reverse pattern for the even-n multipoles (e.g., Fig. III.4). As an indication of the level of uncertainty in the predictions, Table III.8 presents the predictions for magnet design A/D(4 cm) based on separate fits to CBA and Tevatron data. It can be seen that the two sets of predictions are quite close to one another.

Table III.8
Predictions of RMS Multipole Variations in SSC Magnet Designs A and D(4 cm) according to Herrera model based on fits to CBA data and to Tevatron data. Units are 10^{-4} at 1 cm.

	Based on Fit to CBA	Based on Fit to Tevatron	Avg		Based on Fit to CBA	Based on Fit to Tevatron	Avg
a_0	2.1	1.5	1.8 ± .3	b_0	6.4	5.5	6.0 ± .5
a_1	3.3	3.7	3.5 ± .2	b_1	1.8	1.3	1.6 ± .2
a_2	.65	.64	.65 ± .01	b_2	2.6	2.4	2.5 ± .1
a_3	.73	.86	.80 ± .07	b_3	.57	.46	.51 ± .05
a_4	.15	.15	.15 ± .01	b_4	.68	.68	.68 ± .01
a_5	.26	.32	.29 ± .03	b_5	.062	.050	.056 ± .01
a_6	.046	.047	.047 ± .01	b_6	.086	.085	.085 ± .01
a_7	.043	.054	.048	b_7	.024	.020	.022
a_8	.0084	.0085	.0084	b_8	.024	.024	.024
a_9	.0090	.0111	.010	b_9	.0045	.0037	.0041
a_{10}	.0018	.0018	.0018	b_{10}	.0035	.0035	.0035

III.6 Comparison of Models and Suggested Table of RMS Multipole Widths

P.J. Wanderer

a. Intercomparison of Models

It is useful to compare of the models of Fisk, Meuser, and Herrera in order to have a feeling for the uncertainties in the predictions. The comparison is made in several ways: the models themselves, the fits to Tevatron and CBA data, the values for specific mechanical motions, the variation of the errors with coil radius, and the predictions for SSC magnets.

The models themselves: The models are quite different. Fisk extrapolates the measured rms multipole variations in the framework of a two-parameter fit to the Tevatron quadrupole and dipole data. The parameters are the error in angular width and the difference between geometric center and magnetic center of each coil, as built. The parameters describe the quadrupole data well and provide a reasonable fit to the dipole data. From this, Fisk concludes that an extrapolation to SSC dimensions can be made on the basis of a model for the variation of coil angular errors with radius. The extrapolations from Tevatron and CBA data are averaged and the difference between the two is used as a measure of the uncertainty. In addition, Fisk assigns an overall uncertainty of +50% to the predictions.

Meuser bases his fit on the effects of specific mechanical errors, nine angular and six radial. The errors were selected from a much larger list by taking the errors that have the largest effect on the harmonics, given a reasonable estimate of the magnitude of the error. The list of angular errors includes those which vary the overall size and position of the coils and those which provide top-bottom and left-right asymmetries.

The inner and outer coils are treated separately. The motion of the coil center post with respect to the yoke also is considered. Similarly, the list of radial errors includes those which vary the thickness and position of the coils symmetrically and also is a way that generates top-bottom and left-right asymmetries. The magnitude of the mechanical errors is determined by making a least-squares fit to the data. The procedure does not generate a unique solution because several of the error modes affect the multipoles in similar ways. Meuser has checked that different solutions that fit the data equally well give comparable predictions for SSC magnets.

Herrera's model groups construction errors by the resultant symmetry or asymmetry of the coils and links each of four symmetry parameters to the specific multipoles affected by it. Radial and angular variations of the coil size and position are assigned initial values which are effectively modified by the symmetry parameters in the fitting procedure. The coil size and position variations are modified as a group, but the fit is most sensitive to the coil angular position. Thus, Herrera's model contains all but one of the errors used in Meuser's model, but fits them to the data in a quite different way.

Fits to Tevatron and CBA data: The rms difference between the measurements and the fits has been calculated for each of the models. For Meuser's fit, the rms difference is 0.17 for the CBA data and 0.26 for the Tevatron data (in units of 10^{-4} at 2/3 inner-coil radius). For Herrera's fit, the rms difference is 0.34 for CBA and 0.16 for the Tevatron data with the quadrupole terms excluded from the fit. (Herrera's best fit with the quadrupole terms included has an rms difference of 0.27.) Fisk's model gives an rms difference of 0.59 for the Tevatron data, with the decapole and higher terms not included. Overall, the fits of Meuser and Herrera are comparable, and that of Fisk somewhat worse. The agreement between the data and the two best fits is very good when measured against the Tevatron and CBA rms tolerances.

Specific mechanical errors: Because of the different approaches taken by the three models, it is not clear that the sizes of specific mechanical errors can be directly compared. Nonetheless, it is instructive to make a comparison. The errors which are the easiest to understand and which have the largest effect on the multipoles are the symmetric variation in coil size and the top-bottom asymmetry. Values for these two errors are given in Tables III.9a and III.9b.

Table III.9a
Symmetric Variation in Coil Azimuthal Size (mils)

	Tevatron Coils		CBA Coils		
Model	Inner	Outer	Inner	Outer	Notes
Fisk (η)	1.1	1.1	--	--	
Meuser ($\epsilon/4$) (modes 4, 5)	1.1	1.1	1.6	1.6	inner = outer assumed
Herrera $(1+\beta)\phi$	0.7	--	1.2	--	

Note: No entry is made for outer coil variation in Herrera's model because the parameter that controls the inner coil-outer coil difference indicates a large difference that is not understood.

Table III.9b
Top-Bottom Coil Size Differences (mils)

Model	Tevatron	CBA
Fisk (δ)	2.3	--
Meuser ($\epsilon/2$)	0.1	1.4
Herrera $(1+\beta)(1+\alpha)\phi$	1.6	1.2

There is general agreement among the models that coil variations are at the level of 1 to 2 mils, but more precise conclusions cannot be drawn from the values in the two tables. The fits to and predictions of the multipole variations are more consistent than the various mechanical errors used by the individual models.

Variation with Coil Radius: The three models assume that the errors determined from fits to Tevatron and CBA magnet data scale with radius in different ways. The most conservative assumption is made by Herrera, who assumes that the errors (stated in units of length) will remain unchanged. Thus the angular errors will vary as $(\text{radius})^{-1}$. The inner coil radius of the Tevatron dipoles is about twice as large as that of the 4-cm Reference Design magnet, so the Design D angular errors will be roughly twice those of the Tevatron. Meuser assumes that there will be some improvement in the absolute errors as the radius becomes smaller and that the angular errors will go as $(\text{radius})^{-0.7}$. With this assumption, the Design D angular errors are about 1.6 times the Tevatron error. Fisk assumes that the absolute errors result from a buildup of errors on the thickness of individual turns of conductor and so the rms variation should be proportional to the square root of the number of turns. Thus the angular errors go as $(\text{radius})^{-0.5}$, which makes Design D errors 1.4 times Tevatron errors. (Other factors, such as the closeness of the iron, enter in, so these ratios should not be taken literally.)

Predictions for Reference Design D: The predictions of the three models for the multipole widths of Reference Design D magnets are presented together in Table III.10 and on a semilog plot in Fig. III.9.

Generally speaking, the largest of the three predictions is 1.4 times the smallest. Given the difference between the details of the models, the fact that their predictions agree within about 40% lends confidence to the overall picture they present.

Table III.10
Summary of Predictions for the rms Multipole Widths of Reference Design D(4 cm) Magnets due to Placement Errors. Units are 10^{-4} at 1 cm.

No. of Poles	Multipole Coef	rms Multipole Widths Fisk Method	Meuser Method	Herrera Method
4	a_1	3.31 ± .30	3.2	3.5 ± .2
4	b_1	1.61 ± .35	1.7	1.6 ± .2
6	a_2	0.71 ± .23	0.48	0.65 ± .01
6	b_2	1.94 ± .20	1.6	2.5 ± .1
8	a_3	0.72 ± .16	0.54	0.80 ± .07
8	b_3	0.32 ± .14	0.21	0.51 ± .05
10	a_4	0.16 ± .06	0.11	0.15 ± .01
10	b_4	0.62 ± .05	0.48	0.68 ± .01
12	a_5	0.12 ± .08	0.083	0.29 ± .03
12	b_5	0.07 ± .03	0.052	0.056 ± .01
14	a_6		0.026	0.047
14	b_6		0.040	0.085

Notes: (1) The upper and lower uncertainty limits correspond to values scaled from the Tevatron and the CBA data, respectively.

(2) Fisk assigns an additional uncertainty of +50 percent of the width to the uncertainties listed.

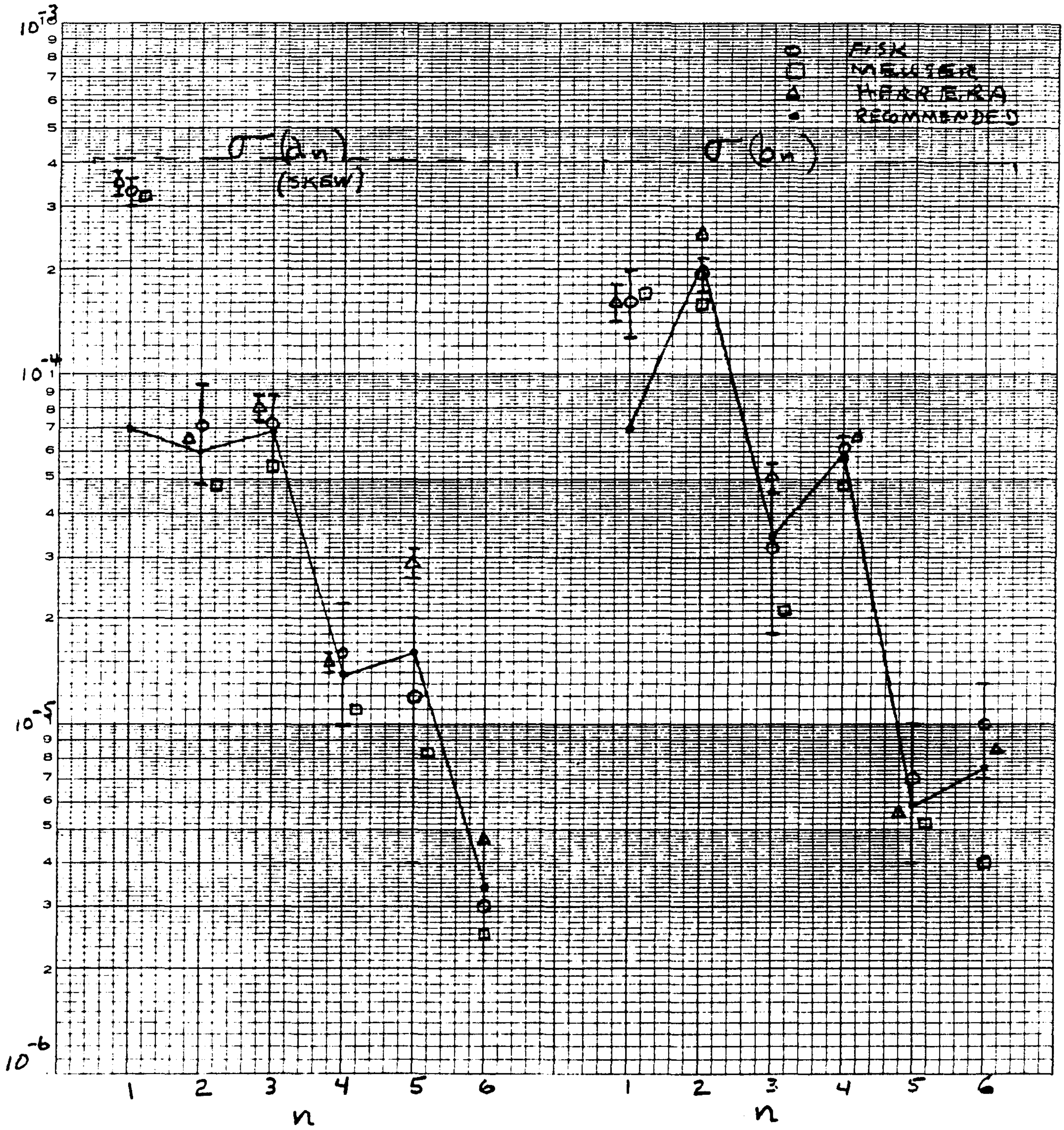

Figure III.9 The rms variation of multipole errors (at 1 cm) projected for SSC magnet designs A and D(4 cm) due to placement errors, based on Tevatron and CBA dipole magnetic measurements, according to the models of Fisk, Meuser, and Herrera (Table III.10). The solid curve connects the recommended values (Table III.11). (The number of magnet poles is 2(n+1)).

b. Suggested Table of Multipole Widths.

A reasonable table of random errors is developed by taking the average of the predictions from the three models. The only exceptions to this are the quadrupole terms for designs A and D, where it was assumed that the coils could be centered in the iron so as to reduce the quadrupole strengths, as was done for Tevatron magnets (see Section III.8). The resultant values are listed in Table III.11, and also in the Summary Table S-1.

Table III.11
Suggested rms multipole widths for reference design D(4cm)

Multipole	rms Width
a_1	0.7
b_1	0.7
a_2	0.61
b_2	2.01
a_3	0.69
b_3	0.34
a_4	0.14
b_4	0.59
a_5	0.16
b_5	0.059
a_6	0.034
b_6	0.075
a_7	0.030
b_7	0.016
a_8	0.0064
b_8	0.021

Taking the dipole field uniformity as a whole ($\delta B/B$ at 1 cm), comparison of the models suggests that Design D magnets will be within 20% to 30% of the values in Table III.11. The uncertainty in an individual multipole is estimated to be about 50%. The data from the eight bores of 3.2 cm magnets (Section III.1), the Fermilab 5-cm magnets, and the first 4.5-meter Design D magnets indicate that the models are substantially correct.

The projected multipole variations for magnet designs B and D(5 cm) (also listed in Table S-1) were scaled from the values for designs A and D(4 cm). The scaling assumption used here was that all dimensional errors scaled as the effective coil radius (r_e) to the minus 0.5 power. Thus the rms variation of the n^{th} multipole coefficient for the D(5 cm) design was calculated as:

$$\sigma(b_n)_{D5} = \sigma(b_n)_{D4}\left[\frac{r_{e\ D4}}{r_{eD5}}\right]^{n+1/2}$$

The effective coil radii were taken as:

for designs A and D(4 cm)	3.0 cm
design D(5 cm)	3.5 cm
design B	3.33 cm

For design B each value was enlarged by a further factor of 1.25 to take into account the 25% increase in dipole field due to the iron yoke in designs A and D, which is absent in design B. (The smaller effect of the iron on the higher multipole fields was ignored.) In addition, the quadrupole coefficients listed for design B are based on the assumption of no improvement via centering in the "no-iron" design B.

III.7 Systematic Multipoles

P. J. Wanderer

Since the publication of the SSC Reference Design, the two-in-one yoke specified for the Reference Design A magnet has evolved to the collared coil design shown in Figure III.1. The systematic multipoles calculated for this yoke at 1-cm radius are given in Table III.12a at low field ($\infty\mu$) and at high field.(9) The variation in multipoles with excitation is small, everywhere less than one unit (10^{-4}). Calculations for two-in-one yokes are more difficult than for one-in-one yokes because of the absence of left-right symmetry. Also, the odd-b terms (quadrupole etc.) become allowed harmonics. For the 3.2-cm aperture SSC R&D magnets (Ref. 35) the calculated and measured values are in good agreement. Specifically, the measured quadrupole coefficient b_1 is 0.5±0.1 unit, as compared to a predicted value of 0.9 unit (Ref. 37). The measured octupole and 12-pole terms are consistent with zero, as expected from a calculation by Morgan. Also good agreement has been obtained between calculation and measurement for a two-in-one CBA yoke (Ref. 38).

An independent calculation of multipoles has been made for a slightly different configuration of yoke and holes (Ref. 10). Although the design of reference 10 was not optimized for minimum multipoles, quadrupole and sextupole terms were held to two units. The differences in the yokes used in the two calculations prevents detailed comparison between the two calculations. Further calculations are being made at BNL.

The systematic multipole strengths predicted for magnet designs B (Ref. 11) and D are given in Table III.12b. The two-unit systematic increase in b_2 from injection to full field in Design D(4 cm) is due to saturation effects in the iron yoke. For Design D(5 cm) the increase is 1.5 unit (Table S-2). The original design D(4 cm) coil configuration C-5 (Ref. 12) has a relatively large 18-pole coefficient (b_8). To remedy this defect the coil configuration PK-15 was recently developed (Ref. 39).

Table III.12a
Systematic Multipole Strengths Predicted for
Two-in-One Design A
(Units are 10^{-4} at 1 cm)

I (A)	Bo,G	Relative Bo/I	b_1	b_2	b_3	b_4	b_6	b_8	b_{10}
μ	-	1.000	-	0.4	-	0.0	0.2	0.8	0.0
400	4124	.997	0.8	-0.9	0.2	0.0	0.2	0.8	0.0
5600	57243	.992	0.3	-0.8	0.1	0.0	0.2	0.8	0.0
6100	62203	.986	0.1	-0.4	0.0	0.0	0.2	0.8	0.0
6600	66903	.980	-0.6	-0.1	0.0	-0.1	0.2	0.9	0.0

Table III.12b
Systematic Multipole Strengths for Magnet Designs B and D(4 cm)
(Units are 10^{-4} at 1 cm)

	b_2	b_4	b_6	b_8	b_{10}
Design B					
(Injection and 20 TeV)	.07	-.07	.09	-.14	.014
Design D(4 cm) - C-5					
Injection	.4	-.1	.2	.9	0
20 TeV	2.4	-.1	.2	.9	0
Design D(4 cm) - PK-15					
Injection	-.05	-.16	-.03	.15	.19
20 TeV	2.0	-.16	-.03	.15	.19

III.8 Effect of Coil-Centering Errors on the Multipoles of Reference Design D Magnets

P.J. Wanderer

Calculations have been made of the multipole strengths generated by horizontal or vertical displacements of the entire C5 coil structure relative to the iron yoke (Ref. 13). The gap between the yoke and the coil is 15.6 mm.

For a horizontal displacement dx, all 72 conductors in the upper midplane of the coil must be modeled. The results of the calculation for the centered coil and the displaced coil are given in the upper portion of Table III.13. Only odd-n normal harmonics (quadrupole, etc.) are generated by horizontal displacements. The table presents the results for the expected odd-n terms as well as for the allowed (even-n)terms. The only non-zero changes are the approximately 2 units in b_1 (quadrupole) and the approximately 0.1 unit in b_7 (16-pole).

For a vertical displacement dy, the entire coil must be modeled. This is not possible with program MDP (the BNL version of two-dimensional GFUN), because MDP is limited to about 120 conductors. Hence an approximate coil structure consisting of 5 radial sectors per quadrant with starting and ending angles for each block the same as the midpoint of the sides of the partially keystoned design was used to study vertical displacement. The multipole strengths of the approximate configuration centered in the iron and of the approximate configuration shifted up 5 mils (0.127 mm) are given in the lower portion of Table III.13. For a vertical displacement, odd-n skew harmonics are expected. The table presents the results for these terms and for the allowed terms. The changes produced by the 5-mil displacement are all less than 0.1 unit except in the skew quadrupole, coefficient a_1, which is about 2 units. (Note that the approximate C5 structure has about 5 units of sextupole without displacement.)

Table III.13
Multipoles (10^{-4}) Generated by a 5-mil displacements
(evaluated at 1-cm radius)

For Horizontal Displacement dx:

	b_1	b_2	b_3	b_4	b_5	b_6	b_7
C5 coil centered	0.00	0.19	0.00	0.01	0.00	0.16	0.00
C5 coil at + dx	1.95	0.20	0.00	0.01	0.01	0.16	0.09

For Vertical Displacement dy:

	a_1	b_2	a_3	b_4	a_5	b_6	a_7
C5 coil centered	0.00	4.75	0.00	0.94	0.00	0.79	0.00
C5 coil at + dy	1.86	4.74	0.06	0.93	0.06	0.79	0.10
+pole position, degrees	90	30	45	18	30	12.9	22.5

In the case of the skew harmonics a_i, the pole sign is indicated by the position in degrees of the positive pole in the first quadrant nearest the positive x axis; the b_i have a field either parallel (+) or antiparallel (-) to the dipole field on the positive x axis; the dipole field is in the (-) y direction.

It is interesting to compare the sensitivity of the quadrupole term to centering errors for the C5 coil, as calculated above, with the sensitivity of the Tevatron magnets. At 2/3 of the C5 coil radius, the sensitivity is 2-mils per unit (10^{-4}) of b_1. For the Tevatron magnets, evaluated at two-thirds of their own radius, the sensitivity is less, 3-mils per unit b_1. This is as expected, since the iron is much farther from the Tevatron coils than in the C5 design.

The sensitivity of the quadrupole term to centering in the iron can be used to reduce the quadrupole terms that are due to manufacturing tolerances. This was done for the Tevatron dipoles where the "smart bolts" were adjusted to minimize the quadrupole terms (Ref. 14). With this adjustment, the rms width of the normal quadrupole was reduced from about 3 units (Table III.1) to 0.5 unit. For Design D dipoles, this procedure would be implemented by measuring the harmonics of the collared coils before insertion in to the iron. U-shaped channels would be placed over the tabs of the collars to position the coils in the iron. Centering would be achieved by the use of channels with different wall thicknesses. The Tevatron quadrupole data imply that the distribution of centering errors had an rms width of 1.5 mils. Carrying the 1.5 mil variation over to Design D gives a quadrupole distribution with an rms width of about 0.7 unit, for both normal and skew terms. With the quadrupole variation minimized, the effect of variation in the next harmonic, the sextupole, would then be reduced by judicious positioning of the dipoles within the cells. Tevatron dipoles were positioned by this method (Ref. 14).

III.9 Multipoles Due to Magnet Ends

P.J. Wanderer

A comparison between measurements for four bores of 3.2 cm 2-in-1 magnets made at BNL and a calculation by Fernow given good agreement for the quadrupole, sextupole, and octupole multipole strengths due to the the magnet ends (Ref. 15). Poor agreement is found for the decapole term. This is the first time this calculation (program MAG3) has been used, and it does a better job of predicting end multipoles than previous calculations at BNL.

The program calculates the contribution of coil segments only (no iron). The iron yoke stops at the end of the straight section, and the program calculates the integrated multipoles from that point outwards. The measured values are simply the difference of long- and short-coil measurements. This gives the end multipoles scaled to the effective dipole length, which is about 4.5 m. (For SSC Reference Design D dipoles, which have an effective length of about 16.7 m, the end multipole strength, relative to whole dipole, would be lower by a factor of four.)

The comparison of the measured and calculated values in Table III.14 shows that the calculations can predict the quadrupole and sextupole terms within several b_n units. This ability could be used in principle to design an end configuration with no sextupole contribution (Ref. 2). The program does not appear reliable for higher multipoles. Unfortunately, even this limited predictive power will probably be lost if the iron is extended part way along the end region. If the iron completely covers the end, the quadrupole term would be reduced naturally, and it might be possible to predict and thereby control the sextupole. However, such a design must also reduce the field enhancement in the saddle region, or else the ends will limit the magnet's performance.

Table III.14
End Multipoles b_n (10^{-4}) at 1 cm for Coil Section SSC-P11.

Multipole	Calculated	Measured (4 bores)
Quadrupole, b_1	10.4	8.4 $\pm$ 1.4
Sextupole, b_2	25.9	27.2 $\pm$ 2.0
Octupole, b_3	0.1	1.6 $\pm$ 0.9
Decapole, b_4	-0.8	-7.2 $\pm$ 1.4

IV. Magnetization Effects in Cosθ magnets

W.S. Gilbert and W.V. Hassenzahl

IV.1 Introduction

Superconductors exhibit diamagnetism that varies from complete exclusion of flux in the soft, or Type 1, superconductors, such as lead, to the very limited exclusion of flux in the hard, or Type II, superconductors, such as the high-field NbTi alloy used in accelerator dipoles. The magnetization effects in these conductors have been calculated from their known superconducting characteristics, based on flux penetration models, by M. Green (Ref. 16).

The magnetization can also be measured directly, and magnetization curves of several NbTi cables have been presented by Ghosh and Kuchnir (Ref. 25) Magnetization for a cable with 19-micron filaments is shown in Fig. IV.1.

According to Green's theory, except for low-field penetration effects, the magnetization should be proportional to critical current density (J_c). Critical currents are difficult to measure at low field, so that assumed values have been used in the region. Comparison is made between the variation of magnetization with magnetic field and the variation of critical current density, relative to their 3 tesla values, in Table IV.1 and shown in Fig. IV.2. For the magnetization data, the difference between the increasing field branch and decreasing field branch is used. Between 0.2 T and 3 T, J_c changes by a factor of 2.85 whereas the magnetization changes by factors of 3.36 and 3.73 for the two conductors considered here. These differences may be due both to an

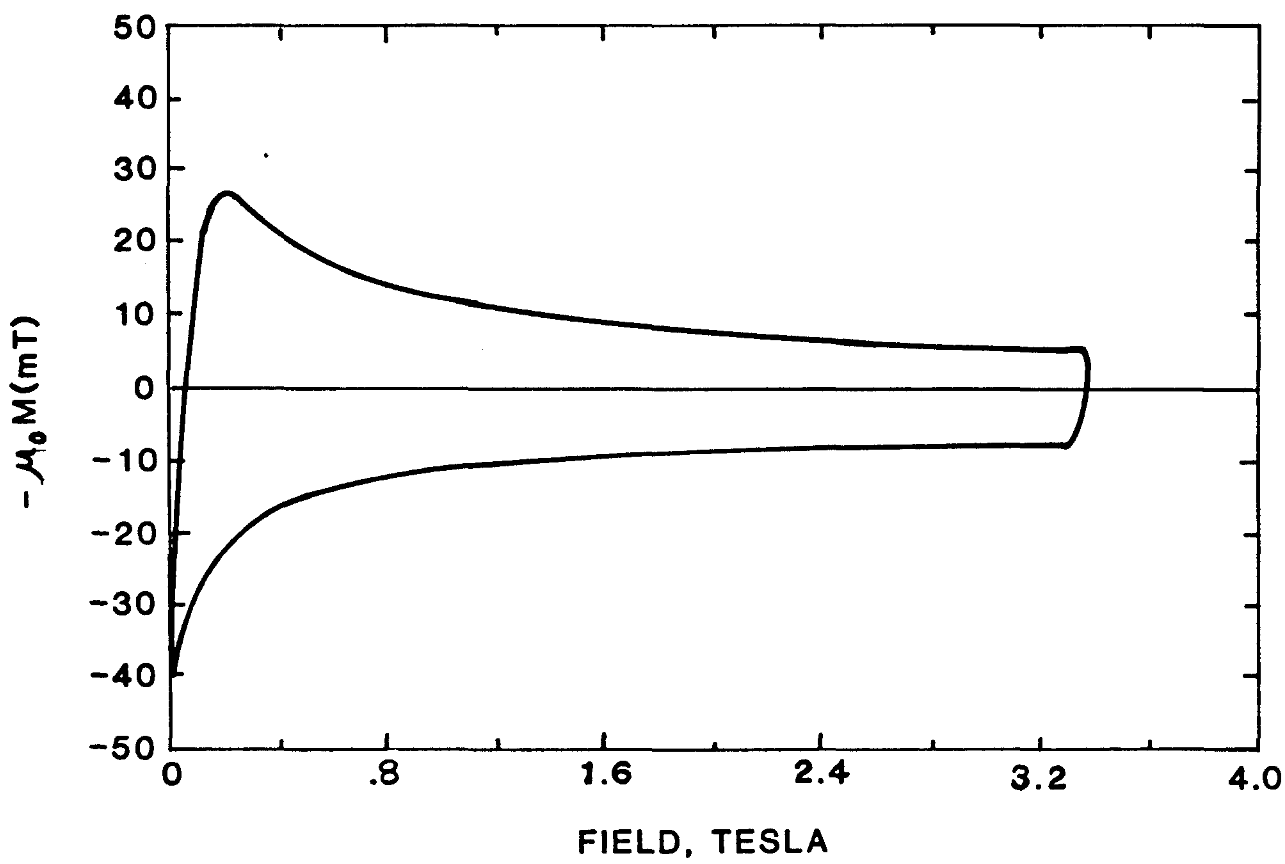

Figure IV.1 Magnetization data for a cable with 19-micron filaments (Ref. 24).

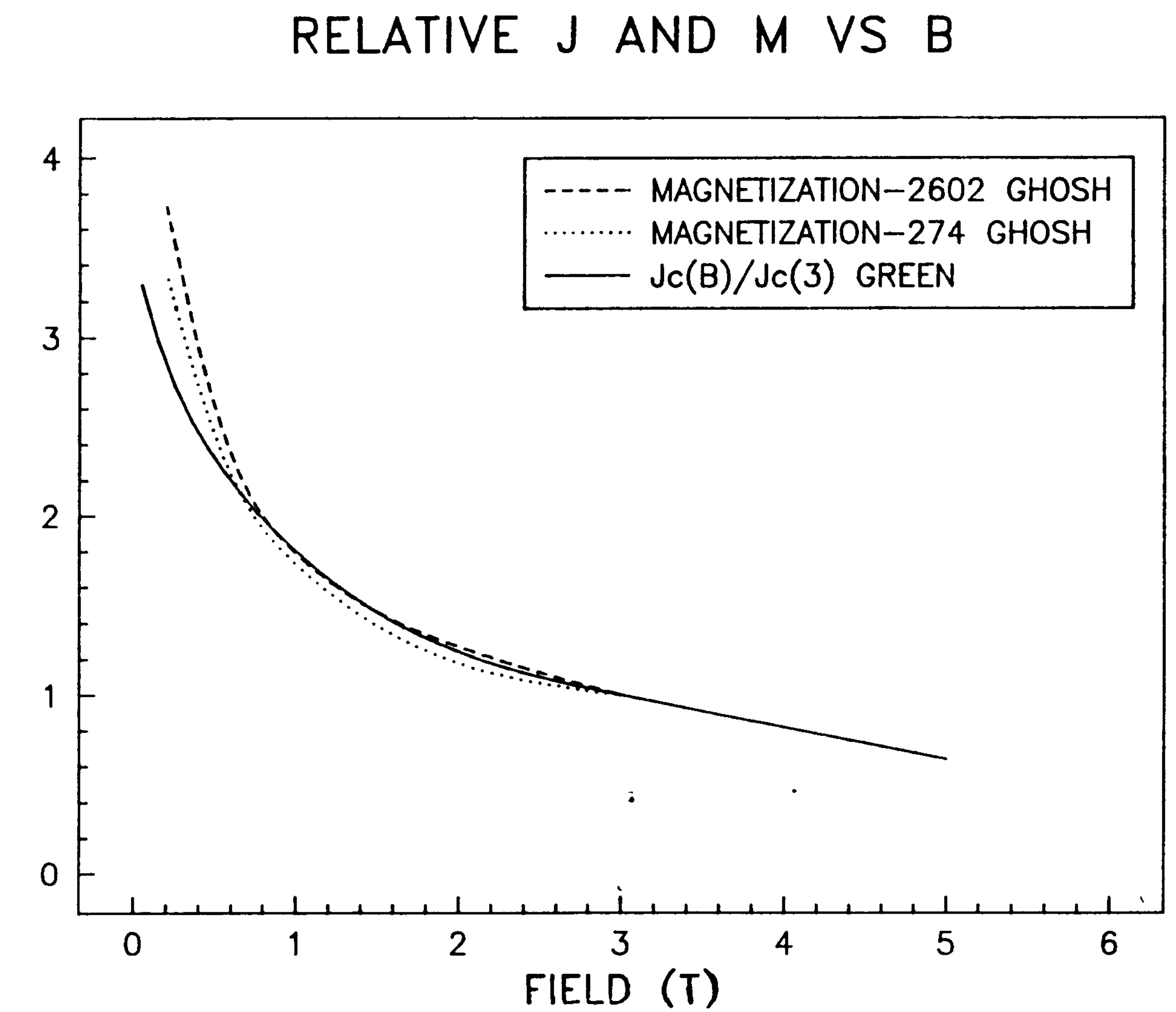

Figure IV.2 Relative variation of critical current density and magnetization with magnetic field strength, normalized at 3T.

incorrect low-field J_c value and to an overly simplified low-field flux-penetration model. Overall the agreement is good, and we should be able to reduce the relatively small apparent differences through more detailed measurements and calculations.

Table IV.1

Comparison of the variation of magnetization and critical current density in two conductors with different filament size.

B (T)	$\frac{J_c(B)}{J_c(3T)}$	M(B)/M3T) 0274 (8.7μ)	2602 (19.3μ)
0.05	3.29	--	--
0.1	3.13	-	--
0.2	2.85	3.36	3.73
0.5	2.32	2.45	2.61
1.0	1.80	1.73	1.79
2.0	1.24	1.18	1.27
3.0	1.0	1.0	1.0
5.0	0.64	-	--

IV.2 Calculated Persistent-Current Multipoles.

Green's theory (Ref. 16) has been found to yield fairly good agreement with experimental data collected from several accelerator dipoles. The basic physical assumption made is that the bulk critical current density in the NbTi is independent of the filament diameter. Using Green's model the magnetic fields produced by persistent-current doublets induced in filament diameters of 20 μm, 8.7 μm, 5.0 μm, 2.0 μm were calculated for magnet types A, B, D(4 cm), and D(5 cm). Because of a code limitation, the same Cu/SC ratio was used in both inner and outer coils. For the increasing-current branch of the magnetization curve, the magnet's central field was cycled up to a peak field of 6.0 tesla (for types A and D), then down to zero, and then up to the field of interest. The decreasing branch has the field being ramped from zero, to 6.0 tesla, and then down to the field of interest. The sextupole fields are given at a reference radius of 1.0 cm both in the units of magnetic field (gauss), and relative to the dipole field, as b_2 in units of 10^{-4}.

Table IV.2 tabulates the data for magnet types A and D(4 cm). Figure IV.3 displays the relative sextupole coefficient b_2 vs. central field up to 4.5 tesla; Figure IV.4 expands the 0-to-1-tesla region. According to this model smaller filaments reduce the error field due to persistent currents and also move the region of rapid change to lower fields since the flux can more easily penetrate a smaller filament.

Table IV.3 and Figures IV.5 and IV.6 present the same type of data for magnet type D(5 cm). The larger winding bore also reduces the sextupole at the reference radius of 1.0 cm.

Table IV.4 and Figures IV.7 and IV.8 present similar data for magnet type B(5.1 cm). The field sweeps are to 5.5 tesla (rather than to the 6.0 tesla maximum used for the D magnets).

Table IV.2
Persistent-Current Sextupole Strengthen Magnet Designs A and D(4 cm)
For Four Sizes of Superconductor Filaments, evaluated at 1 cm
$B_o b_2$ in Gauss;
b_2 in 10^{-4} units.

		20 μ		8.7 μ		5.0 μ		2.0 μ	
Field (tesla)		$B_o b_2$	b_2	$B_o b_2$	b_2	$B_o b_2$	b_2	$B_o b_2$	b_2
<u>Current Increasing</u>									
6.0→0.0→	0.05	7.65	153.0	3.03	60.60	1.39	27.80	0.13	2.60
	0.10	3.78	37.80	0.02	0.20	-0.72	-7.20	-0.49	-4.90
	0.15	0.76	5.07	-1.49	-9.93	-1.23	-8.20	-0.58	-3.87
	0.20	-1.42	-7.10	-2.01	-10.05	-1.34	-6.70	-0.59	-2.95
	0.25	-2.86	-11.44	-2.18	-8.72	-1.40	-5.60	-0.60	-2.40
	0.30	-3.72	-12.40	-2.25	-7.50	-1.41	-4.70	-0.61	-2.03
	0.35	-4.17	-11.91	-2.29	-6.54	-1.40	-4.00	-0.62	-1.77
	0.40	-4.38	-10.95	-2.29	-5.72	-1.38	-3.45	-0.62	-1.55
	0.5	-4.51	-9.02	-2.24	-4.48	-1.36	-2.72	-0.60	-1.20
	1.0	-4.14	-4.14	-1.98	-1.98	-1.18	-1.18	-0.47	-0.47
	3.0	-2.49	-0.83	-1.08	-0.36	-0.62	-0.21	-0.25	-0.08
	4.5	-1.70	-0.38	-0.73	-0.16	-0.42	-0.09	-0.17	-0.04
<u>Current Decreasing</u>									
0→6.0→	0.0	12.08	-	7.34	-	5.55	-	3.80	-
	.05	9.01	180.20	4.47	89.40	2.82	56.40	1.34	34.60
	.10	8.05	80.50	3.80	38.00	2.30	23.00	1.02	10.20
	.15	7.50	50.00	3.46	23.07	2.06	13.73	0.87	5.80
	.20	7.11	35.55	3.24	16.20	1.91	9.55	0.79	3.95
	.25	6.81	27.24	3.08	12.32	1.80	7.20	0.74	2.96
	.30	6.56	21.87	2.95	9.82	1.72	5.73	0.70	2.33
	.35	6.34	18.11	2.84	8.11	1.65	4.71	0.67	1.91
	.40	6.14	15.35	2.74	6.85	1.59	3.98	0.65	1.63
	.50	5.77	11.54	2.56	5.12	1.49	2.98	0.60	1.20
	1.00	4.59	4.59	2.02	2.02	1.17	1.17	0.47	0.47
	3.00	2.45	0.82	1.07	0.36	0.62	0.21	0.25	0.08
	4.50	1.64	0.36	0.73	0.16	0.42	0.09	0.17	0.04

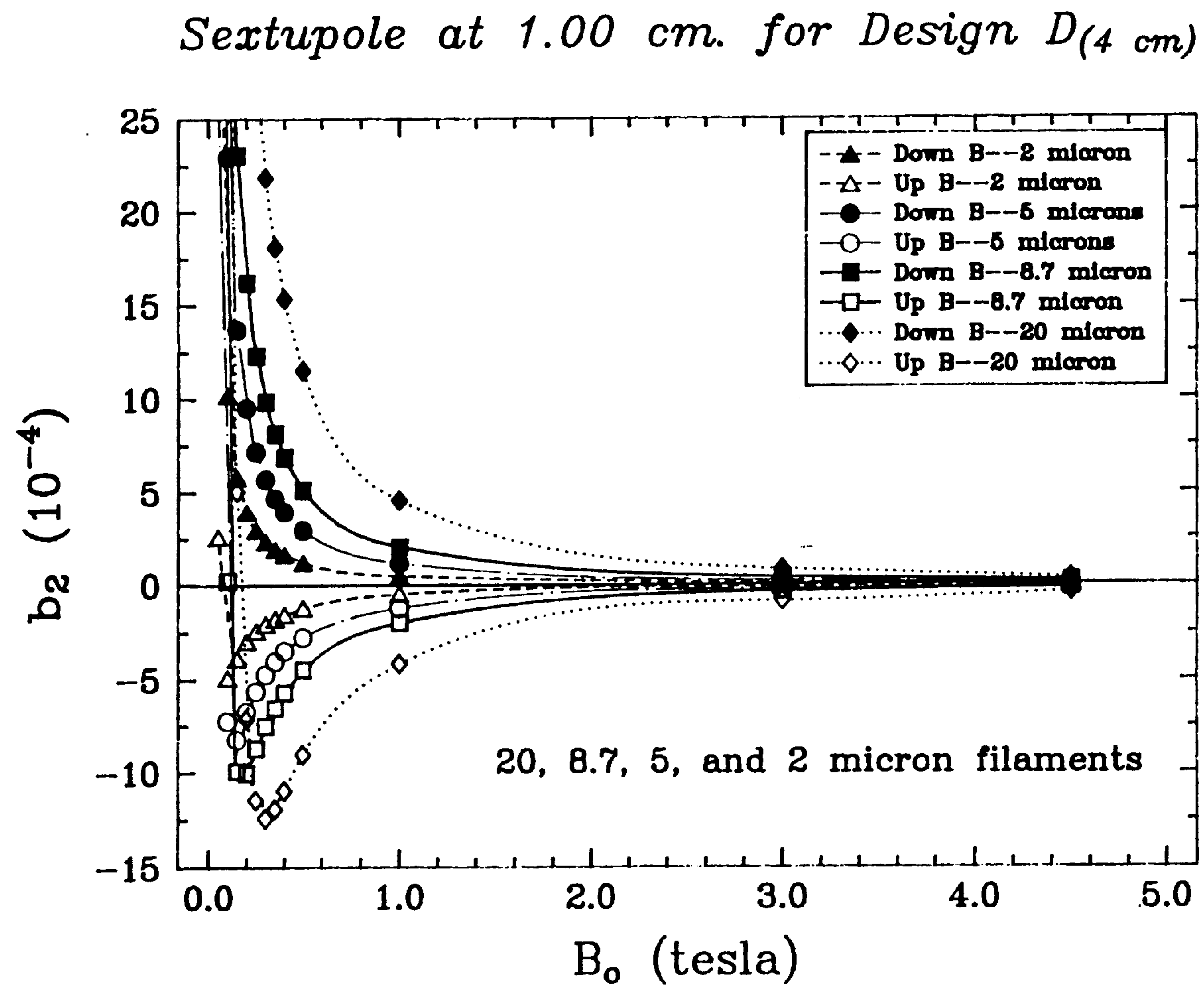

Figure IV.3 Persistent current sextupole strength at 1.0 cm for designs A and D(4 cm) for several filament diameters.

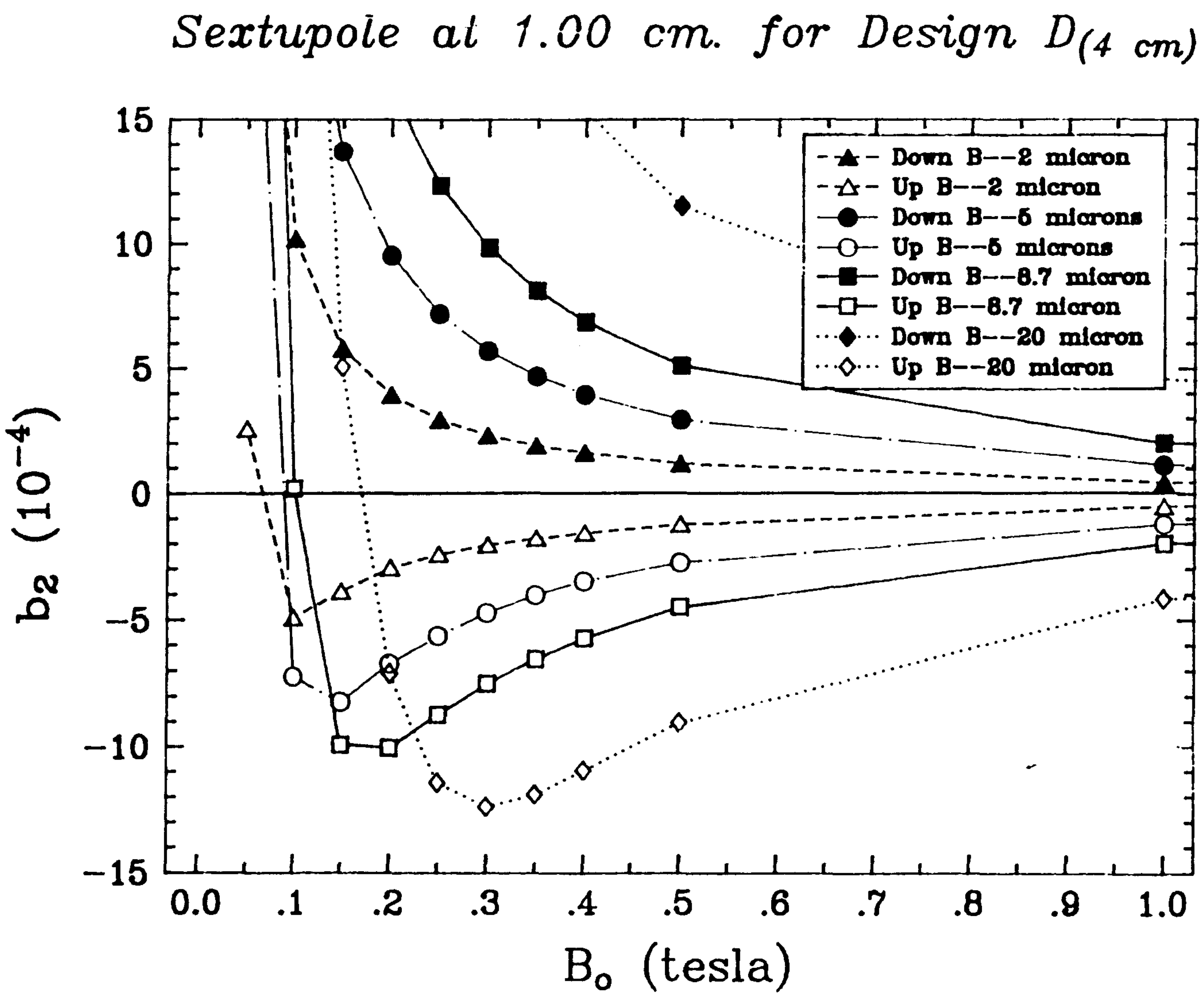

Figure IV.4 Persistent current sextupole strength for designs A and D(4 cm) in the lower excitation range.

Table IV.3
Persistent-Current Sextupole Strength in
Magnet Design D(5 cm) at 1 cm.
B_ob_2 in Gauss,
b_2 in 10^{-4} Units.

	20 μ		8.7 μ		5.0 μ		2.0 μ	
Field (tesla)	B_ob_2	b_2	B_ob_2	b_2	B_ob_2	b_2	B_ob_2	b_2
<u>Current Increasing</u>								
6.0→0.0→ 0.5	4.96	99.20	2.00	40.00	0.94	18.80	0.12	2.40
0.10	2.53	25.30	0.09	0.90	-0.40	-4.00	-0.29	-2.90
0.15	0.62	4.13	-0.87	-5.80	-0.75	-5.00	-0.35	-2.33
0.20	-0.76	-3.80	-1.23	-6.15	-0.83	-4.15	-0.36	-1.80
0.25	-1.69	-6.76	-1.35	-5.40	-0.87	-3.48	-0.37	-1.48
0.30	-2.26	-7.53	-1.41	-4.70	-0.88	-2.93	-0.38	-1.27
0.35	-2.53	-7.31	-1.43	-4.09	-0.87	-2.49	-0.39	-1.11
0.40	-2.72	-6.80	-1.44	-3.60	-0.87	-2.18	-0.39	-0.98
0.50		-	-1.41	-2.82	-0.86	-1.72	-0.38	-0.76
1.0	-	-	-1.26	-1.26	-0.76	-0.76	-0.31	-0.31
3.0	-	-	-0.71	-0.24	-0.41	-0.14	-0.16	-0.05
4.5	-	-	-0.49	-0.11	-0.28	-0.06	-0.11	-0.02
<u>Current Decreasing</u>								
0→5.0→ 0.0	7.74	-	4.70	-	3.55	-	2.44	-
0.05	5.80	116.00	2.89	57.80	1.83	36.60	0.87	17.40
0.10	5.19	51.90	2.46	24.60	1.49	14.90	0.66	6.60
0.15	4.83	32.20	2.24	14.93	1.34	8.93	0.57	3.80
0.20	4.58	22.90	2.09	10.45	1.24	6.20	0.52	2.60
0.25	4.39	17.56	1.99	7.96	1.17	4.68	0.48	1.92
0.30	4.23	14.10	1.91	6.37	1.11	3.70	0.46	1.53
0.35	4.09	11.69	1.84	5.26	1.07	3.06	0.44	1.26
0.40	3.96	9.90	1.77	4.43	1.03	2.58	0.42	1.05
0.50	3.74	7.48	1.66	3.32	0.96	1.92	0.39	0.78
1.00	2.98	2.98	1.31	1.31	0.76	0.76	0.30	0.30
3.00	1.61	0.54	0.71	0.24	0.41	0.14	0.16	0.05
4.50	1.08	0.24	0.49	0.11	0.28	0.06	0.11	0.02

Similar, but smaller, magnetization effects are calculated for the decapole and 14-pole field components. The magnitude of those components also vary roughly with the filament diameter. The agreement between experiment and theory is not quite as good for the decapole as for the sextupole, as will be discussed in Section IV.4b. The total excursion of the 14-pole magnetization b_6 is much less than 1 unit in the magnetic excitation region of interest, and can be neglected.

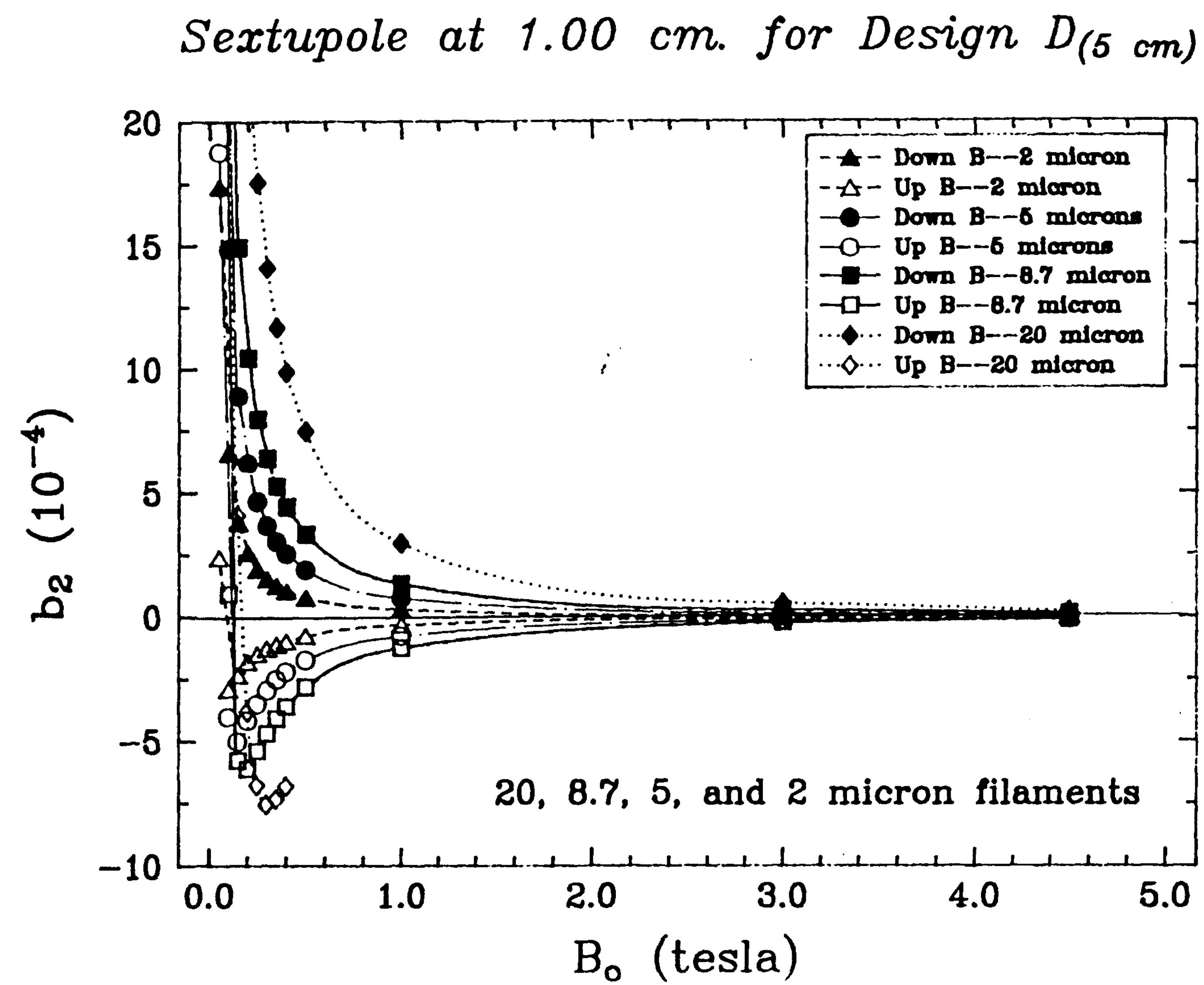

Figure IV.5 Persistent current sextupole strength at 1 cm for design D(5 cm) for various filament diameters.

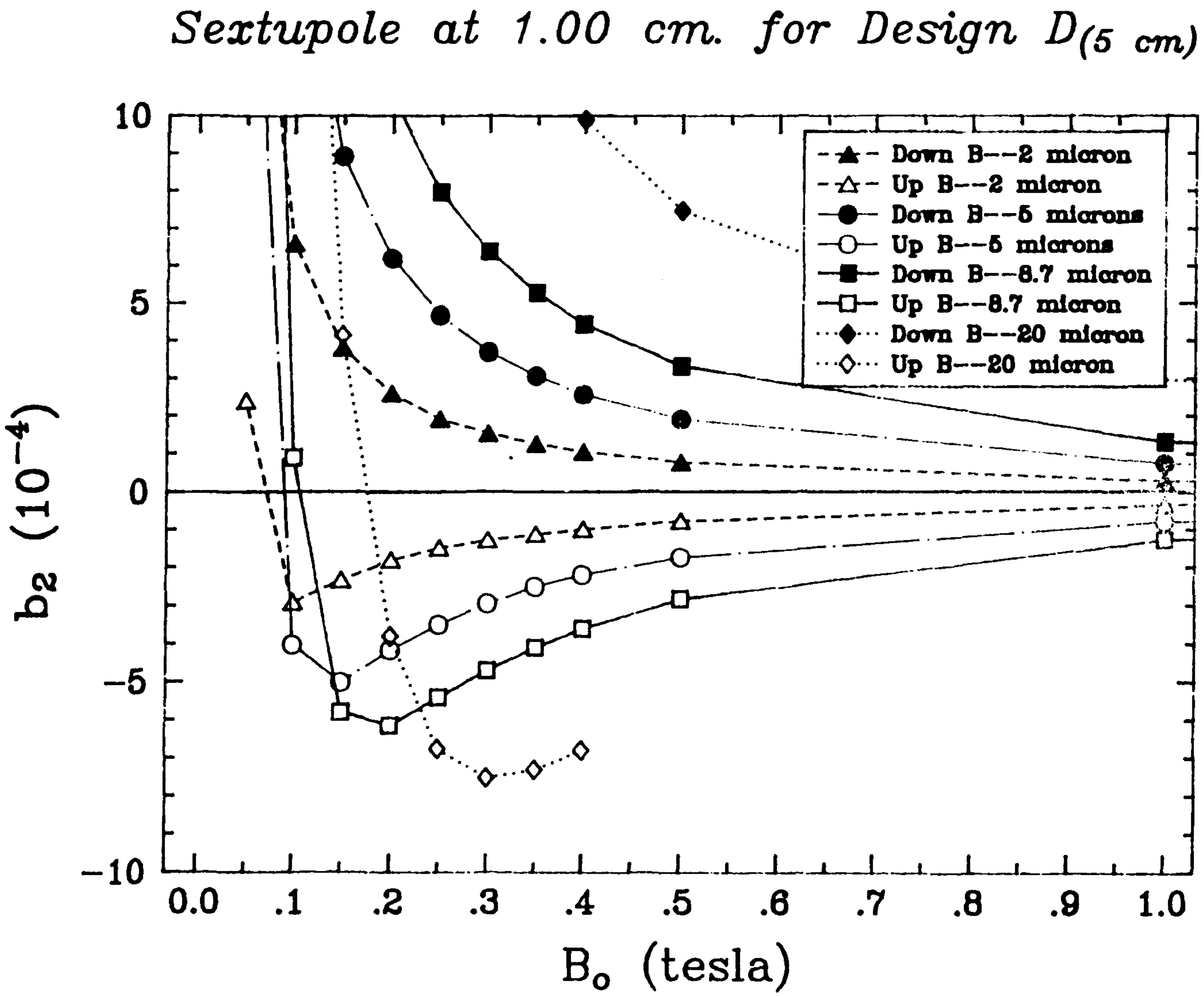

Figure IV.6 Persistent current sextupole strength for design D(5 cm) in the lower excitation range.

Table IV.4
Persistent-Current Sextupole Strength in
Magnet Design B(5 cm), at 1 cm.
B_ob_2 in Gauss,
b_2 in 10^{-4} Units.

		20μm		8.7μm		5.0μm		2.0μm	
Field (tesla)		B_ob_2	b_2	B_ob_2	b_2	B_ob_2	b_2	B_ob_2	b_2
Current Increasing									
5.5→0→	0.5	5.07	101.40	2.19	43.80	1.13	22.60	0.23	4.60
	0.10	2.89	28.90	0.37	3.70	-0.28	-2.80	-0.33	-3.30
	0.15	1.10	7.33	-0.71	-4.73	-0.77	-5.13	-0.36	-2.40
	0.20	-0.30	-1.50	-1.21	-6.05	-0.88	-4.40	-0.37	-1.85
	0.25	-1.32	-5.28	-1.41	-5.64	-0.89	-3.56	-0.39	-1.56
	0.30	-2.03	-6.77	-1.47	-4.90	-0.88	-2.93	-0.40	-1.33
	0.40	-2.72	-6.80	-1.44	-3.60	-0.89	-2.23	-0.40	-1.00
	0.50	-2.94	-5.88	-1.42	-2.84	-0.88	-1.76	-0.38	-0.76
	1.0	-2.63	-2.63	-1.28	-1.28	-0.75	-0.75	-0.30	-0.30
	3.0	-1.52	-0.51	-0.66	-0.22	-0.38	-0.13	-0.15	-0.05
	4.5	-0.89	-0.20	-0.39	-0.09	-0.22	-0.05	-0.09	-0.02
Current Decreasing									
0→5.5→	0.0	7.48	-	4.55	-	3.43	-	2.36	-
	0.05	5.68	113.20	2.85	57.00	1.81	36.20	0.87	17.40
	0.10	5.07	50.70	2.40	24.00	1.46	14.60	0.64	6.40
	0.15	4.73	31.53	2.19	14.60	1.30	8.67	0.55	3.67
	0.20	4.48	22.40	2.04	10.20	1.20	6.00	0.50	2.50
	0.25	4.29	17.16	1.94	7.76	1.14	4.56	0.47	1.88
	0.30	4.14	13.80	1.86	6.20	1.08	3.60	0.44	1.47
	0.35	4.00	11.43	1.79	5.11	1.04	2.97	0.42	1.20
	0.40	3.88	9.70	1.73	4.33	1.01	2.53	0.41	1.03
	0.50	3.66	7.32	1.63	3.26	0.94	1.88	0.38	0.76
	1.00	2.91	2.91	1.28	1.28	0.74	0.74	0.30	0.30
	3.00	1.49	0.50	0.65	0.22	0.37	0.12	0.15	0.05
	4.50	0.83	0.18	0.38	0.08	0.22	0.05	0.09	0.02

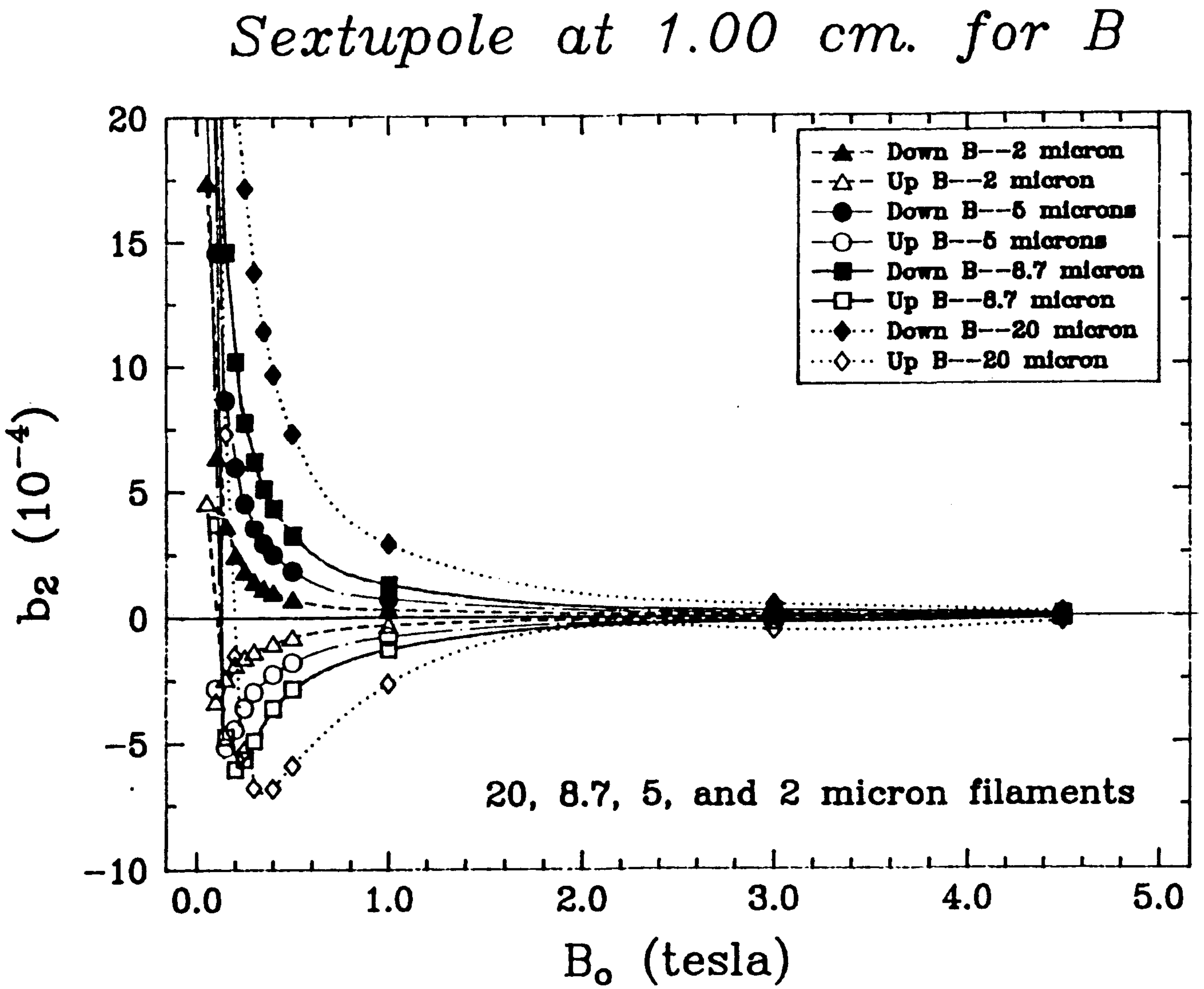

Figure IV.7 Persistent current sextupole strength at 1 cm for design B for various filament diameters.

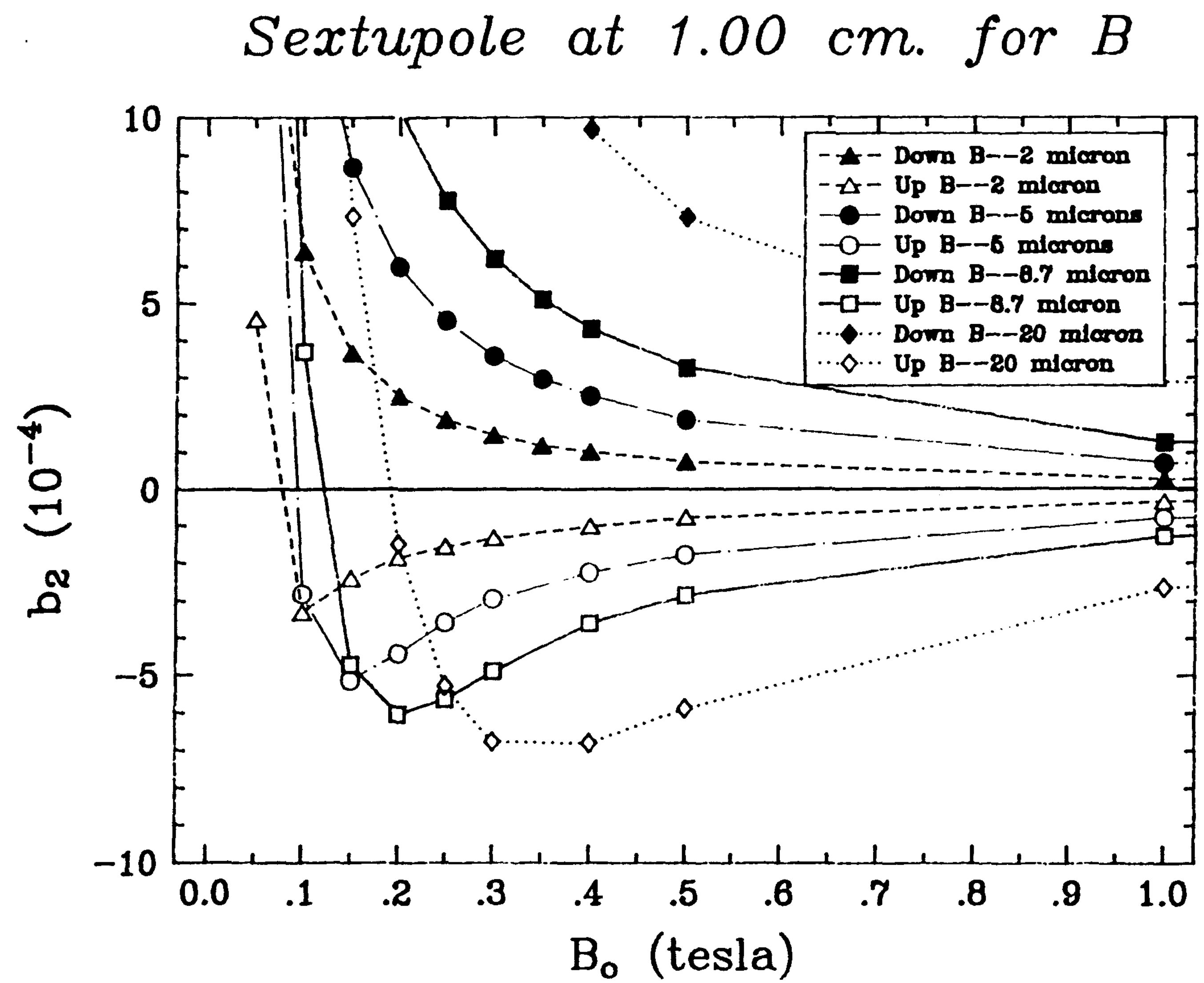

Figure IV.8 Persistent current sextupole strength for design B in the lower excitation range.

IV.3. <u>Is magnetization proportional to filament diameter?</u>

As discussed above, Green's model, for a given bulk critical current density, yields a magnetization field error proportional to filament diameter except for the effects due to field penetration and to transport current. Some recent experimental data indicate that for filaments smaller in diameter than 5 microns the effects of surface currents, which are proportional to the total surface area of the filaments, may become comparable with the bulk currents and result in remanent fields that do not decrease linearly with smaller filament diameter. The evidence for these surface currents comes from magnetization measurements on fine-filament materials, as listed below:

a. Carr and Wagner paper in 1983 ICMC (17). Magnetization measurements of 1.6 μm NbTi filaments shown in Fig. IV.9 display asymmetric magnetization, which they explained by invoking large surface currents.

b. Sampson et al., BNL measurements Feb. 14, 1985 (18). The same superconductor used above was drawn down to 1.25 μm filament diameter and the asymmetric magnetization curve was confirmed, Fig. IV.10.

c. Dubots et al., Marcoussic Lab., ASC 1984 (19). AC loss measurements on filaments ranging from 0.1 to 10 μm show that losses no longer decrease linearly with filament diameter as the filaments get smaller than 1 to 2 μm. They quote the Carr paper and cite surface currents for this lack of linearity. See Fig. IV.11.

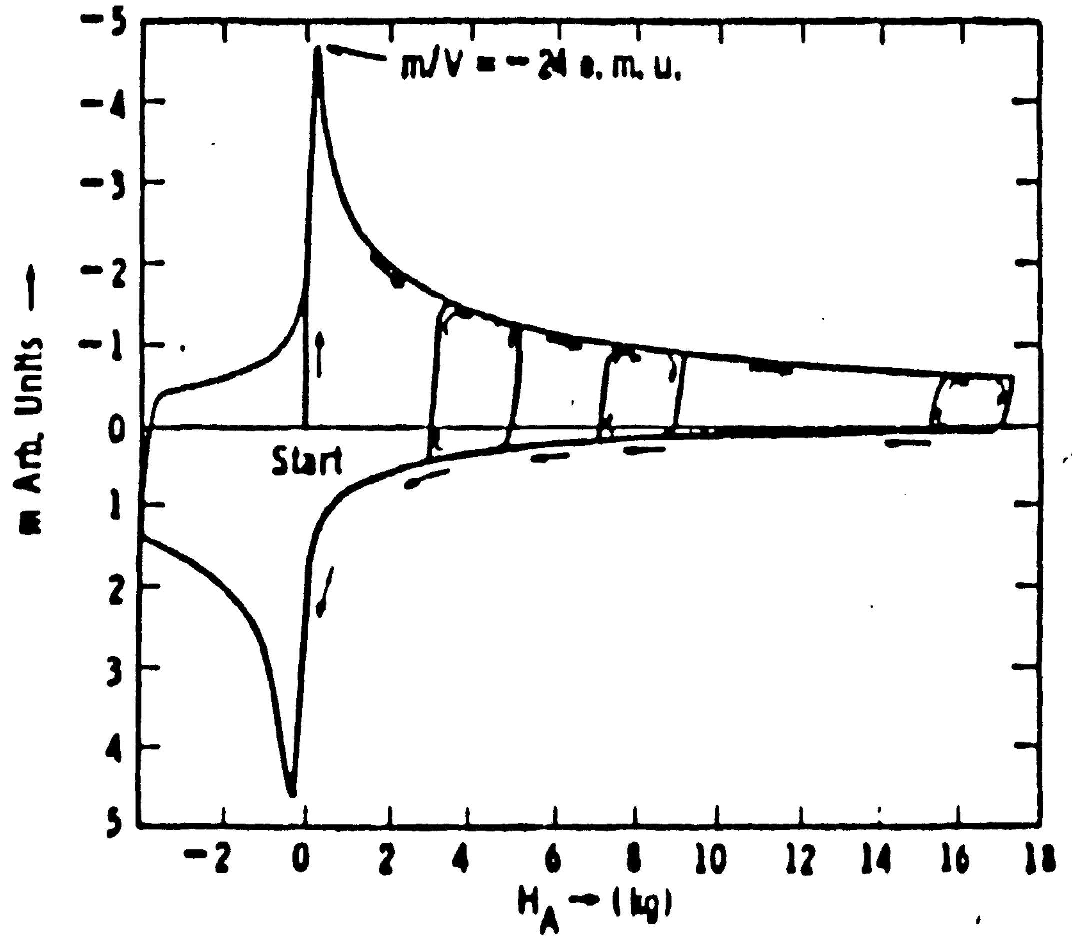

Figure IV.9 Asymmetric magnetization in 1.6-micron NbTi filaments measured by Carr and Wagner, attributed to surface currents.

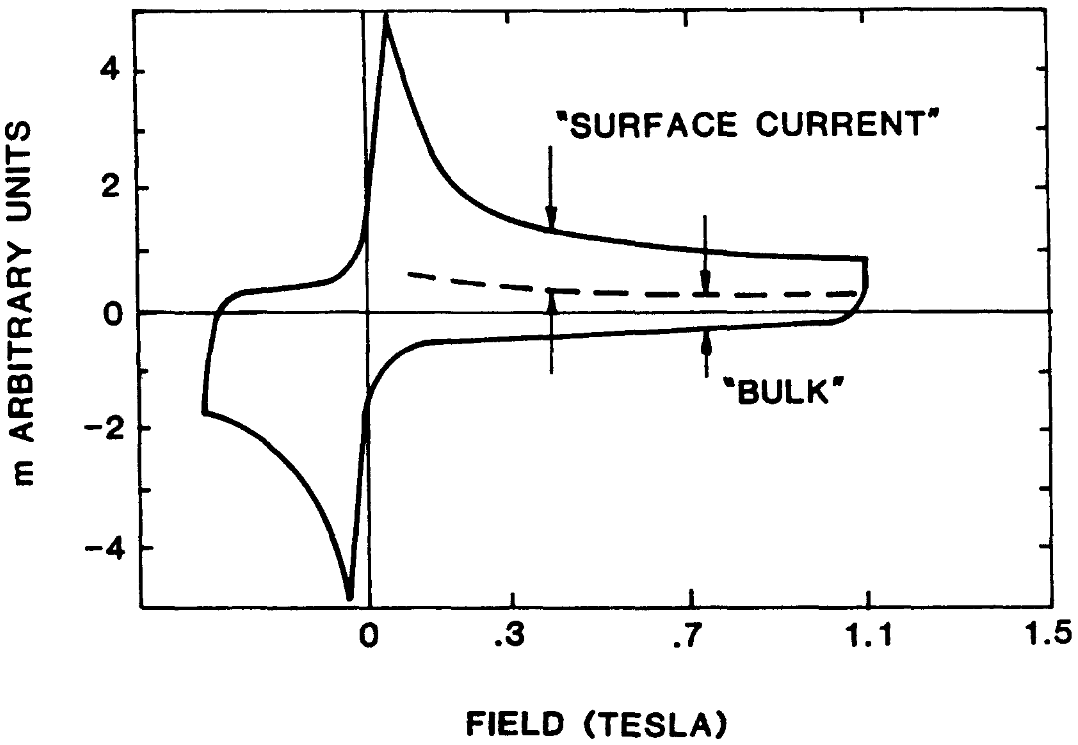

Figure IV.10 Asymmetric magnetization in 1.25-micron NbTi filaments measured by Sampson and Ghosh.

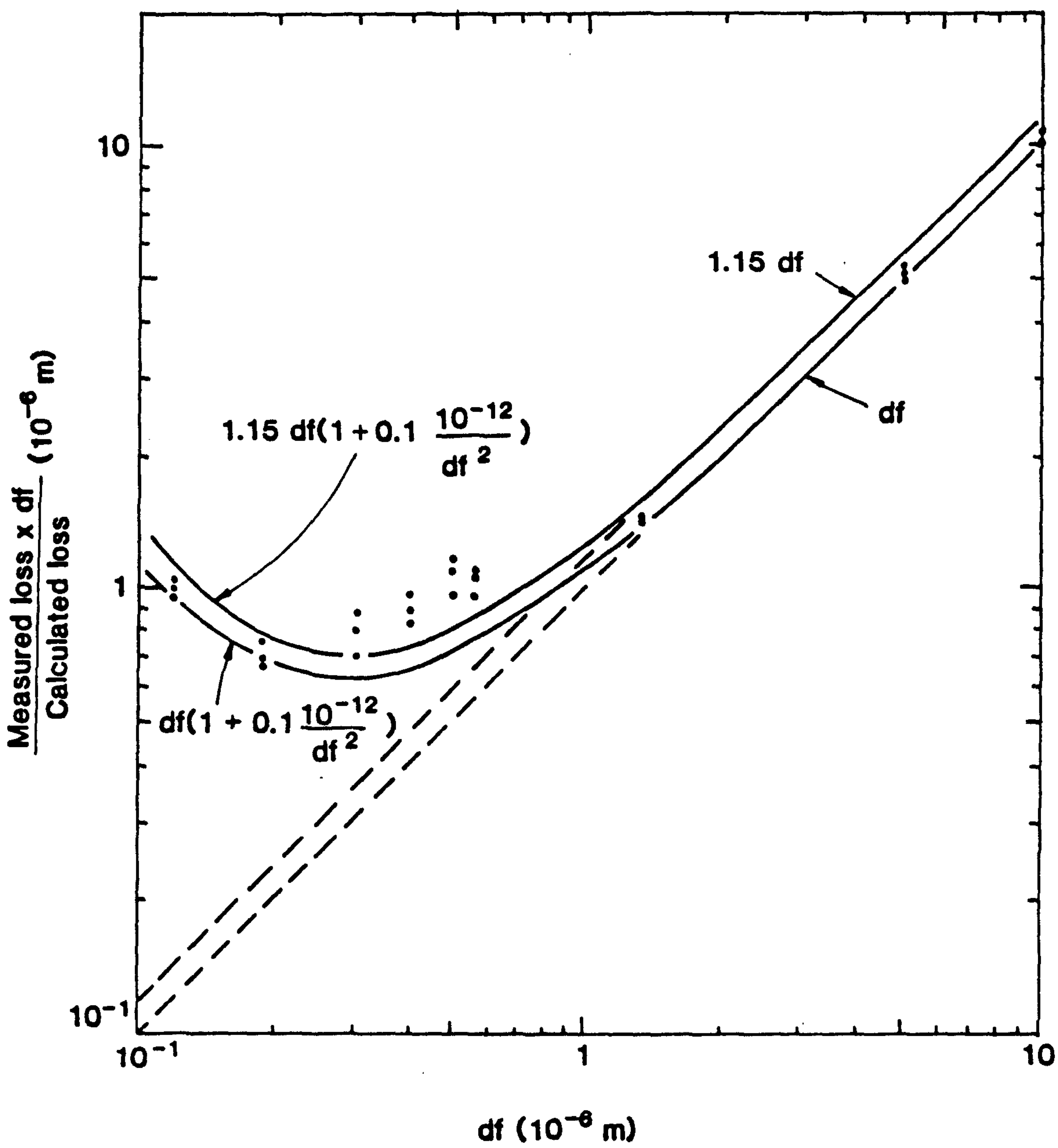

Figure IV.11 Ratio of measured hysteretic losses to calculated hysteretic losses multiplied by the diameter of the filament df for filament diameters ranging from 0.1 to 10 microns.

d. Very recent measurements of total magnetization for fine-filament conductor indicates that in some cases the magnetization is nearly proportional to filament diameter (Ref. 23), as shown in Fig. IV.12. The magnetization curve for the 3-micron material is more symmetric than the curves in Figs. IV.9 and IV.10, which may be due to different superconductor material or processing. The (transport) critical current density of the Furukawa material measured for this figure is greater than 2500 Amp/mm^2 (at 4.5 K, 5 T) for all filament diameters. By contrast, the critical currents of the two samples measured for Figs. IV.9 and IV.10 were lower and decreased with filament diameter. The difference between the bulk properties (magnetization) and the transport properties (critical current) of these materials indicates the importance of good manufacturing processes. Further experimental investigation will be required to resolve the question as to which production techniques result in linear magnetization behavior. For SSC applications, it is significant that the data of Fig. IV.12 establish that linearity is a good approximation down to 3-micron filament diameter.

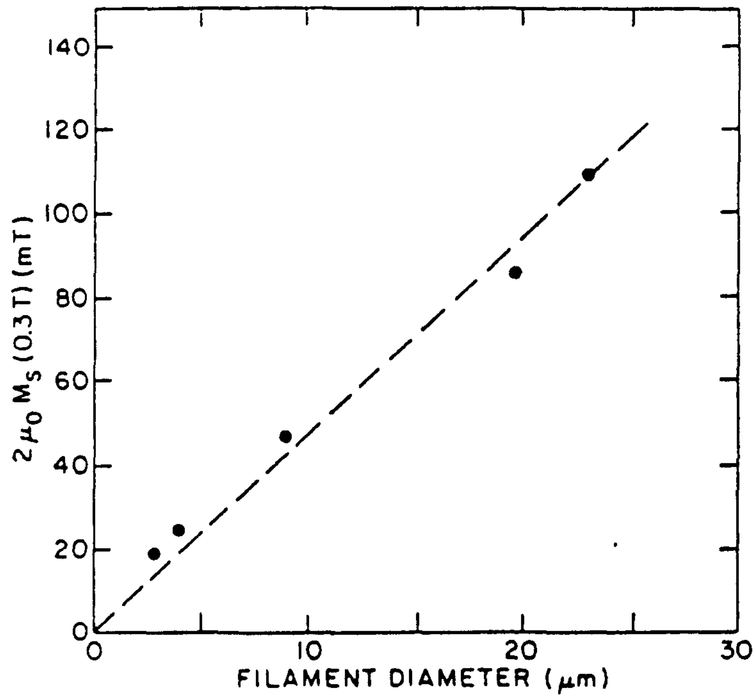

Figure IV.12 Measured magnetization versus filament diameter.

IV.3A Additional Observations of the Effect of filament size on multipole fields.

The dependence of magnetization on filament size and critical current are addressed explicitly in the equations developed by Green (Ref. 16). The multipole coefficients depend on a factor Γ,

$$\Gamma = \frac{2\epsilon\, d_f J_c(B)[1 - J_t/J_c(B)]\beta}{1 + \lambda}$$

where ϵ depends on the penetration, d_f is the filament diameter, $J_c(B)$ is the critical current, J_t is the transport current, β is a coil packing factor, and λ is the copper-to-superconductor ratio.

If this expression correctly describes the multipole amplitudes, then for two coils having identical geometries, but with superconductors of different filament diameters, the relative amplitude of the multipoles should be

$$R = \frac{\Gamma_1}{\Gamma_2} = \frac{\epsilon_1 d_{f1}}{(1+\lambda_1)} \frac{J_{c1}(1+\lambda_2)}{\epsilon_2 d_{f2}\, J_{c2}}$$

There are not many instances where two coils have been constructed in the same forms with very different conductors. One example, however, is in the quadrupoles at Fermilab. Two types of quadrupoles were made in the same form but with different superconductors. One was the main doubler-saver quadrupole, and the other was a special set of low-beta insertion quadrupoles. These coils and some of the measurements of remanent 12-pole were described by Brown, Fisk and Hanft (Ref. 20). See Fig. IV.13. The filament

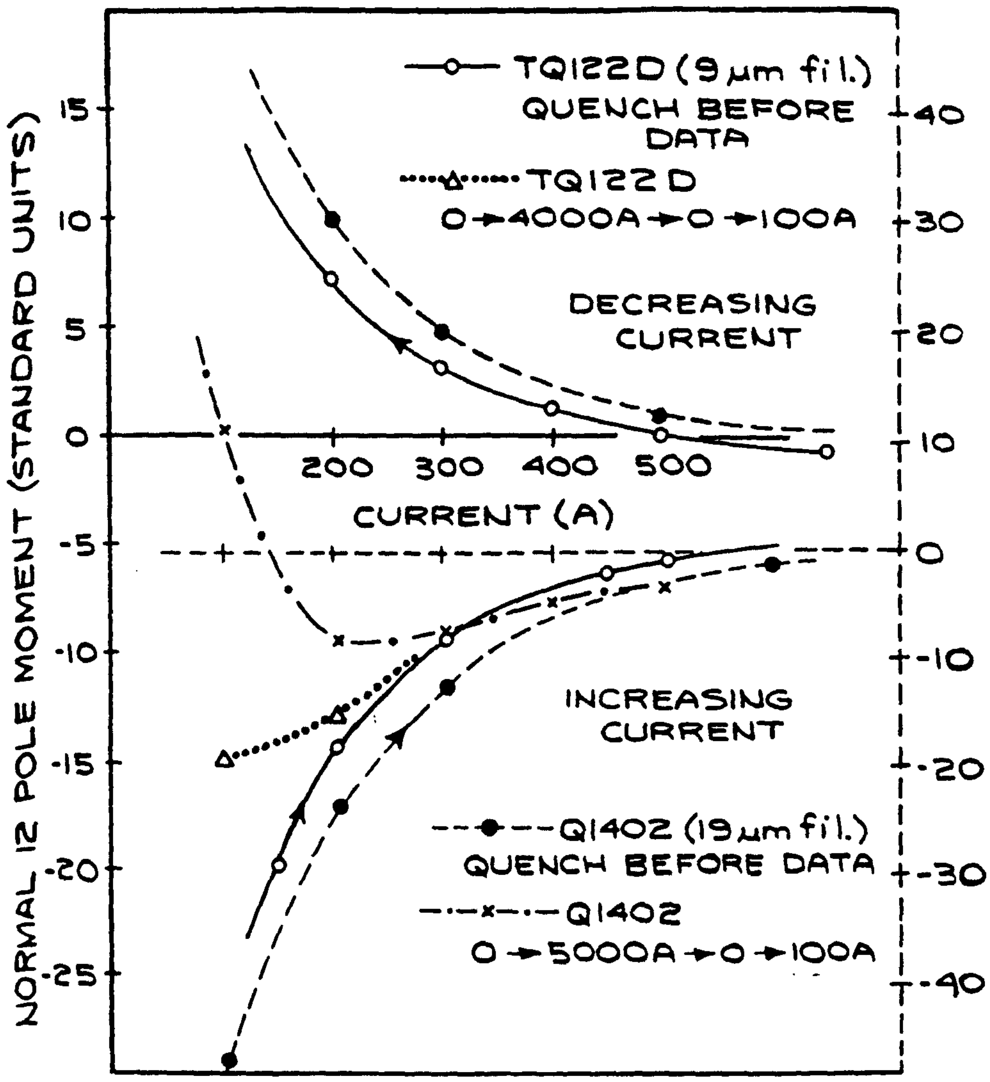

Figure IV.13 Remanent 12-pole magnetization in Tevatron quadrupoles with 9-micron (left scale) and 19-micron (right scale) filaments.

diameter is 8.7 μm for the doubler-saver quads and is 19.3 μm for the low-beta quads. The copper-to-superconductor ratio is 1.8 in the doubler-saver quads and 1.37 in the low-beta quads, and the ratio of critical current densities is 0.933 (21). Plugging these values into the formula above, and assuming $\epsilon_1 = \epsilon_2$, we obtain

$$R = \frac{8.7}{2.8}\,\frac{2.37}{19.3}\,0.933 = 0.356$$

The experimentally observed ratios at 300, 400, 500, and 600 A are 0.36, 0.39, 0.37 and 0.40, respectively, which indicates that the theory is quite reasonable.

This comparison is expected to be valid where saturation of the superconducting filaments is complete, a condition that is satisfied above 300 A. Note that in making the comparison at a fixed current and field the quantity $(1 - J_t/J_c(B))$ has been neglected. This value is nearly unity at low fields in any case, but is in fact slightly different for the two quadrupoles mentioned here.

A similar comparison can be made for the magnetization in two similar conductors used for the construction of 3.2-cm-bore dipoles at Brookhaven National Laboratory (22, 23). The measurements are given in Table IV.5.

Table IV.5
Measured Magnetization Multipoles and Conductor Characteristics for 3.2-cm Dipoles.

	CBA NbTi (6 bores)	HiHo NbTi (2 bores)
Magnetization sextupole $-b_2$ at 0.3T	-30.0 ± 1.6	-63.1 ± 1.1
Magnetization decapole $-b_4$ at 0.3T	8.0 ± 0.9	16.8 ± 0.5
I_{ss} at 5T (kA)	5.56	7.30
Cu/SC	1.7	1.3
fil diameter (μm)	9	21
$2\mu_0 M_s$ at 0.3T (mT)	47	85

The observed ratio of the multipoles for the two conductors is 2.1 ± 0.1. Using the measured magnetization, this ratio is predicted to be 2.1, in good agreement. However, critical currents measured at 5T predict a ratio of 3.0, indicating that the shape of the I_{ss} vs. B curve is not the same for the two conductors.

IV.4 Comparison of theory with experimental data.

In reference (16) good agreement is shown between the calculations done by Green and measurements made with the BNL-CBA magnets in the low-field region, below 0.4 tesla. Since then, comparisons have been made with other accelerator dipoles and to considerably higher fields.

a. Tevatron dipole--Brown, Fisk, Hanft (20).

Figure IV.14 shows the theoretical calculation for the Tevatron dipole and measured data on the remanent sextupole field. The calculation uses magnetization data from Ghosh and Kuchnir (Fig. IV.1) for the cable used in construction of the magnet. The filament size is 8.7 microns. The calculations are carried out in a manner similar to that of M.A. Green except that the product $\epsilon(B)J_c(B)d_f$ is replaced by $\frac{3}{2\pi}M(B)(1+Cu/SC)$.

b. LBL-SSC model magnet D-12C-2.

Figure IV.15 compares the calculation of the sextupole harmonic, b_2, for an LBL-SSC model D(4 cm) magnet with 20 μm filaments with measurements of a model magnet with such a conductor (Ref. 26). As can be seen, the agreement is good below 0.4 tesla, but at higher fields the calculation slightly overestimates the effect. Figure IV.16 displays the same data in a different form; the absolute difference in sextupole field in the increasing and decreasing field directions is shown. Again it can be seen that the agreement is quite good below 0.4 tesla, but that the theory gives an overestimate at larger fields.

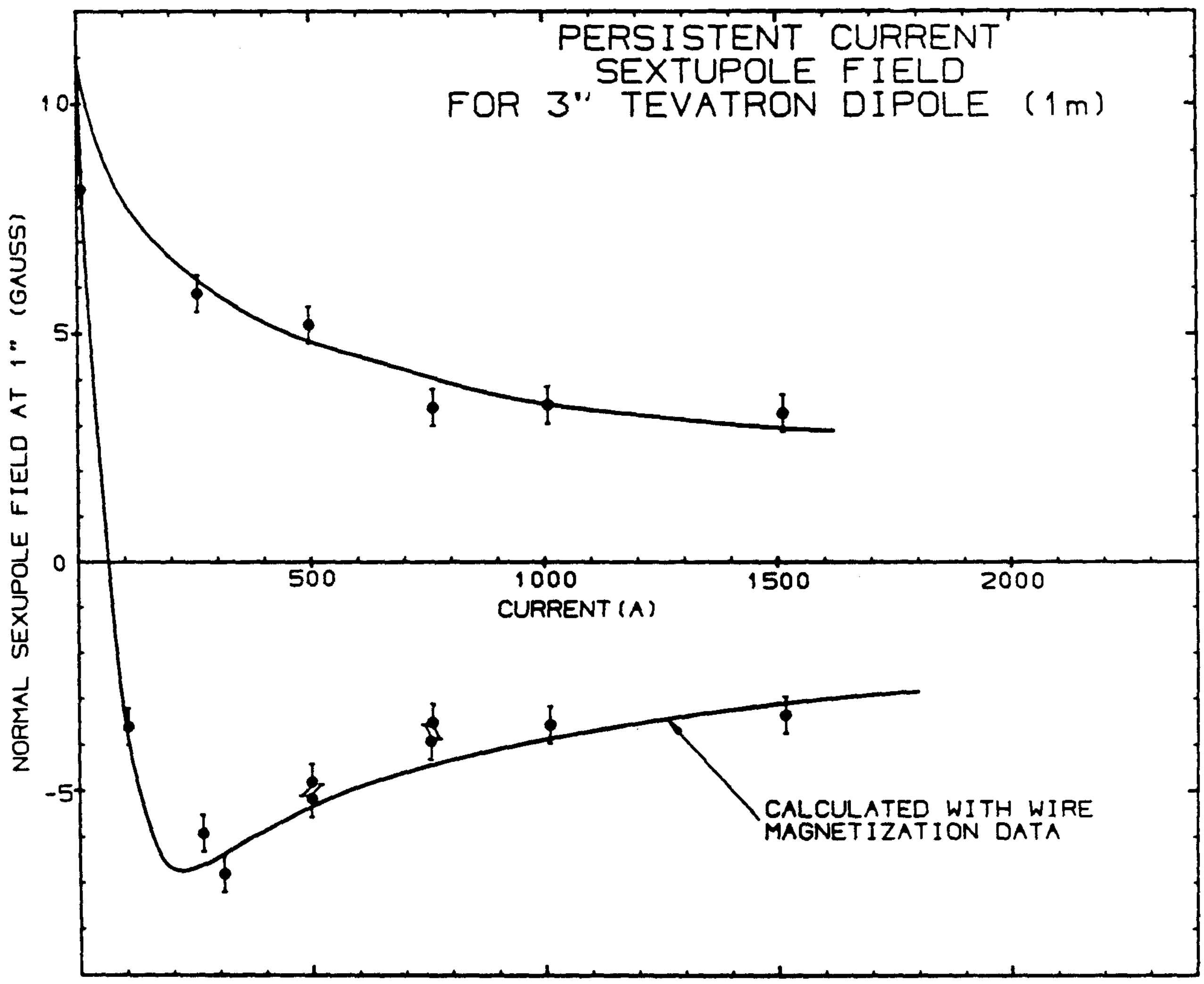

Figure IV.14 Measured and calculated persistent-current sextupole strength in Tevatron dipoles versus dipole current. The dipole strength is 1.0 tesla at 1,000 amperes.

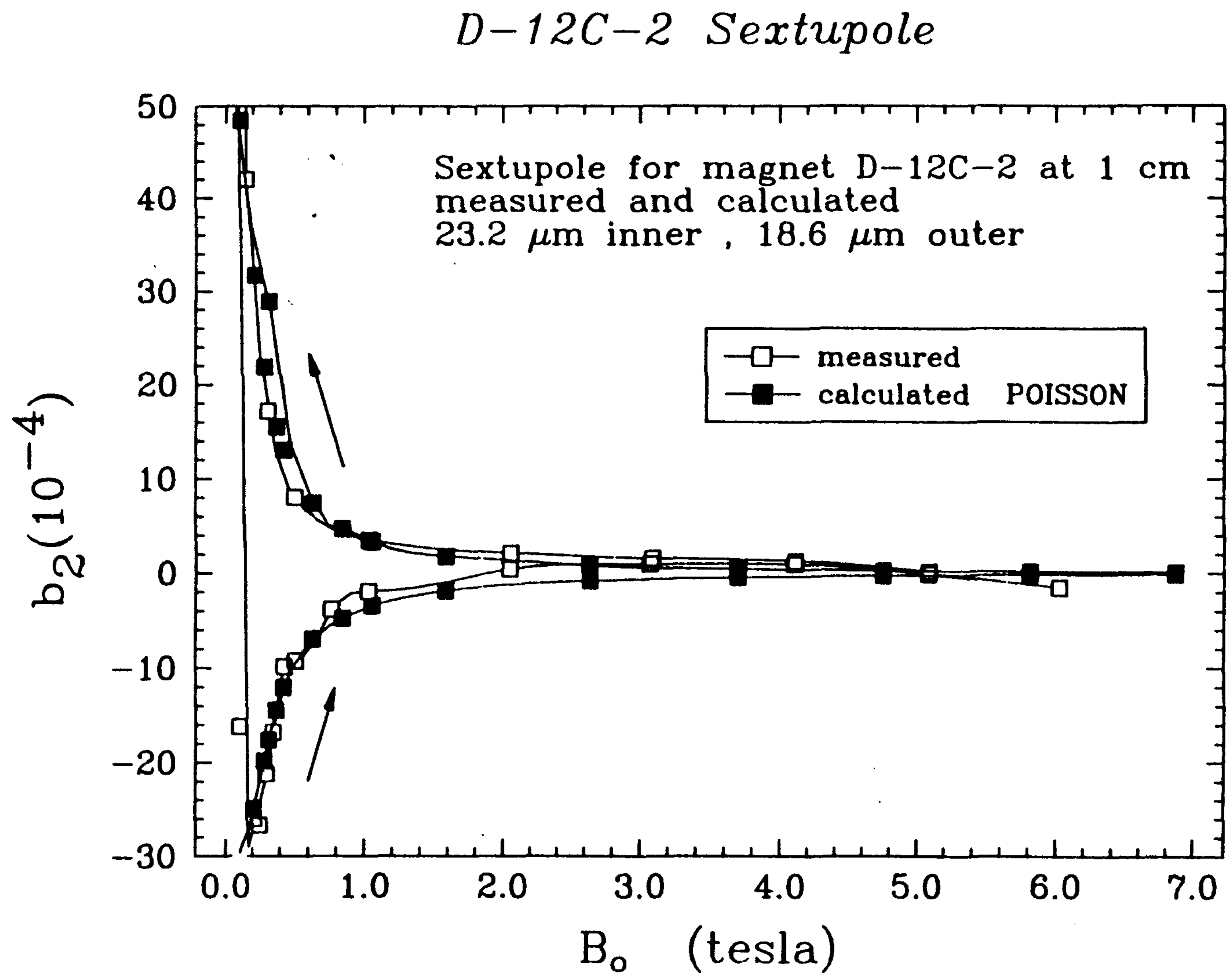

Figure IV.15 Measured and calculated persistent-current sextupole coefficient for the LBL model magnet D-12C-2 (D(4 cm) design).

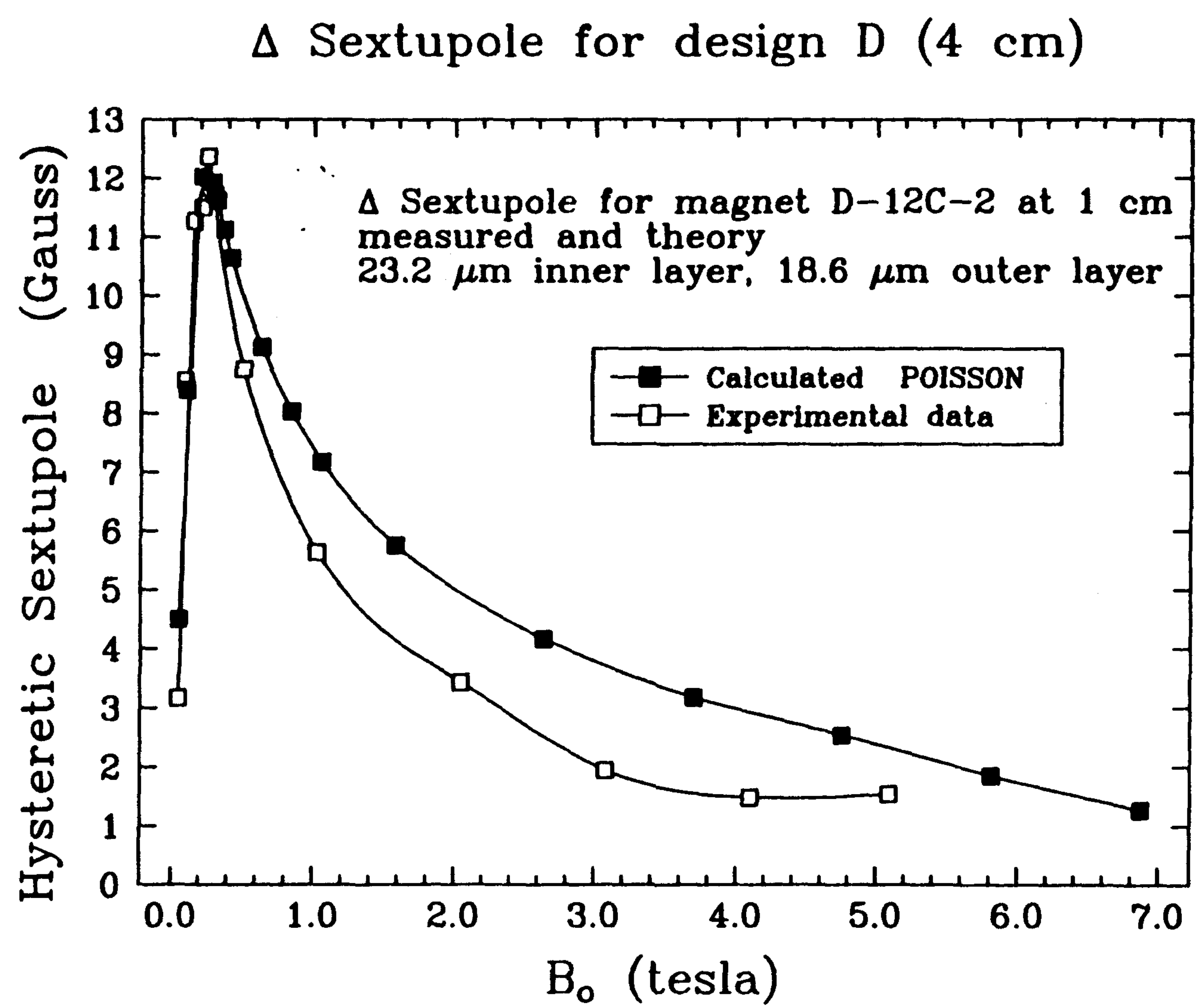

Figure IV.16 Measured and calculated persistent-current sextupole strength at 1 cm for the LBL model magnet D-12C-2. Same data as in Figure IV.15 displayed in a different form.

Calculations of magnetization effects using the Program POISSON have been made by S. Caspi (Ref. 24) for increasing and decreasing fields between 0.05 and 6.9 tesla with the resulting sextupole and decapole harmonics being compared with magnetic measurements. The steps needed to use POISSON to calculate the magnetization effects in this dipole magnet are as follows:

1. The M-H curve for the superconducting cable used was measured at BNL by Sampson and Ghosh, up to a field level of 3.2 tesla. This curve is similar to Fig. IV.1 and appears as the solid squares in Fig. IV.17.

2. The M-H curve was extrapolated from 3.2 tesla to the magnet's peak field of 7.0 tesla using the proportionality between magnetization and the conductor's measured critical current density. These values also appear as solid squares in Fig. IV.17 and are magnetization values with no transport current.

3. A dilution factor is introduced to account for the insulation, air spaces, and materials other than the superconductor and copper.

4. Certain geometrical corrections are introduced for different filament sizes and different copper-to-superconductor ratios.

5. A transport-current correction is introduced. At the magnet short-sample limit, the transport current is 100 percent of that possible, so that the magnetization is zero (at 7.0 tesla here).

6. The magnetization curves for the inner and outer cables, with transport current, are shown in Figures IV.17 and IV.18 for LBL magnet D-12C-2, which is a D (4 cm) magnet.

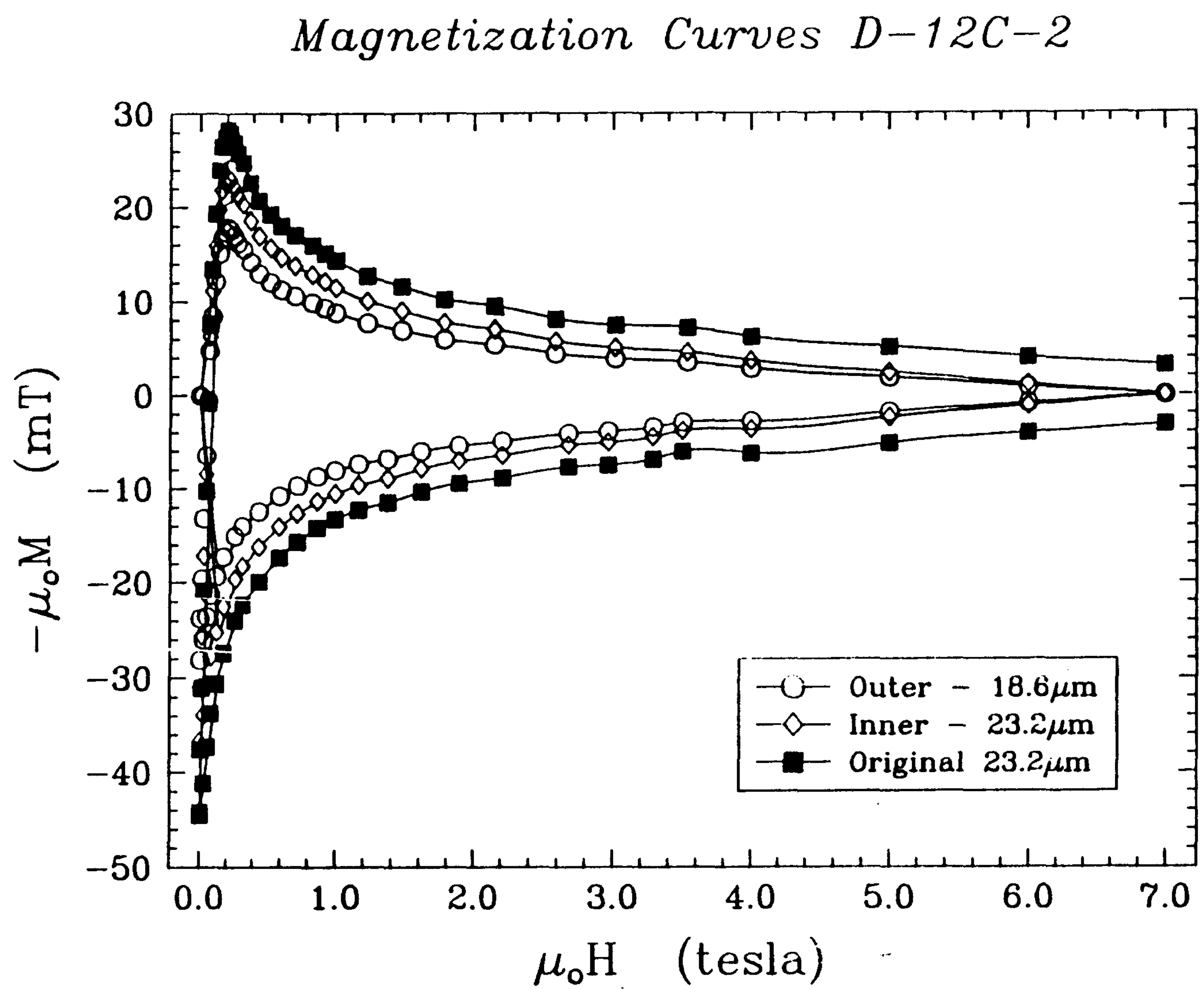

Figure IV.17 Magnetization curves for the cables used in LBL model D-12C-2. The "original" curve up to 3.2 tesla is the wire-magnetization data (no transport current) measured by Sampson and Ghosh. The "outer" and "inner" curves are corresponding magnetization curves for the parameters of the outer and inner coils, including transport current.

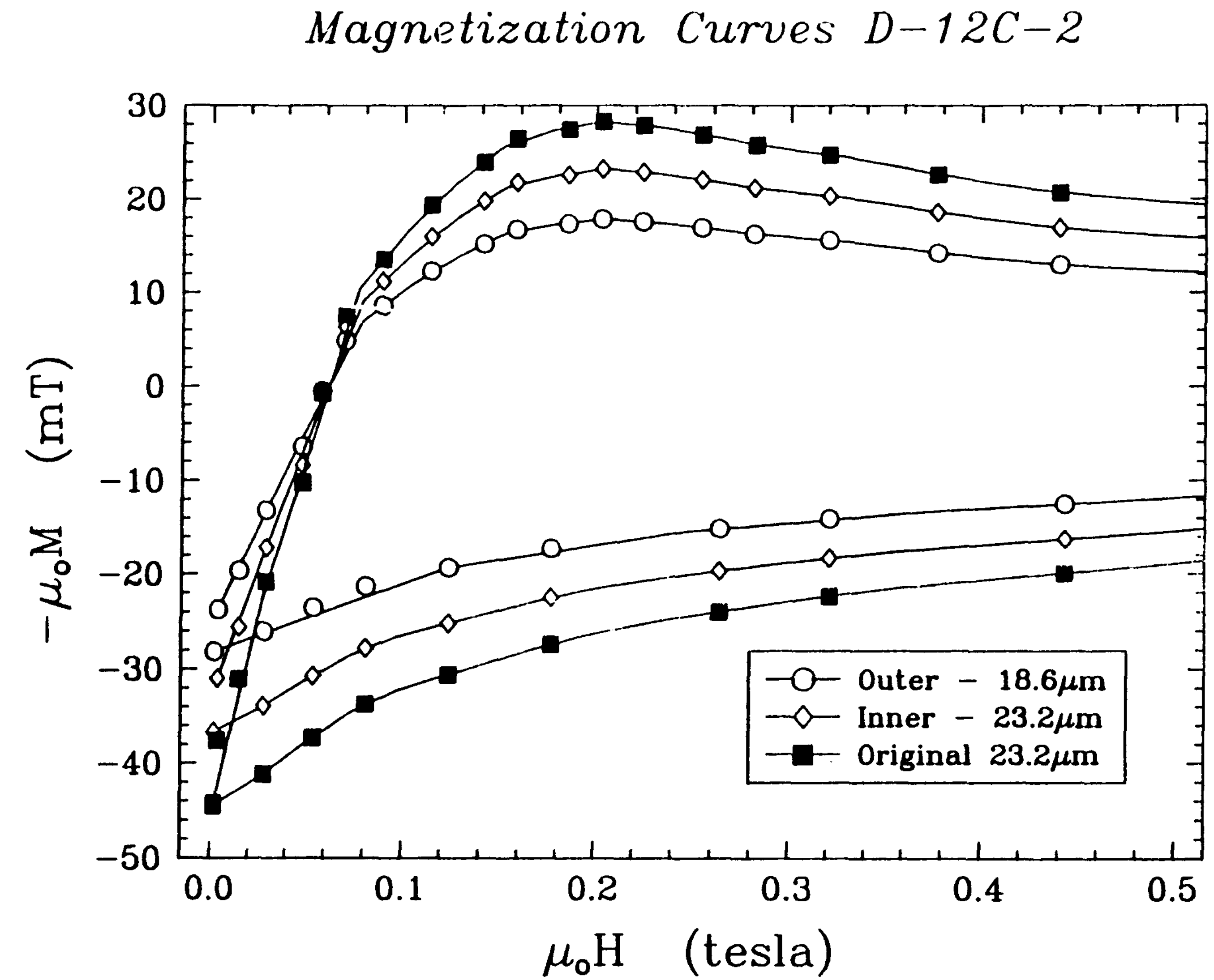

Figure IV.18 Magnetization curves for LBL model D-12C-2. The data of Figure IV.17 shown with an expanded scale.

7. Finally these corrected magnetization curves are transformed into a "μ" table for the superconductor. POISSON then treats, in a self consistent way, the superconductor as a special type of iron and calculates the magnetic field and magnetization induced multipoles within the magnet aperture.

The magnetization decapole is much smaller than the sextupole so that the decapole measurement and calculation are both close to the limits of experimental error and computer precision. Figure IV.19 shows reasonably good agreement between the measured and calculated decapole harmonic, b_4. The same data are displayed as hysteretic decapole in Fig. IV.20.

c. Improvements of theoretical models.

There are modifications that are being made in the theoretical models to describe more closely the details of the magnet construction and to tie together the measured magnetization data with the flux penetration model:

1. M. Green model. More detailed models for surface current and filament flux penetration have been incorporated. Changes are being introduced in the assumed superconductor low-field critical-current densities to make them consistent with the measured magnetization. Past calculations require the same superconductor for the inner and outer magnet layers so that graded magnets had the properties of the two layers averaged. Different superconductor properties can now be used in different coil regions, and new calculations will be done shortly.

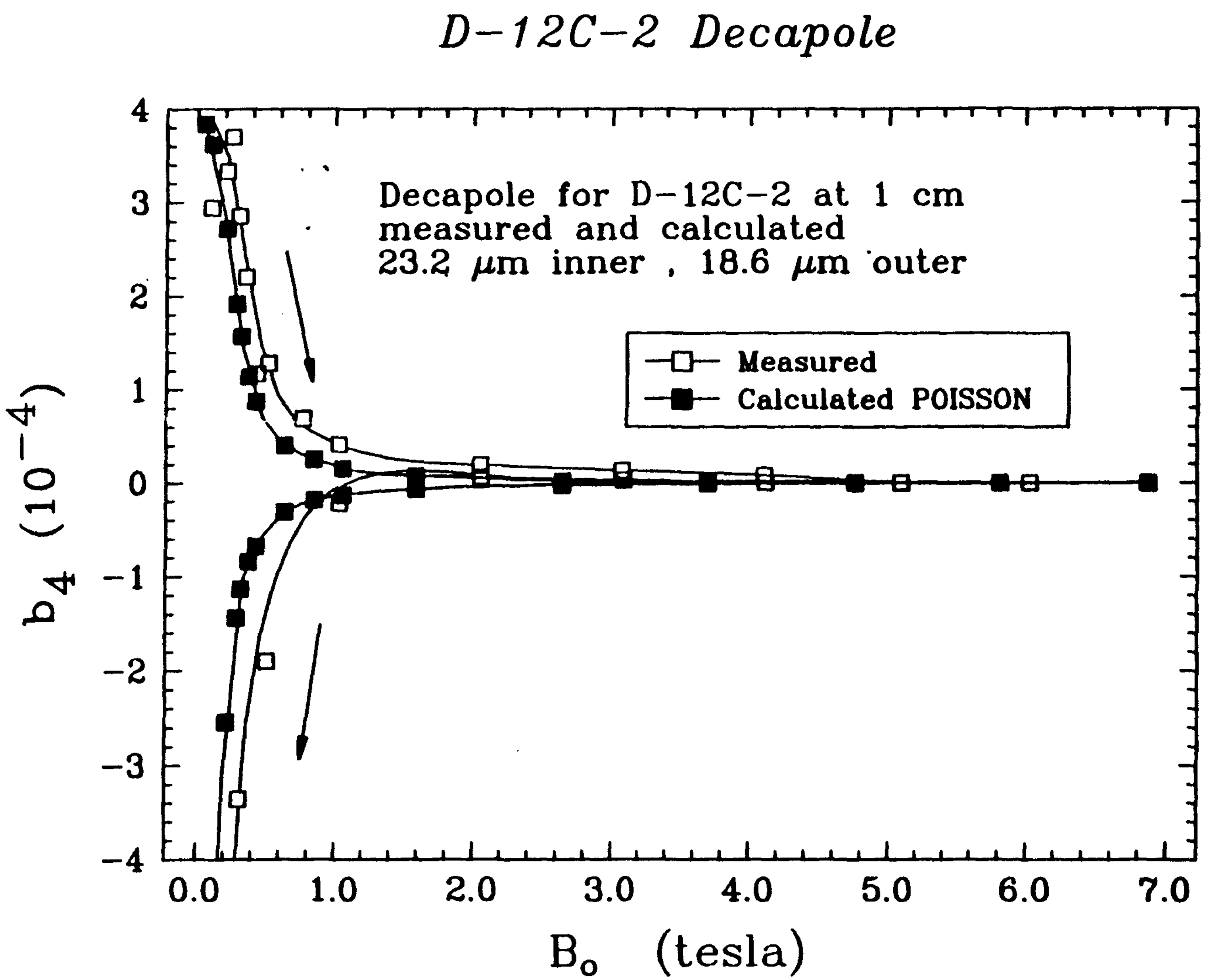

Figure IV.19 Measured and calculated decapole coefficient in LBL model D-12C-2.

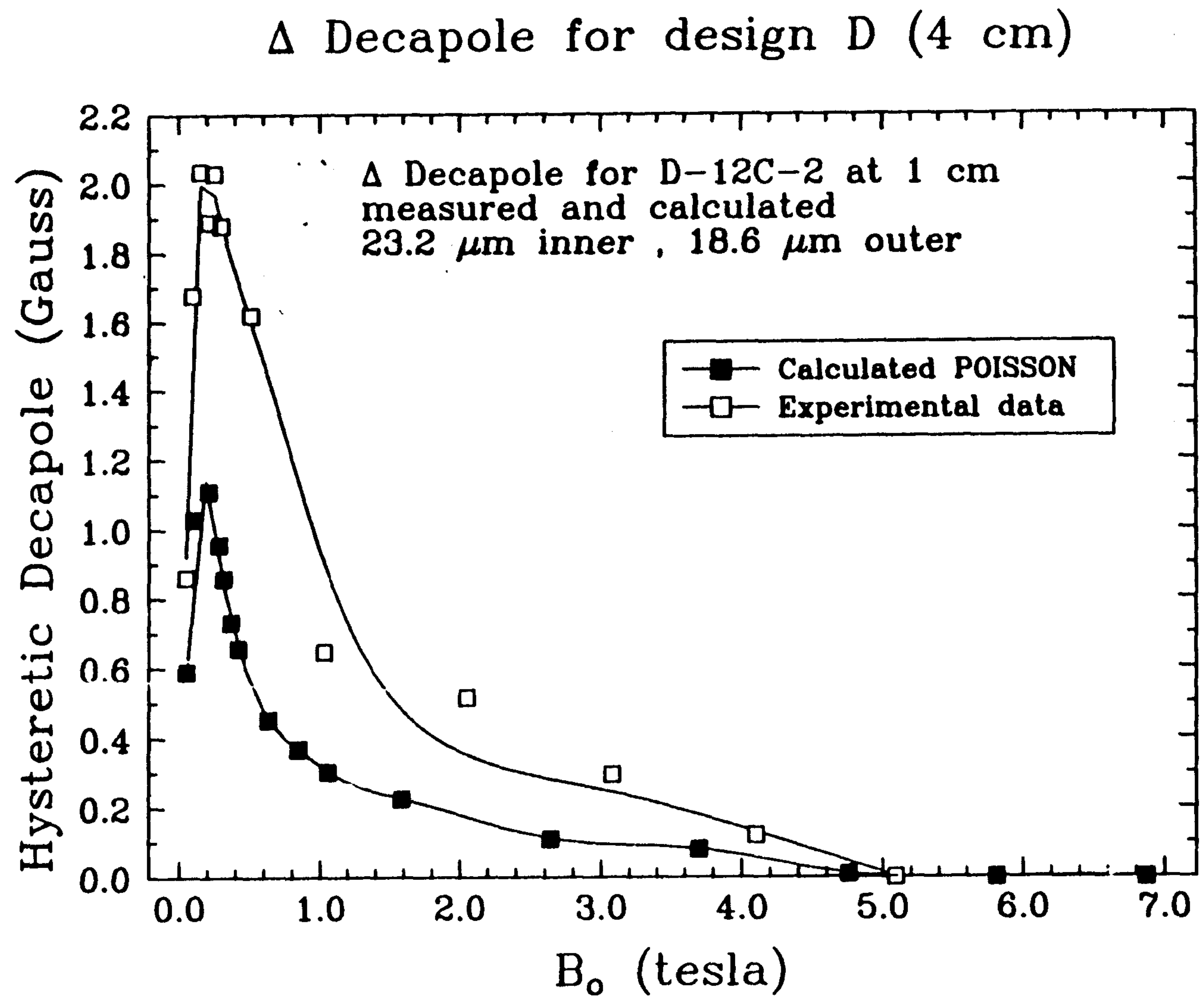

XBL 858-3193

Figure IV.20 Measured and calculated decapole strength for LBL model D-12C-2.

2. POISSON method. A variety of detailed but small geometrical corrections are required to use properly the directly measured magnetization curves in the POISSON program. This procedure has produced reasonable agreement between magnet experimental magnetic measurements and predictions from this program.

IV.5 The Variation in Remanent Field Strength at Low Fields

W.V. Hassenzahl

The variation in remanent field strength at low fields will limit the effectiveness of driven, series-connected correction coils and other correction methods (discussed in Section IV.6) that correct only the average error fields. It would be useful if we could understand the variation in persistent-current magnetization in terms of available data on critical current density.

Data are available on the remanent magnetic fields at 0.7 tesla of the Tevatron dipoles and on the critical current density J_c at 5 tesla of the conductor used for these magnets. We will compare these two independent measurements to determine the correlation between variations in magnetization and in critical current density. The rms variations are used as monitors because data are not available as to the J_c values of the conductors in the individual magnets.

The rms variation in the remanent sextupole field is about 9% for Tevatron dipoles with a roughly gaussian distribution (27) as shown in the solid curve of Figure IV.21. This variation is presumably produced by the variation in critical current density at low fields. However, measurements of the 5-tesla critical currents of all the billets used to make the Tevatron conductor indicate an rms variation of only 4.5% to 6.5% (Ref. 28 and 29), as illustrated in Figure

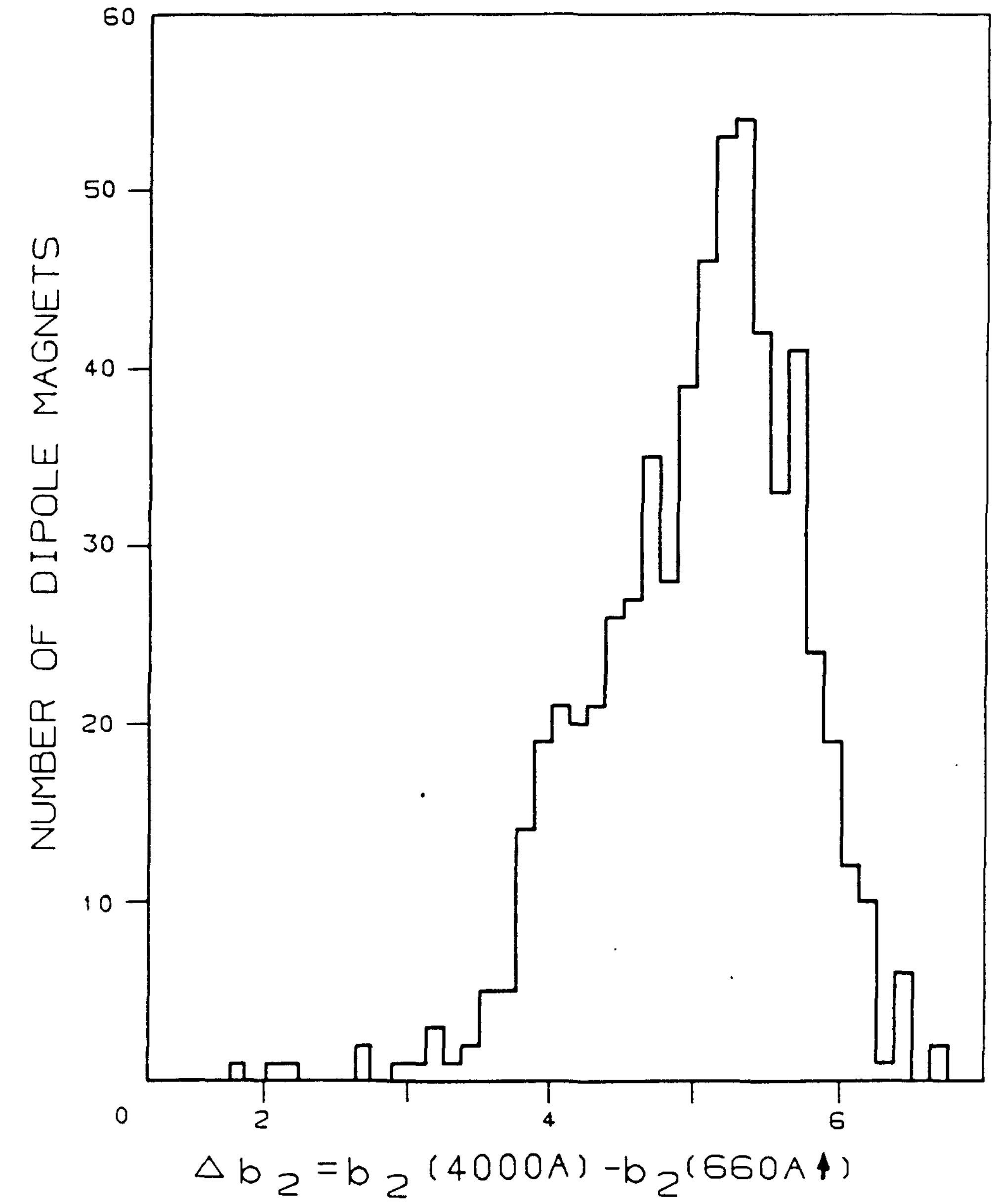

Figure IV.21 Variation in the remanent sextupole field in Tevatron dipoles. The rms variation is 9%. About 600 magnets were included in this sample. (Some 300 were excluded because they showed a systematic variation or because their data were suspect.)

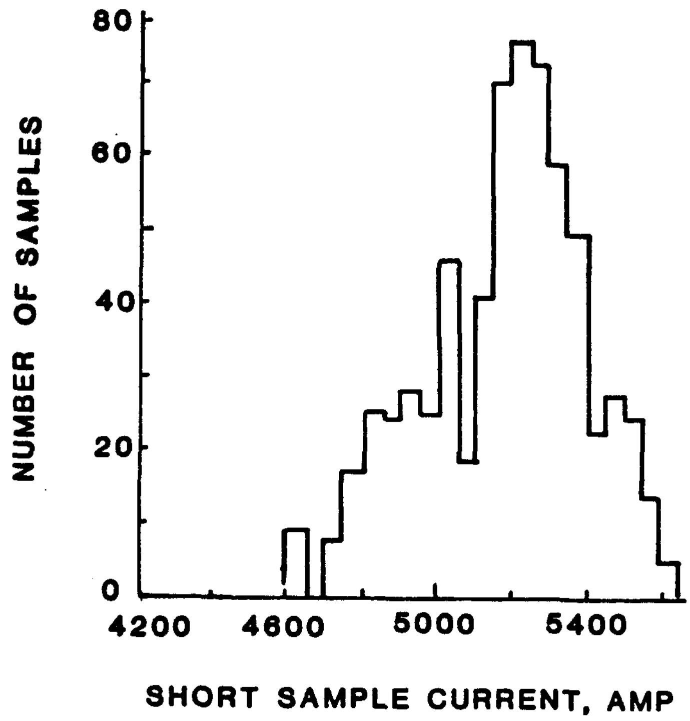

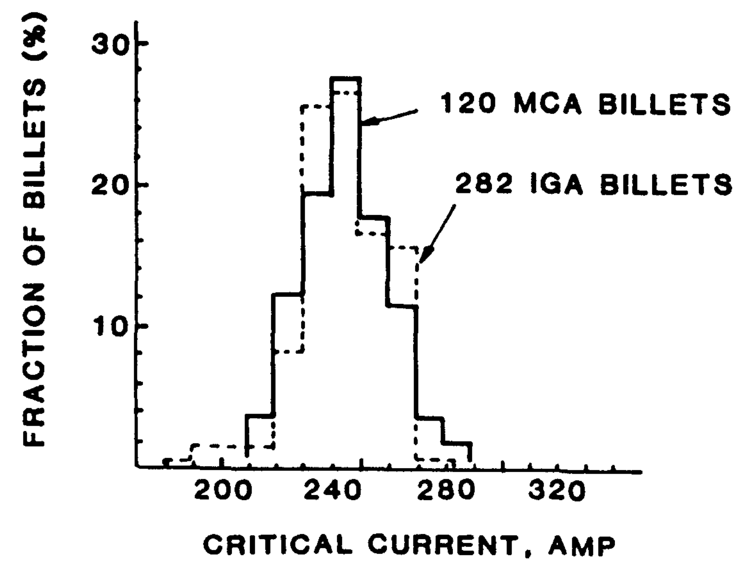

Figure IV.22 Variation in critical current density at 5 tesla. The top distribution is for cable used in Tevatron dipoles (Ref. 28); the rms variation is 4.5%. The bottom distribution is for CBA cable (Ref. 29); the MCA billets have an rms variation of 6.6% and the IGC billets 6.5%.

IV.22. Tannenbaum et al (29) present data at resistivities of 1.3 x 10^{-11} ohm-cm and 10^{-12} ohm-cm. Although both the mean critical current and the absolute variation are greater by about 14% at 10^{-11} ohm-cm, in each case the rms variation is about 6.5%. All of these variations in critical current density are considerably smaller than the 9% variation in the magnetization.

This difference between the variations in remanent field strengths and critical current data cannot be completely explained at present. It is possible, since good critical current data does not exist at low fields, that the variation in J_c is much larger at 0.7 T than at 5.0 T.

In the summary Table S-1 (pp. 4 and 5) of projected rms variation of multipole strengths for SSC magnets, a 10% random variation in magnetization fields has been used. This variation may be too large, since there were no specifications for magnetization at low fields in procurement of Tevatron conductor. With proper attention to manufacturing techniques, the variation in magnetization could very well be smaller.

IV.6 The Effect of Temperature Variation Along a String of Magnets on the Remanent Sextupole Component.

W.V. Hassenzahl

For this evaluation we use the measurements of the residual sextupole component as a function of temperature described by Wanderer (30). This effect is the direct result of the change in critical current in the superconductor as a function of temperature. At 3.7 K, the residual sextupole b_2 in CBA dipoles was 55 units, and at 4.83 K, the value was 43 units. This amounts to a 24 percent change, or 21.2 percent per degree.

In the SSC Type A magnet system, there is an allowable variation of temperature in a 10-magnet cell of 0.25 K. The actual variation will probably be less, but we use 0.25 K as a conservatively large value here. This temperature variation implies a 5.3 percent variation in the remanent sextupole field. If the SSC magnets have 10 units of sextupole at injection (of course, this will be corrected to an average value of zero by some method), then the excursion along the cell will vary almost linearly from the low-temperature offset of 0.27 units, to the high-temperature offset of -0.27 units. Thus, the variation in sextupole will be saw-tooth in appearance and will have σ of about 0.15 unit (10^{-4}).

The proposed refrigeration scheme for the Type B magnets is different from that for the Type A magnets. The temperature variation will be about the same magnitude, but over a much longer string of magnets. In addition, the winding diameter is considerably larger for these magnets; thus, the variation in sextupole at the beam will be smaller for the type B system than for the Type A system.

IV.7 Local Sextupole/Multipole Field Correction Methods

W.V. Hassenzahl

Three possible multipole correction schemes have been proposed and tested, though none of them has as yet been fully developed. The first two schemes involve specially-made multipole coils placed inside the main magnet to correct one or more of the multipole components of the field. (Note: We consider below only the sextupole component). In the first case, the correction coil is powered by an external power supply, and in the second it is "self powered" by the flux linkage with the sextupole in the magnetic field. Though we consider here only the case where the correction coil is internal to the main coil, as shown in Fig. IV.23, in fact, for the powered case, it could be external to the main dipole coils. The third approach uses the inherent diamagnetic property of superconducting filaments to produce multipole fields that cancel the fields produced by the persistent currents in the main dipole windings (33). To achieve this result, conductors of the appropriate size and shape are placed inside the bore as shown in Fig. IV.24.

Each of these three techniques is described in more detail below, and then a comparison of the three approaches is given in the final section (Table IV.5).

a. Multipole Correction Coils.

A coil system made of six identical coils with alternating polarity on the surface of a tube produces a nearly pure sextupole field. This field can be made to work in opposition to that of the undesirable sextupole component produced by the dipole.

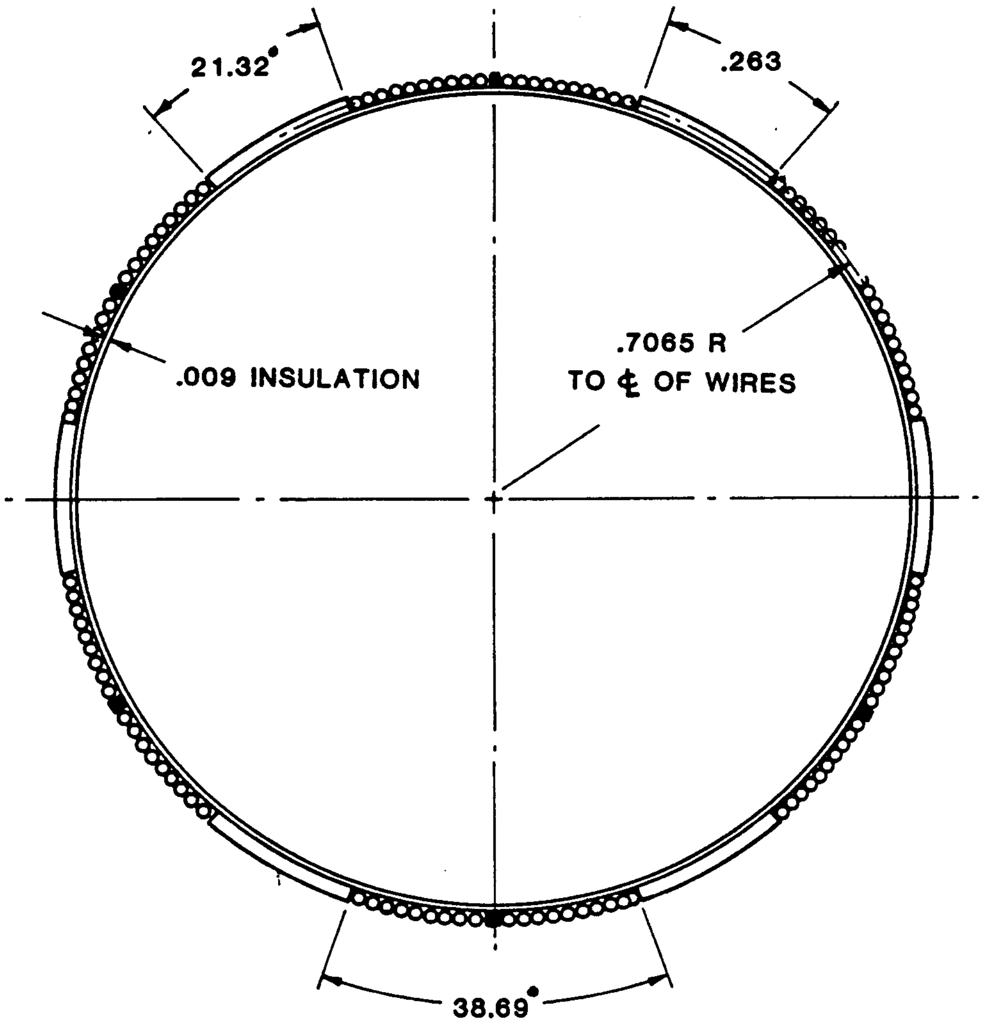

Figure IV.23 Cross section of a sextupole correction coil, driven or self powered.

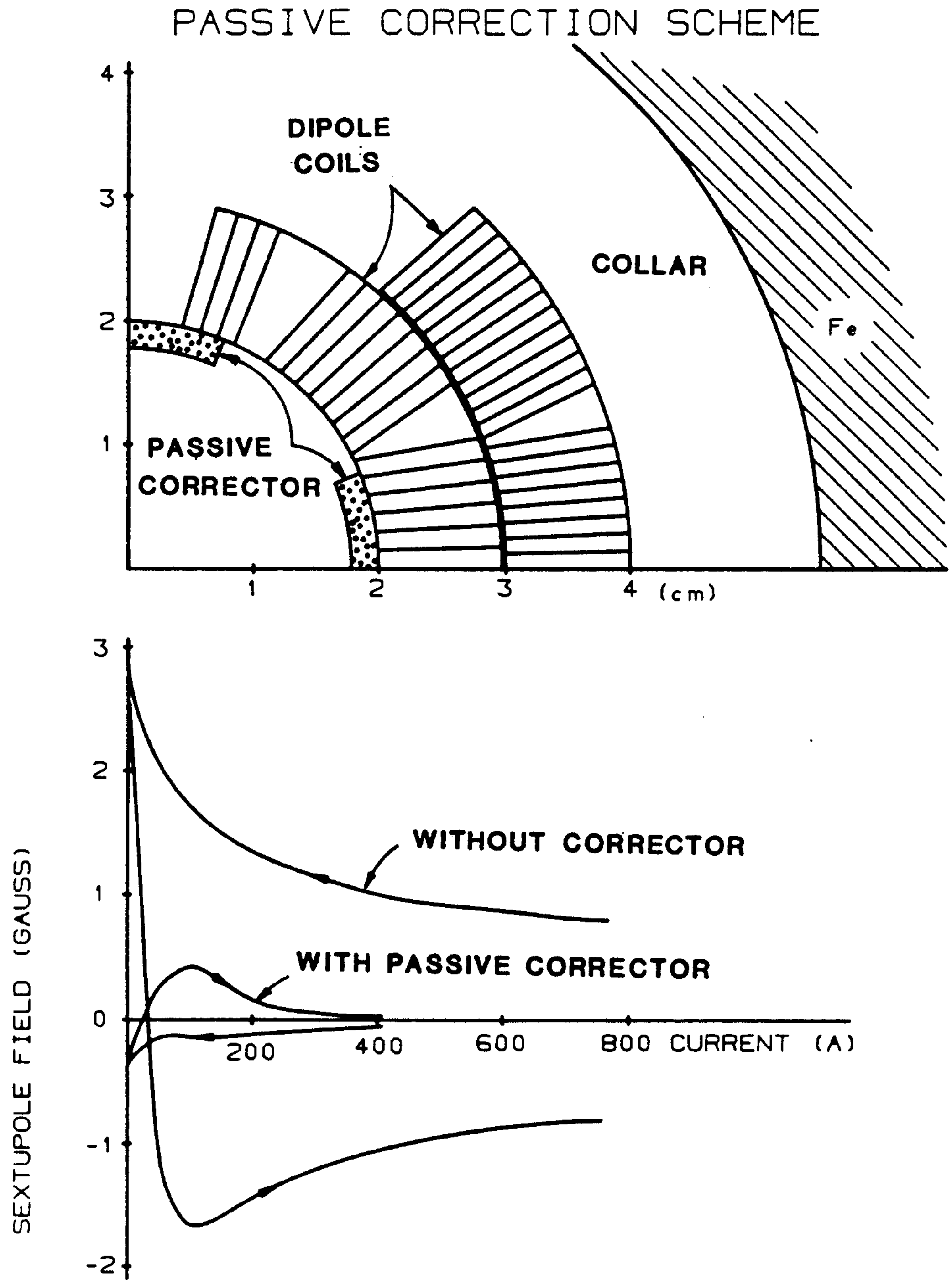

Figure IV.24 (Top) Quadrant of a passive correction scheme in a D(4 cm) dipole. The dotted areas represent the passive correction elements. (Bottom) The calculated persistent-current sextupole strength without and with the passive corrector.

In the case of the externally powered coil, the current supplied to the sextupole coil is adjusted to produce a field that bucks the error sextupole field in the main dipole. This field could be as high as, say, 0.10 percent of the main field, or 65 Gauss at the bore tube for the design A magnets at maximum field. This level sets the limit for the amount of superconductor needed in the correction coils. Noting that the radius of the sextupole coil is about half that of the dipole and that the relative field strengths is 0.1 percent, as mentioned above, about 0.05 percent of the conductor required for the main coil is needed for this type of correction. This is probably smaller than could be fabricated easily. Thus an estimate of 0.2 percent is assumed, giving a safety margin of 4.

The current in this type of coil is varied according to a predetermined plan based on a knowledge of the main-coil error field. Therefore, the fields of all the main dipoles must be measured (at room temperature), and, depending on the accelerator requirements, the dipoles may have to be positioned selectively on the basis of their sextupole component. Every few cells the current ramp in these correction elements would change slightly to maintain the local, average sextupole at zero. This would be accomplished by a pair of current leads and a power supply driven in a predetermined field ramp.

The self-powered sextupole correction coil requires exactly the same quantity of conductor as the driven coil. However, it does not require an external power supply or current leads. Because the driving forces for the current in this coil is the coupling to the sextupole in the dipole, the coil must exhibit essentially zero coupling to the much larger dipole field. This is accomplished by fabricating the sextupole coil as accurately as possible initially, by measuring the dipole component of this sextupole coil, and by minimizing the dipole component by adding a small correction loop.

In this approach, it may be possible to eliminate detailed field measurements of the main dipoles, but all the correction coils must be measured and corrected to eliminate the dipole coupling, unless fabrication and assembly tolerances can be improved considerably over those now available. In addition, because the performance of this system depends on a persistent current joint, which will inevitably have some decay characteristics, both the main dipole and sextupole correction coil must be brought to the normal state after some predetermined operating period. Both coils could then start off fresh, so to speak, at zero current and zero field.

The assembly bore tube for the self-powered coil must be as close to round as possible over its entire length. An error of 0.25 mm can produce an effective dipole area in the coil of almost 10 mm^2 per meter.

b. <u>Passive Internal Superconductor for Multipole Correction</u> In this scheme, the inherent diamagnetic characteristic of the superconductor, which in the main dipole produces the remanent sextupole at low fields, is used to correct this error field. Superconductor that does not carry the main coil current is placed at the inside periphery of the windings in a distribution that cancels the remanent field sextupole. The conductor need not be of the same type as the main dipole conductor but its magnetization properties must be selected for this application.

Because the effect may be considered second order, the quantity of superconductor required to accomplish this correction is larger than for the two previous approaches. On the order of 3 to 10 percent of the main coil superconductor is required, depending on the filament diameters used in the main coils and in the passive corrector. As the effect depends on filament size, the use of larger filaments, assuming critical current can be maintained at the same time, can reduce the total volume of superconductor in the corrector. Of course, in this case, the superconductor must be made especially for the correction element. The design of the correction element must give sufficiently low sextupole at injection.

Of the three types of correction being considered, this approach will require the most extensive research and development program.

c. Costs of Multipole Correction Schemes. The cost of the three schemes for correction are estimated to be between 40 and 65 x 10^6\$ (31,34).

Table IV.6
A comparison of the three schemes for correcting the sextupole components in the SSC dipoles.

	Sextupole Driven	Correction Coil Self-Powered	Passive
Corrects remanent sextupole at injection	Yes	Yes	Yes
Corrects Sextupole due to assembly tolerances and iron saturation	Yes	Yes	No
Requires detailed measurement of dipole field	Yes	No	Yes
Requires magnet selection due to high field sextupole	Yes	No	Yes
Uses spare conductor	No	No	Maybe
Requires high precision assembly	Yes	Yes[2]	No
Requires field measurement of correction element and zero dipole component	No	Yes	NA
Requires power supplies and current leads	Yes	No	No
Special monitoring to be developed	No	Maybe	Maybe
Requires occasional rewarming above T_c	No	Yes	No
Conductor requirement, % of main dipole	0.2	0.2	3-10
Causes physical aperture to decrease or coil aperture to increase	No	No	Yes[2]
Requires precise and rigid support	No	Yes	No

IV.8 Fine-Filament Nb-Ti R and D

R. Scanlan

During 1985 significant progress has been made in establishing the technical feasibility of fine-filament NbTi. Intermagnetics General Corp. (IGC) have produced a .015" diam. wire with 3.7 μm filaments and a J_c value of 2711 A/mm^2 at 5T. Magnetic Corp. of American (MCA) have made a .0045" diam. wire with 4 μm filaments and a J_c (5T) = 2497 A/mm^2, and Furukawa Electric Co, have made a .0089" diam. wire with 2.85 μm filaments and a J_c (5t) = 2380 A/mm^2. These results show that fine filaments are feasible; however, in each case the quantity produced was small, and the process was not production scale. We will now discuss several problems that must be solved in the large scale manufacture of fine-filament NbTi and several R&D programs that are in progress.

Conventional production of Nb-Ti superconductor consists of a hot extrusion (500°-600°C) of NbTi in a copper matrix. During this extrusion and the prior heating of the billet, a layer of titanium-copper intermetallic compound perhaps 1-2 μm thick, can form around the filaments. This brittle intermetallic layer does not co-reduce, and it can become equal to the filament diameter at final wire size; this results in extensive filament breakage and sometimes strand breakage. This problem can be eliminated by enclosing the NbTi rods at extrusion size in a barrier material, such as Nb, which prevents the titanium-copper intermetallic formation. This barrier needs only be 0.1 to 0.2 mm thick, and will be reduced to an insignificant fraction of the filament cross section at final filament size.

Another problem can arise from the introduction of foreign particles during the billet preparation operations. Any "dirt" consisting of micron size particles, or any inclusions of this size in the NbTi rods or the copper components, can result in filament breakage at the final wire size. This type of problem is insidious since processing may proceed successfully until the final wire size in approached. Also, the size of inclusion which is tolerable depends upon the desired filament size, e.g., a one micron diameter inclusion is acceptable for a 20 micron filament, but not for a 2 micron filament. This problem can be eliminated by careful selection of raw materials and by clean room practice in billet assembly.

When a large number of rods are stacked in a billet, as is necessary to achieve fine filaments, a large void fraction is present, and this can lead to non-uniform reduction in the extrusion step. The filaments are necked down locally, and this also leads to filament breakage. This problem can be eliminated by compacting the billet before extrusion.

When these potential problems are eliminated by proper processing and quality control, there is no metallurgical reason why a J_c value of greater than 2400 A/mm^2 cannot be achieved in filaments less than 2.0 μm in diameter. In fact, the increased total reduction in area of the NbTi filaments may mean that it is possible to introduce more heat treat/cold work cycles and hence raise the value of J_c.

We have discussed these potential problems and the proposed solutions with the superconducting materials manufacturers. Several manufacturers have responded with proposals to investigate the production of high J_c, fine-filament Nb-Ti. The deliverable items include material from which we can determine J_c and construct model magnets, and an economic analysis of the fabrication method. The details of these projects are listed in Table IV.7.

The LBL/BNL team is investigating a two-level cable with material from two sources. First, we will process some standard 500-filament material to a wire size of 0.009" diameter; this will produce filaments of about 7 μm diameter. This wire will be used to fabricate a 7-strand cable which will then be used to replace the 0.0255" diameter monolithic strands in our standard Rutherford cable. Next, material from the Supercon R&D program will be drawn, with appropriate heat treatments, to a 0.009" diameter wire with 2 micron filaments. This material will also be evaluated in a two-level cable.

A preliminary estimate of the costs for fine filament Nb-Ti produced by these alternate methods has been made. The rough estimate of the costs of fine-filament Nb-Ti indicates a 15 to 30% premium compared with the costs of conventional 20 μm filament material. More accurate cost information will be obtained at the end of the R&D work (Sept. 1985).

Table IV.7 - Fine-Filament R&D Efforts

Organization	Billet Size & Cu:SC Ratio	Final Wire Size & Filament Size	Quantity	Delivery Date
IGC				
PHASE I	6" Diam. Billet 1.8:1	.0255" Diam. Wire 4μm Filaments	100 lbs.	July 1985
PHASE II	10" Diam. Billet 1.3:1	.0318" Wire 2μm Filaments	400 lbs.	Nov. 1985
	10" Diam. Billet 1.8:1	.0255" Diam. Wire 2μm Filaments	400 lbs.	Nov. 1985
SUPERCON				
PHASE I	12" Diam. Billet 1.3:1	.0318" Diam. Wire 8μm Filaments .009" Diam. Wire For 2-Level Cable 2μm Filament	400 lbs.	Aug. 1985
PHASE II	12" Diam. Billet 1.8:1	.0255" Diam Wire 2μm Filaments	400 lbs.	Oct. 1985
LBL HYDRO-STATIC BILLETS	6.5" Diam. Billet 1.3:1	.0318" Diam. Wire 2.5μm Filaments	200 lbs.	Oct. 1985
	6.5" Diam. Billet 1.8:1	.0255" Diam. Wire 2.5μm Filaments	200 lbs.	Oct. 1985

References

1. R. Hanft, et. al, "Magnetic Field Properties of Fermilab Energy Saver Dipoles," IEEE Trans. on Nucl, Sci., NS-30, 3381 (1983).

2. E. Bleser, et. al. Superconducting Magnets for the CBA Project, Nucl. Inst. Methods A235, p. 435 (1985). BNL Report 34863 (1984).

3. R. Fernow, P. Wanderer, and E. Willen, Private Communication, November 11, 1984.

4. H.E. Fisk, Proc. of the Ann Arbor Workshop on Accelerator Physics Issues for a Superconducting Super Collider, p. 119-123 (1983), M. Tigner, Ed., University of Michigan, Ann Arbor, Michigan.

5. K. Asano, et. al., "SSC Magnetic Field Quality Considerations", Proc. of the 1984 Snowmass Conference on the Design and Utilization of the Superconducting Super Collider; to be published.

6. J. Herrera, et. al. Proc. SSC Accel. Study Conf., Ann Arbor, Mich., Dec 1983.

7. J. Herrera, Proc. Accel. Summer School, Fermilab, 1984.

8. J. Herrera, et. al. "Random Errors in the Magnetic Field Coefficients of Super Conducting Magnets," submitted to 1985 Part. Accel, Conf., Vancouver, B.C.

9. R.C. Fernow and G.H. Morgan, "Coil Design for the 40-mm Collared SSC Dipole (SSC C5)", BNL SSC Tech Note 19, 1984 (unpublished). Reference Design D uses coil cross-section C5.

10 S. Caspi, "SSC 2-in-1 Iron Design", LBL SSC Mag-30, LBID-992, 1985 (unpublished).

11. SSC Reference Design Study, p. 358, May 1984.

12. G.H. Morgan, SSC Tec. Note 23, BNL, Feb 1985.

13. G. Morgan, "Effect of Coil Centering Errors on the Harmonics of SSC-C5", BNL Magnet Division Note 117-1, SSC-MD-90, 1985, (unpublished).

14. L.P. Michelotti and S. Ohnuma, IEEE Trans. Nuc. Sci., NS-30, 4, 1983, p. 2472.

15. R.C. Fernow, "End Multipoles for the 32-mm SSC Dipoles," BNL Magnet Div. Note 102-1, SSC-MD-77, 1984.

16. M.A. Green, "Fields Generated within the SSC Magnets due to Persistent Currents in the Superconductor," Proc. of the Workshop on Accelerator Physics Issues for a Superconducting Super Collider, M. Tigner (Ed.) pp. 126-131 (1983); (see references therein) Univ. of Michigan, Ann Arbor, Michigan.

17. W.J. Carr, Jr. and G.R. Wagner, "Hysteresis in a Fine Filament NbTi Composite," Fifth International Cryogenic Materials Conf., ICMC held in Colorado Springs, Colorado, August 15-17, 1983.

18. W.B. Sampson, 2/14/85, Private Communication.

19. P. Dubots, F. Fevrier, J.C. Renard, J.P. Tavergnier, J. Goyer, and Hoang Gia Ky, "NbTi Wires with Ultra-Fine Filaments for 50-60 Hz use: Influence of the Filament Diameter Upon Losses," ASC 84, San Diego, CA.

20. Brown, Fisk and Hanft, Persistent Current Fields in Fermilab Tevatron Magnets ASC84, San Diego, CA.

21. A.K. Ghosh, private communication.

22. P.J. Wanderer, BNL Magnet Division Note 125-4 (SSC-MD-93), March 1985.

23. A.K. Ghosh, W.B. Sampson, and P.J. Wanderer, "Magnetization, Critical Current, and Injection Field Harmonics in Superconducting Accelerator Magnets," Part. Accel. Conf., Vancouver, 1985, and BNL Report #36628 (1985).

24. S. Caspi, M. Helm, and L.J. Laslett, "The Use of Poisson to Calculate the Effects of Magnetization in Superconducting Magnets, LBL-19810, June 1985.

25. A.K. Ghosh, M. Kuchnir: Magnetic Measurements of Some Superconducting Cables, TM-1286 (Fermilab) Dec 14, 1984.

26. W.S. Gilbert, 2/85, Private Communication.

27. R. Hanft, private communication, 2/85.

28. F. Turkot, W.E. Cooper, R. Hanft, and A. McInturff, "Maximum Field Capability of Energy Saver Superconducting Magnets," IEEE Trans. Nuc. Sci., NS-30, Aug 1983, p. 3387.

29. M.J. Tannenbaum, M. Garber, and W.B. Sampson, "Correlation of Superconductor Strand, Cable, and Dipole Critical Currents in CBA Magnets," IEEE Trans, Magnetics, Mag-19, 3, May 1983, p. 1357.

30. P.J. Wanderer, "Measurement of Magnetization Effects as a Function of Temperature in a CBA Dipole," BNL Magnet Div. Note #58-15 (1984).

31. Goodzeit, 2/15/85, Private Communication.

32. W.A. Wenzel, GIN-246, Oct 23, 1984; GIN-247, Dec 5, 1984; GIN-249, Jan 15, 1985.

33. B.C. Brown and H.E. Fisk, "A Technique to Minimize Persistent Current Multipoles in Superconducting Accelerator Magnets," Proc. Design and Utilization of the SSC, Snowmass, July 1984, p. 336.

34. W.V. Hassenzahl, "Local/Multipole Field Correction Methods", SSC-Mag-45, June 1985.

35. P. Dahl, et al., "Performance of Four 4.5-meter Two-in-One Superconducting R&D Dipoles for the SSC," Proc. of 1985 Particle Accel. Conf., Vancouver, B.C., May 1985, and BNL 36627 (1985).

36. H.E. Fisk, "SSC Magnetic Field Quality Considerations," Proc. Design and Utilization of the SSC, Snowmass, 1984, p. 329.

37. P. Wanderer, BNL Magnet Division Note #149-11, 1985.

38. S. Kahn, R. Gupta, G. Morgan, and P. Thompson, "Comparison of Magnetic Field Calculations to Measurements on a CBA 2 in 1 Magnet System," 1985 Particle Accel. Conf., Vancouver, B.C., and BNL Report #36625 (1985).

39. G. Morgan, private communication.

40. S. Pissanetsky, TAC-1218/84.

41. S. Pisanetsky, TAC-384/21.

42. S. Pissanetsky, TAC-1084/01.

Appendix A

Correction For Saturation in Superferric Dipoles

W. A. Wenzel

Efficient use of the steel required in all active designs for the SSC dipoles must accommodate the saturation characteristics. We have found that this is feasible with a rectangular aperture, so that at all field levels now under consideration the steel can be used to make substantial savings in superconductor requirements. There is a well defined transition at about 2T between current distributions characteristic of low-field (ferric) operation and high-field (super) operation. The former requires a rectangular coil, and the latter implies a rectangular equivalent of the well known $\cos\theta$ distribution for the non-ferric designs. In the transition region the higher multipoles in the field are small. In principle, therefore, the two current distributions may be optimized separately in the asymptotic regions to produce an overall design with excellent dynamic range. In the simulation studies described below the low-field rectangular current distribution is supplemented by correction currents that effectively transform part of the distribution to the appropriate high-field configuration.

A. Conductor Shaping

Figure A.1 shows quadrants for three geometries that have been simulated using POISSON for 1010 steel. In the $1 \times 2\text{-in}^2$ rectangular aperture, the field multipoles were obtained on a circle of radius 1cm. At each dipole field the sensitivity of each multipole to each correction current was obtained as a derivative based on linear differences. The validity of the linear approximation was checked using redundant information. For the configuration of Figure A.1a at an intermediate field value (2.7T) a linear

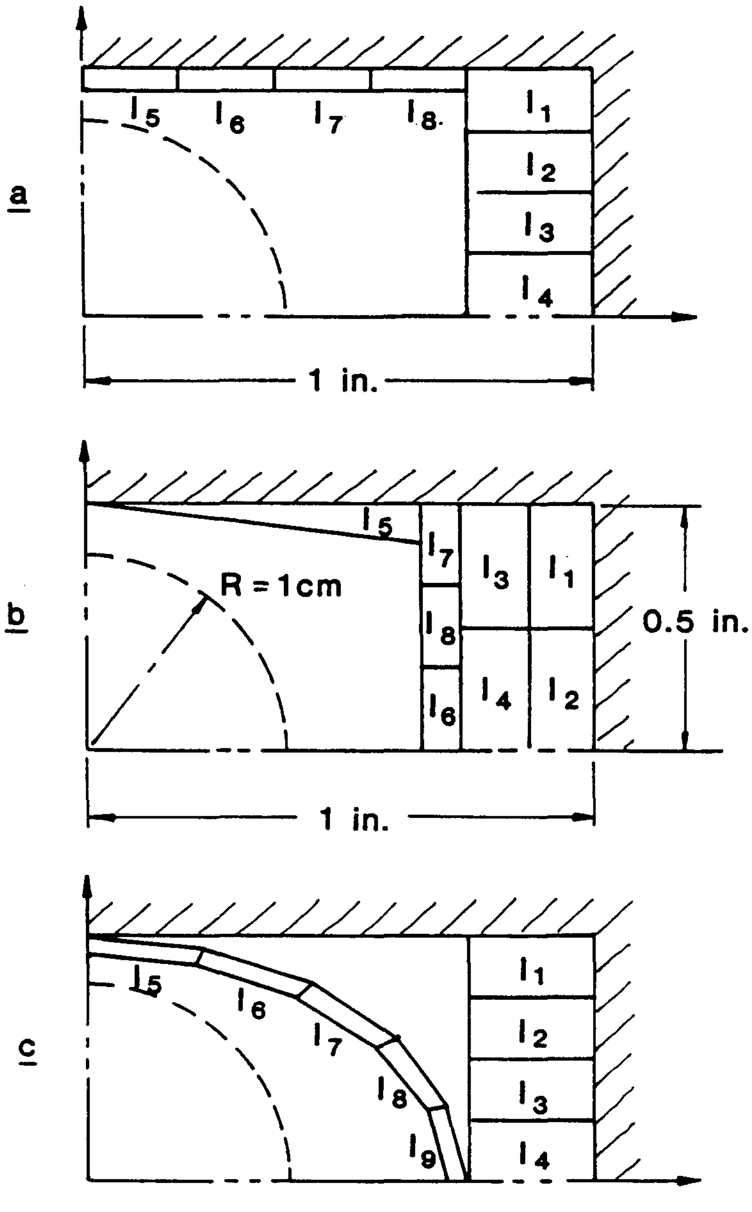

Figure A-1. Three correction-current configurations for a picture-frame superferric magnet.

matrix equation was solved to obtain uniquely the four correction currents which gave zero values for the four multipoles b_2, b_4, b_6, and b_8. At other dipole fields (2.0, 3.2, 3.7 and 4.1T) the same ratios were preserved among the four correction currents as the total correction was adjusted to eliminate the sextupole. Table A.1a shows that the residual values of the decapole and higher multipoles also are suppressed at all fields to less than 10^{-4} of the dipole field. The uniformity of the performance up to 4.1T suggests that this approach can be pushed well beyond 4T.

From Table A.1 we see the the fraction of the total current which appears in the correction windings, each of which has the same polarity as the main windings, is 7.5 percent at 2.7 T, and the required accuracy of power supply regulation for the total correction current is 0.77 percent for a 10^{-4} relative sextupole error. The ampere-turn efficiency, the ratio of the current that would be required if there were no saturation to that actually required, is very high for this configuration. Table A.2 shows the sensitivities of the multipole components to both the magnitude and horizontal position of each current used in simulation a.

In the simulations we have found it easier to find the appropriate current distributions using equally spaced current elements which differ in relative strength. A more useful approach for magnet design would be equal-current conductors with position adjusted to achieve the equivalent distribution.

B. Dipole Decoupling

The correction currents shown in Figure A.1b and A.1c, unlike A.1a described above, are decoupled from the dipole field; i.e., the first horizontal moment of the correction current is zero. The primary advantage of

Table A.1

Multipole content, current requirements and ampere-turn efficiencies for correction current configuration a, b, c as shown in Figure A1. $b_n = B_n/B$. The upper (lower) numbers in each pair refer to the uncorrected (corrected) multipoles. The magnitude of the correction currents are scaled to eliminate the sextupole at each dipole field. The ratios of correction current elements are optimized at 2.7T and taken to be constant at all fields (see Table A.2). At 60kA the simulated field is too low because the return saturates ($B \geq 2.37T$).

Quadrant Current (kA)	Eff. $\frac{BG}{8\pi I}$	Correction Current (kA)	B_0(G)	$b_2(10^{-4})$	$b_4(10^{-4})$	$b_6(10^{-4})$	$b_8(10^{-4})$
Configuration a (SSC 21)							
20	0.994	0	19680	6.32	0.41	0.04	0.11
20	0.994	0.077	19674	0	-0.06	0.04	0.11
30	0.912	0	27084	120.08	10.20	-0.03	-0.06
30	0.907	2.253	26910	0	0	-0.03	-0.04
40	0.824	0	32618	239.15	21.47	0.26	-0.18
40	0.815	5.671	32270	0	0.29	0.06	-0.18
50	0.754	0	37299	329.10	29.43	0.37	-0.22
50	0.749	9.393	37063	0	-0.25	0.39	-0.28
60	>0.694	0	>41199	392.19	34.88	0.60	-0.31
60	>0.692	12.561	>41056	0	0.75	0.56	-0.40
Configuration b (SSC 18)							
20	0.995	0	19682	6.50	0.79	-0.34	0.22
20.12	0.988	0.12	19670	0	0.43	-0.36	0.26
30	0.914	0	27119	122.3	10.65	-0.47	0.07
33.55	0.817	3.55	27137	0	0.93	-0.69	0.49
40	0.826	0	32673	242.6	21.94	-0.23	-0.06
48.79	0.674	8.79	32534	0	1.14	-0.67	0.78
50	0.756	0	37402	334.1	29.99	-0.12	-0.13
64.14	0.587	14.14	37270	0	0.77	-0.58	-0.04
Configuration c (SSC 22)							
20	0.994	0	19680	6.33	0.45	0.06	-0.10
20.06	0.992	0.059	19689	0	0.27 (.38)	0 (.01)	0.11
30	0.913	0	27093	119.4	10.24	-0.03	-0.24
31.85	0.866	1.853	27284	0	0 (1.5)	0 (-.32)	0
40	0.824	0	32620	239.2	21.56	0.27	-0.38
44.69	0.748	4.686	33058	0	-2.98 (0)	0.57 (0)	-0.17
50	0.754	0	37299	329.1	29.46	0.39	-0.43
57.53	0.669	7.533	38092	0	-6.25 (-2.0)	1.11 (.35)	-0.22
60	0.694	0	41199	392.19	34.92	0.61	-0.51
70.02	0.608	10.025	42143	0	0.75 (-3.5)	0.56(.46)	-0.40

Table A.2

Correction-current distributions for three configurations and sensitivity to errors in correction current in configuration a.

A. Correction current distributions for configurations a, b and c at 2.7T.

	$\sum \lvert I_{nc} \rvert$	I_5	I_6	I_7	I_8	I_9
	kA	kA	kA	kA	kA	kA
Configuration a	2.22521	0.0573	0.2367	0.2060	1.7521	-
b	3.5455	0.9770	0.6145	0.9770	-0.9770	-
c	1.8525	0.1393	0.4706	0.5470	0.0344	-0.6612

B. Sensitivity of multipole content for configuration a at 2.7T to errors (in percent) in each correction current.

$\Delta b_2/\Delta I/I$ (10^{-4}/%)	-0.068	-0.372	-0.175	-0.689	-
$\Delta b_4/\Delta I/I$	0.046	0.084	-0.035	-0.232	-
$\Delta b_6/\Delta I/I$	-0.031	0.019	0.016	-0.009	-
$\Delta b_8/\Delta I/I$	0.017	-0.029	0.002	0.010	-

C. Sensitivity of multipole content for configuration a at 2.7T to horizontal placement errors in each correction current.

$\Delta b_2/\Delta x$ 10^{-4}/mil	0.012	0.022	-0.065	-0.287
$\Delta b_4/\Delta x$	0.014	0.061	0.027	-0.047
$\Delta b_6/\Delta x$	-0.019	-0.039	0.005	0.038
$\Delta b_8/\Delta x$	0.013	0.018	-0.007	0.004

this approach is that quench protection may be easier. The disadvantage is that some of the correction current opposes that in the main windings, so that more superconductor is required at a given dipole field.

Configuration b has equal (absolute values of) currents in three of the coils including the triangular one of the poletip. The current in the fourth coil is constrained by the dipole decoupling condition. The total current is adjusted to eliminate the sextupole component at each field. Table A.1b shows that the higher multipoles are $<10^{-4}$ of the dipole field. At 2.7T configuration b requires 12 percent more total current than configuration a, in which the single-polarity correction currents aid the dipole field.

Configuration c uses the elliptical beam pipe to define the positions of the correction currents. Because these are closer to the center, less total current is needed than for configuration b, but 6 percent more current is needed at 2.7T than for configuration a. More significantly, configuration c does not use as effectively the same current distribution at all fields. Following the procedure used for a, we obtain results (Table A.1c) showing that a negative decapole term grows at high fields. The extremes of the variation are reduced by normalizing at a higher field (3.3T instead of 2.7T). These results are shown in parentheses. It is apparent that correction windings work best on the polefaces, i.e., as near as possible to where the greatest saturation effects occur.

C. Excitation of Dipole Field

The magnetic properties of the steel may be parameterized by

$$B = H + M/(1+H_0/H) \qquad (1)$$

where B is in Gauss and H is in Oersteds. For the 1010 steel used in our simulation $M \approx 21400$ G, $H_o \approx 10$ Oe. With a little help from the simulations we may calculate how much saving in superconductor current is possible if the steel is used efficiently. The total path reluctance in a quadrant is evaluated to determine the required current for a given field.

$$4\pi I = Bg/2 + \int H d\ell \qquad (2)$$

where I is the quadrant current in emu, g is the gap height in cm and ℓ is the return distance in the steel. An important condition for good field quality over a wide dynamic range is that the shape of the flux pattern in the steel does not change much with field strength. We assume that there is enough steel so that the outside surface of the flux return never saturates. Then the opening angle between neighboring flux lines leaving the poletip (Figure A.2a) determines the depth of the saturated field region in the steel. From POISSON we learn that the field falls off almost linearly from the poletip, so we may describe the field in the steel by

$$B(x,\ell) = B_p(x)[1- \ell/f(x)] \qquad (3)$$

where x is measured along the poleface, B_p (=B secθ) is the field in the steel at the boundary and f is the fall-off distance. Making the approximation, appropriate for B > M, that $H(x,\ell) = B(x,\ell) - M$, we find for each value of x

$$\int H d\ell = \frac{f}{B_p}\int_M^{B_p} (B-M)dB = \frac{f}{2B_p}(B_p-M)^2 = \frac{f_o B}{2}(1-b)^2 \qquad (4)$$

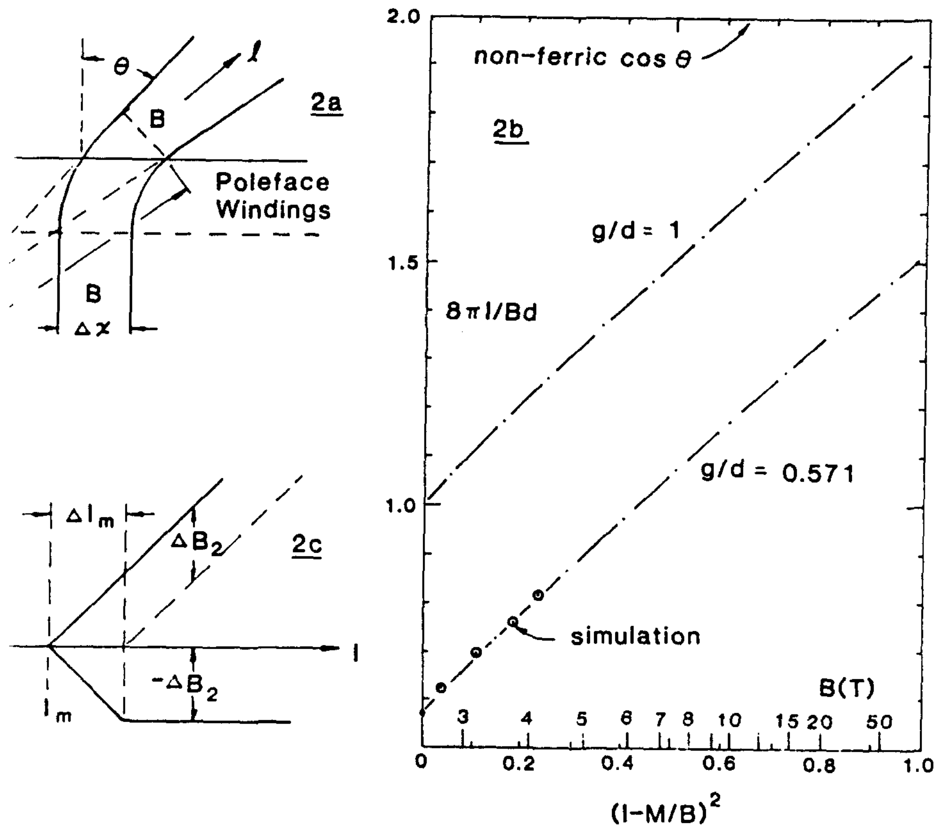

Figure A-2. Superferric design features (a) Divergence of flux lines in the steel pole tip, (b) Excitation-current efficiency as a function of field strength. g is the magnet gap, d is the effective width of the dipole, (c) graph indicating sensitivity of sextupole strength to error in magnetization.

where $f_o \equiv f(o)$ and b=M/B. The dependence of f on x is determined from (4) and Figure A.2a by

$$f = \cos\theta \frac{dx}{d\theta} = \frac{f_o(1-b)^2 \sec\theta}{(\sec\theta - b)^2} \tag{5}$$

The ratio f_o/d, where d is the effective width of the dipole field, is obtained from (5) by integrating in x from 0 to d/2 and in θ from 0 to θ_m, the value of θ at x = d/2. From (2) and (4) we obtain

$$\frac{8\pi I}{Bd} = \frac{g}{d} + 1/2\int_o^{\theta_m} \frac{d\theta}{(1-b\cos\theta)^2} \tag{6}$$

$$= \frac{g}{d} + (1-b^2)/2\left[\frac{b\sin\theta_m}{1-b\cos\theta_m} + \frac{2}{(1-b^2)^{1/2}}\tan^{-1}\left(\frac{1+b}{1-b}\right)^{1/2}\tan\frac{\theta_m}{2}\right]$$

As a function of $(1-b)^2$ the results of the simulation from the Table are shown in Figure A.2b. [Through an oversight the 60kA simulation does not include sufficient steel, so that the return field on the median plane is $\geq$ 2.37T. We estimate that the simulated reluctance is 5-10 percent too high and the field value is ~2 percent too low.] As a guide for extrapolation we show the predictions of (6) for θ_m = 30 degrees. The reluctance scales linearly with d, but it is essentially independent of g because differences in the return associated with the latter involve essentially unsaturated steel. For different values of g/d, therefore, the lines of constant θ_m are vertically offset but parallel.

The sloping upper curve in Figure A.2b is for a ferric design with g/d = 1, a value characteristic of high-field non-ferric $\cos\theta$ designs. The latter are represented by the flat line corresponding to the general relationship for

$\cos\theta$ configurations $4\pi I = Bd$. Figure A.2b shows that even the g-displaced ferric design, for which the conductor shape has not been optimized at high fields, requires at most 2/3 as much current at 5T and 3/4 as much at 7.5T as the non-ferric $\cos\theta$ solution with the same coil aspect ratio.

D. Sensitivity of B and B_2 to M

In the ferric mode ($B < M$) B depends only on the excitation current I; but for $B > M$ the precise value of M is relevant. From Figure A.2b we see that approximately

$$8\pi I/Bd = g/d + (1-M/B)^2 \tag{7}$$

The sensitivity of the dipole field to M is given by

$$(M/B)dB/dM = 2(M/B)(1-M/B)/(g/d+1-M^2/B^2) \tag{8}$$

For $g/d = 0.6$, the largest (worst) value for this ratio is 0.39, occurring at $B = 1.61M = 3.45T$.

Figure A.2c shows how the sensitivity of the multipoles to M may be estimated. An error in M implies an error in transition current, $\Delta I_m = I_m \Delta M/M$. Using the calculated sensitivity of the uncorrected sextupole to the main-winding current, dB_2/dI, we find

$$\Delta B_2/B = (I_m/B)(dB_2/dI)(\Delta M/M) \tag{9}$$

For $I_m = 23kA$, $B = 2.3T$ (worst case), $dB_2/dI = 42G/kA$ and taking $\Delta B_2/B \leq 10^{-4}$, we find $\Delta M/M \leq 2.4 \cdot 10^{-3}$. This limit implies a worst case fractional uncertainty in the dipole field $\Delta B/B \leq 0.93 \cdot 10^{-3}$.

Quality control will be necessary in the production, selection and measurement of the steel. Magnets in the same string, i.e. sharing the same currents, must be matched. Scrambling steel from different production runs can be used to minimize the magnet measurement program.